PETROLEUM ENGINEERING 685

Directed Studies

Summer 2018

Probabilistic volumetric evaluation of potential turbidite prospects from offshore Uruguay.

Student Name: Pablo Rodriguez **Student Number:** 324002078

ABSTRACT

This project is motivated by the importance of turbidite reservoirs in the South Atlantic Ocean region. It consists of a probabilistic volumetric evaluation of five potential turbidite prospects recognized within 3D seismic data acquired in the last 6 years of exploration in the offshore Uruguay.

For the probabilistic volumetric analysis, some key parameters, used to define the probability distribution functions, were obtained from the study of several scientific publications about turbidite fields located in sedimentary basins along the Atlantic Ocean. As a result from this activity, a database of reservoir and fluid properties was created.

Finally, the main result of this project is the quantification and categorization (SPE 2007) of the Prospective Resources of the five potential turbidites that were object of this analysis.

Acknowledgement

I would like to thank ANCAP, the national oil company of Uruguay, for the permission to use its seismic and well data in this project.

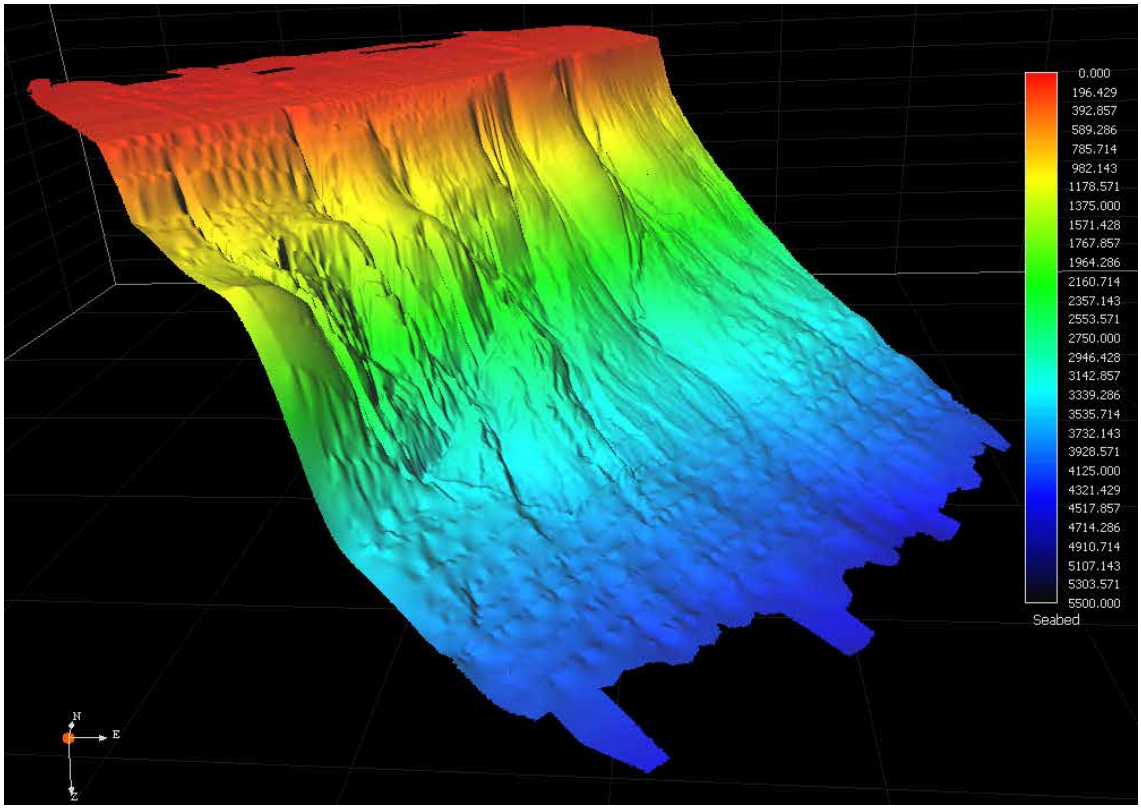

Fig. 1 – Offshore Uruguay seismic interpreted seafloor

INDEX

List of Figures

List of Tables

1. Objective

This project consists of a probabilistic volumetric evaluation of a set of potential turbidite prospects recognized in the offshore Uruguay. It is motivated by the importance of turbidite reservoirs in this region of the Atlantic Ocean.

In "PETE692 – Professional Study" this work will be extended with a probabilistic economic evaluation for each prospect.

2. Introduction

Turbidite reservoirs have been drilled in the offshore of Brazil since the 70s. They became an objective of great interest for exploration and an important source for Brazil's current hydrocarbon production (Bacoccoli and Toffoli 1998). Turbidites have been also a popular target in places like West Africa and the southern region of North Falkland Basin, amongst others.

In the last 10 years of exploration in the offshore of Uruguay, nearly 41,000 km^2 of 3D seismic were acquired and several prospects were recognized. One of them was drilled by Total in 2016. The objective of that well was a Cenozoic turbidite, which resulted to be a good quality reservoir, but without hydrocarbons. It was also the first ever-drilled turbidite in the offshore of Uruguay and it is a current world record in matters of water depth (Wood Group Mustang 2018).

The first part of this analysis consists in the compilation of a database of turbidite reservoir and fluids parameters. These values are used, as analogous, to support the parameters for the probability distribution functions (PDF) of key reservoir variables used in the volumetric assessment of the different prospects.

The next part of this study is a detailed interpretation of 3D seismic in order to get the Gross Rock Volume (GRV) for each prospect. For this purpose, seismic amplitude maps are created to constrain the different volumes and therefore calculate the maximum, optimistic and conservative cases. The definition of the maximum GRV, named P01, is done using the entire interpreted volume of the turbidite body, the definition of the optimistic GRV (P10 volume) is based in the zones where relatively high amplitude anomalies are observed and the definition of the conservative GRV (P90 volume) encompasses only the zones where the highest seismic amplitudes are recognized.

With all the compiled and estimated data, a probabilistic volumetric analysis is carried out using the volumetric formula (Wright 2015; Cronquist 2001) for Estimated Ultimate Recovery (EUR):

$$EUR_{oil} = \frac{7{,}758 * A * h * \frac{N}{G} * \varphi * (1 - S_w)}{B_{oi}} * RF = \frac{6.29 * GRV * \frac{N}{G} * \varphi * (1 - S_w)}{1{,}000{,}000 * B_{oi}} * RF$$

Where *GRV* is expressed in m^3 leading to an EUR_{oil} in MMbbls.

Assuming a Black Oil reservoir fluid, the EUR for associated gas is calculated as:

$$EUR_{associated\_gas} = \frac{EUR_{oil} * GOR}{1{,}000{,}000}$$

Where Gas-Oil Ratio (GOR) is expressed in scf/STB leading to an associated gas EUR in trillion cubic feet (TCF).

3. Database of turbidite reservoir parameters

In this project several turbidite fields were studied in order to obtain reservoir and fluid properties that could be used, as analogous, for potential turbidites recognized in the Uruguayan Exclusive Economic Zone (EEZ).

From offshore Brazil the fields which were selected are: Albacora, Albacora Leste, Marlim, Marlim Sul, Barracuda, Espadarte, Namorado, Frade and Roncador, all located in Campos basin. The analized turbidites from other regions of the globe comprise: Jubilee field, located offshore Ghana, and the Sea Lion Complex, located offshore Falkland Islands. Their locations are shown in **Fig. 2.**

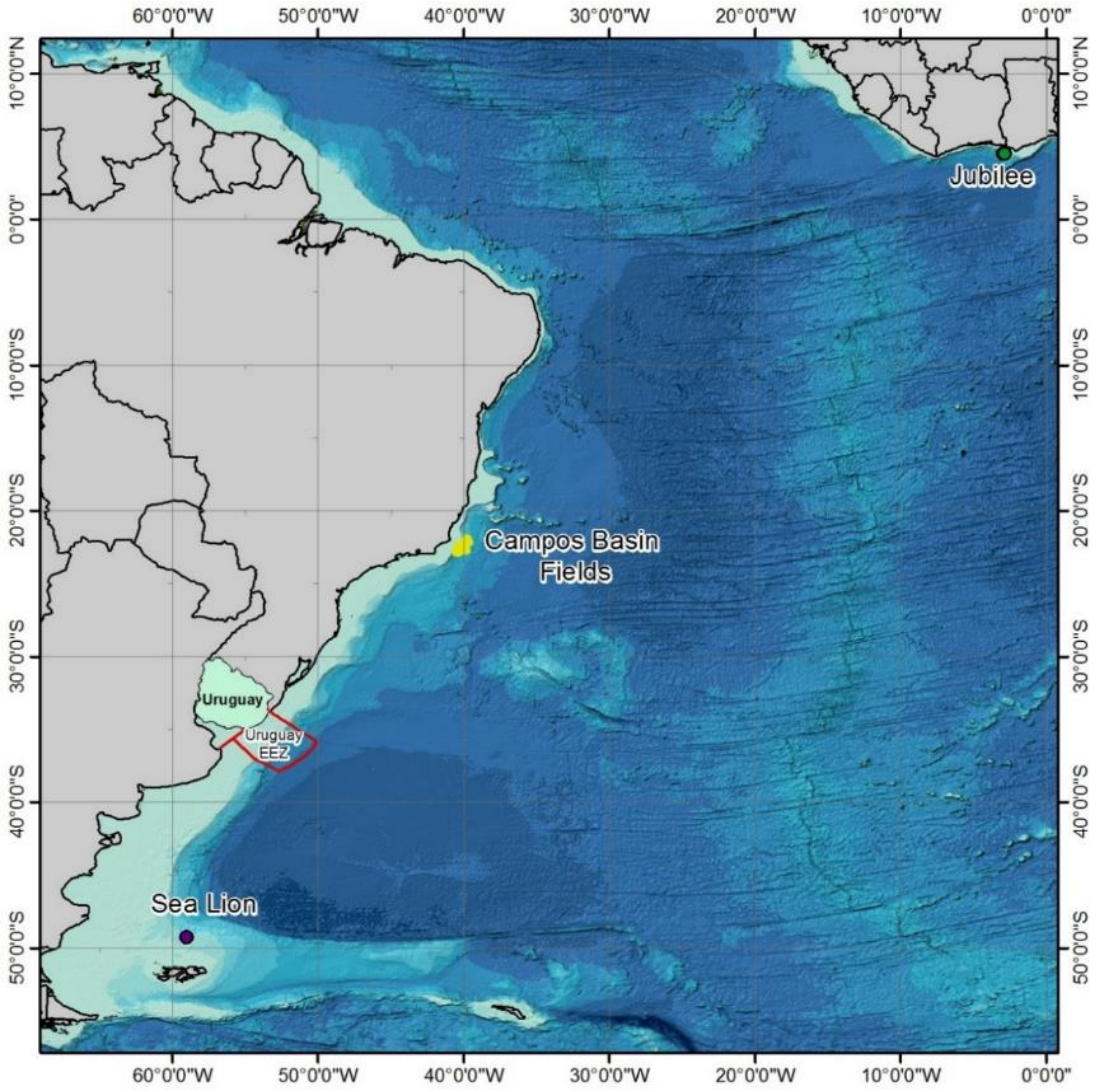

Fig. 2 – Location of turbidite fields analyzed for this report

From the review of various publications about the mentioned fields, **Table 1** was constructed. The information it contains includes field name, location data (country and sedimentary basin), reservoir age, water depth limits, reservoir depth, porosity, gas-oil ratio, oil density, water saturation (S_w), area, gross thickness, net to gross ratio (N/G), net pay, recovery factor (RF) and initial oil formation volume factor (B_{oi}). In the last column, there is a list of the different publications that were consulted for each particular field. The PDF obtained from fitting the datasets of N/G, S_w, GOR and RF are shown from **Fig. 17** to **Fig. 20,** respectively.

Field	Country	Basin	Age	Water Depth (m)		Total Depth (m)		Porosity (%)			GORi (scf/stb)			°API			Sw (%)		
				Min	Max	Min	Max	Min	Avg	Max	Min	Avg	Max	Min	Avg	Max	Min	Avg	Max
Albacora	Brazil	Campos	Oligocene/Eocene/Albian	100	1050	2500	3260	17.0		29.0	365	492	663	26.0		29.0	18.3		30.7
Albacora Leste			Miocene	800	2000	2350	2480		30.0		337		393	16.5		21.5		22.8	
Marlim			Oligocene/Miocene	500	1100	2500	2700		30.0		337	449	1123	18.0		25.0		15.0	
Marlim Sul			Oligocene/Miocene	800	2600	3100	3300		32.0		337	449	1123	13.0		29.0			
Barracuda			Oligocene/Eocene/Paleocene	600	1200	2400	3200	19.0		31.0	365		561	20.0	25.0	26.0	10.0	20.0	35.0
Espadarte			Eocene	750	1500	3050	3350	25.7	29.0	31.8		505		18.0	26.0	29.0		54.0	
Namorado			Albian/Cenomanian	130	240	2940	3200	20.0	23.0	30.0		1123			28.0	31.0	10.0	18.0	20.0
Frade			Miocene/Oligocene	1050	1300	2000	2450	29.0		34.0	345		423	15.0		22.4			
Roncador			Maastrichtian	1500	1900	2890	3505	24.0	28.5	30.0	434		635	18.0		31.0	23.0		18.0
Jubilee	Ghana	Tano Basin	Turonian	1200	1500	3000	4000	15.0	21.0	30.0		1200		36.0	37.0	38.0	10.0		40.0
Sea Lion	UK	North Falkland Basin	Aptian	375	475	2359	2477	15.0	22.0	25.0	243		498	24.5		29.3	15.0	35.0	50.0

Field	Area (km^2)	Gross Thickness (m)		N/G (%)			Net Pay (m)			RF (%)	Boi (rb/stb)			Sources
		Avg	Max	Min	Avg	Max	Min	Avg	Max		Min	Avg	Max	
Albacora	94		210	40		90		94		25		1.032		Awad 1997; Bonet et al. 1999; Candido and Cora 1990; Gasperi and Catuneanu 2014
Albacora Leste	141						5	16.8	35	25				Candido and Cora 1992; Lemos et al. 2006; Loureiro et al. 2006
Marlim	152		130		86			44.5		40				Bampi et al. 2010; Candido and Cora 1992; Figuereido et al. 2007; Olivera 2008; Weimer 2004
Marlim Sul	572						10		40		1.108		1.194	Acosta et al. 2005; ANP 2016a; Capeleiro Pinto et al. 2001; Da Silva et al. 2004; Figuereido et al. 2007; Souza 1989
Barracuda	157									32				Alves et al. 2005; Assis et al. 1998; da Costa Filho 2005; Rangel et al. 2003
Espadarte	146								53	33				Albertao et al. 2005; ANP 2016a; Hernandes et al. 2008; Pires et al. 2010; Reid et al. 2009
Namorado	20	60	150		50			53		40		1.439		Bacoccoli et al. 1980; Ferreira et al. 1990; Guardado et al. 1989; Silva et al. 2007
Frade	20	60									1.129		1.173	ANP 2016b; Bergeron and Parvez 2007; Ecologus 2006
Roncador	143		240					61	205	25	1.180		1.290	Cysne and Mihaguti 2008; Minami et al. 2000; Padua et al. 1998; Rangel et al. 1998; Rangel et al. 2003; Rodriguez et al. 2003
Jubilee	110	250	271	30		80	20		100		1.570		1.690	Dailly et al. 2017; Hanley et al. 2009; McLaughlin 2012; Sills and Agyapong 2012
Sea Lion	115		69		75			35		25		1.200		Bunt 2015; Farrimond et al. 2015; Griffiths 2015

no published data was found

Table 1 – Reservoir and fluid properties of the analyzed turbidite fields

4. Interpretation of geophysical data

4.1 – Geological and geophysical database

The geological and geophysical database used in this project comprises three 3D seismic surveys: UR13_3D, BG12_3D and TO12_3D, and well data from three offshore wells: LOBO and GAVIOTIN, drilled by Chevron in 1976, and RAYA, drilled by Total in 2016. The geographical location of these datasets is shown in **Fig. 3.**

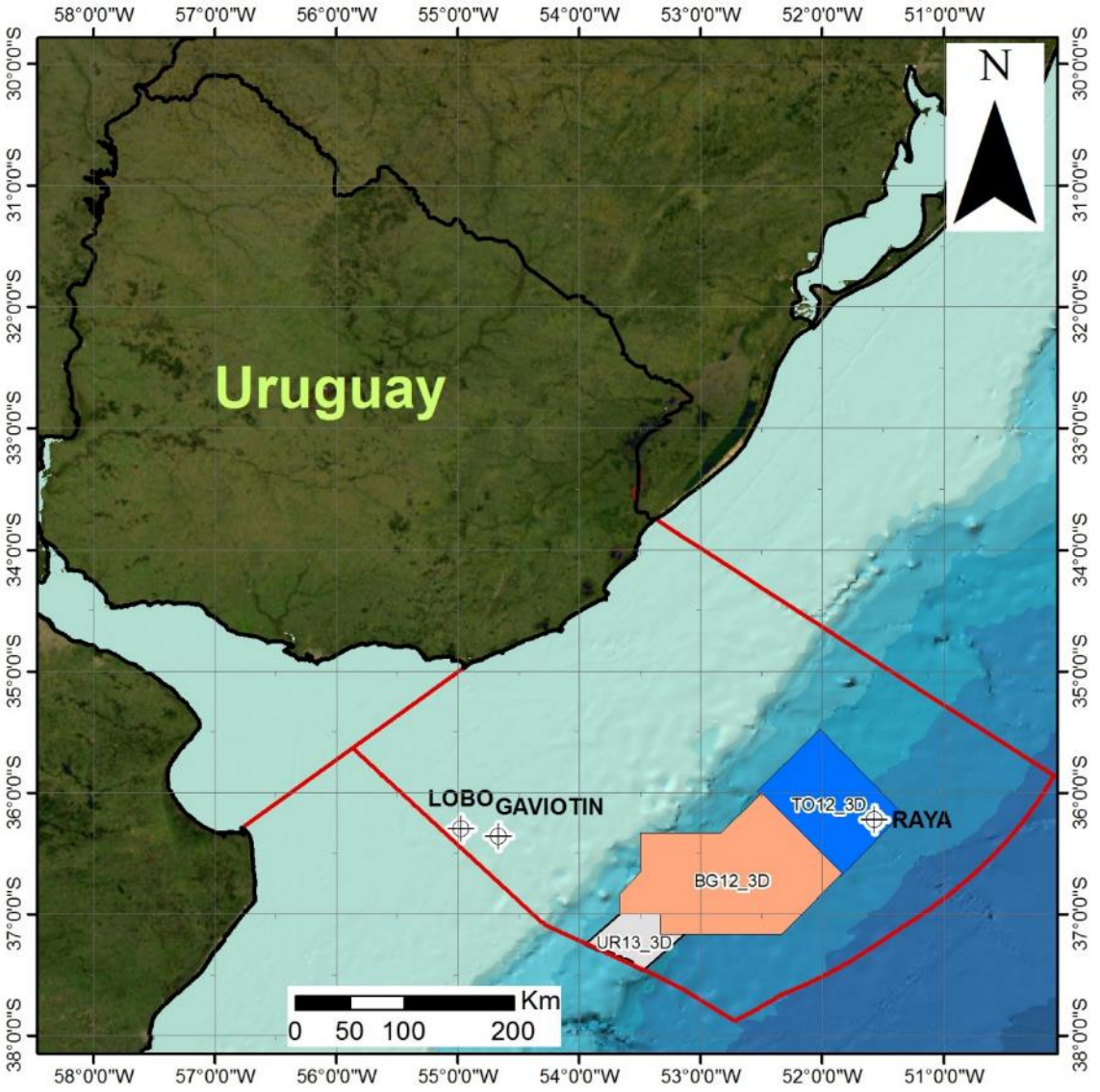

Fig. 3 – Offshore Uruguay 3D seismic and well data used in this project

4.2 – Geological framework

In the offshore of Uruguay there are three passive margin type sedimentary basins **(Fig. 4):** Punta del Este Basin, Pelotas Basin and Oriental del Plata Basin (Morales et al. 2017a).

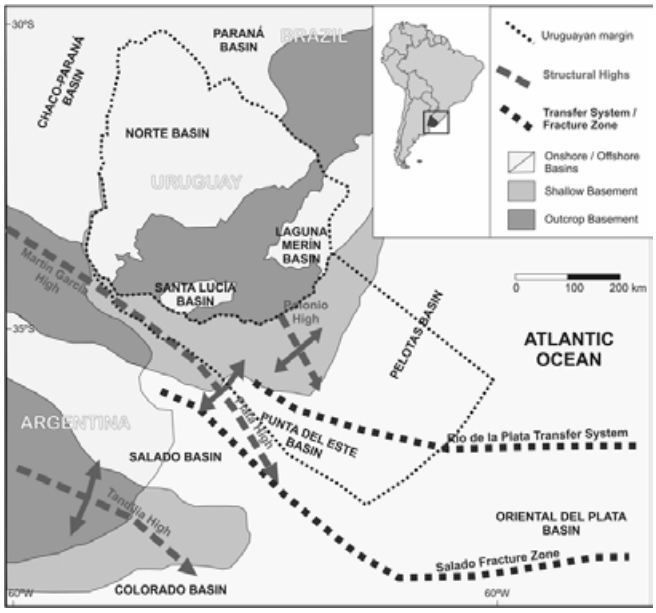

Fig. 4 – Sedimentary basins of Uruguay (Morales et al. 2017a)

Punta del Este basin, which encompasses the south-western portion of the margin, presents the main geological structures found in the offshore of Uruguay. They are associated to rift faulting during the South Atlantic break-up. In the north-eastern portion of the margin, which covers the southernmost part of the Pelotas basin, the rift sequence is not significant; it only presents some minor structures.

The sedimentary infill of these basins consists of sediments from three different phases: pre-rift, syn-rift and post-rift (passive margin).

The passive margin phase starts in the Cretaceous and continues to the present (Conti et al. 2017). Due to the absence of significant deformation of the sedimentary sequences, the main hydrocarbon plays are stratigraphic, such as turbidites, basin floor fans, channels and pinch-outs.

The recognizance of the turbidite prospects analyzed within this report implied a previous sequence stratigraphy analysis of the main depositional sequences that comprise the sedimentary infill of the basins. From that analysis, different system tracts were defined in order to identify potential turbidites related to sea-level variations.

This project was focused in five potential turbidites. Three of them are Cretaceous turbidites and are located within the area of the UR13_3D survey, one is a Cenozoic turbidite located within the area of the BG12_3D survey, while the last one is a Cretaceous turbidite located within the area of the TO12_3D survey (Fig. 3).

4.3 – Offshore Uruguay speculative petroleum systems

For the sedimentary basins of the offshore of Uruguay there are only speculative petroleum systems defined in the literature. Hydrocarbon generation and migration is supported by fluid inclusions found in cuttings from LOBO and GAVIOTIN wells (Tavella and Wright 1996; Soto et al. 2016) and also by gas indications in GAVIOTIN wireline logs (**Fig. 15** and **Fig. 16**).

In Morales et al. (2017b) and Morales (2013) four speculative (conventional) petroleum systems are proposed for offshore Uruguay. They are based on analogies with other offshore basins as well as the onshore basins of Uruguay:

A) Pre-rift marine petroleum system (Fig. 5), which is restricted to the proximal sectors of the offshore basins:

- Source Rocks (depicted as black diamonds in the seismic section of Fig. 5): pre-rift marine Devonian and Permian oil-prone shales.
- Reservoirs (depicted as yellow squares in the seismic section of Fig. 5): pre-rift fluvial-deltaic and aeolian Permian sandstones.
- Seals (depicted as blue diamonds in the seismic section of Fig. 5): pre-rift Permian marine shales, Mesozoic lacustrine shales and basalts of the syn-rift sequence.

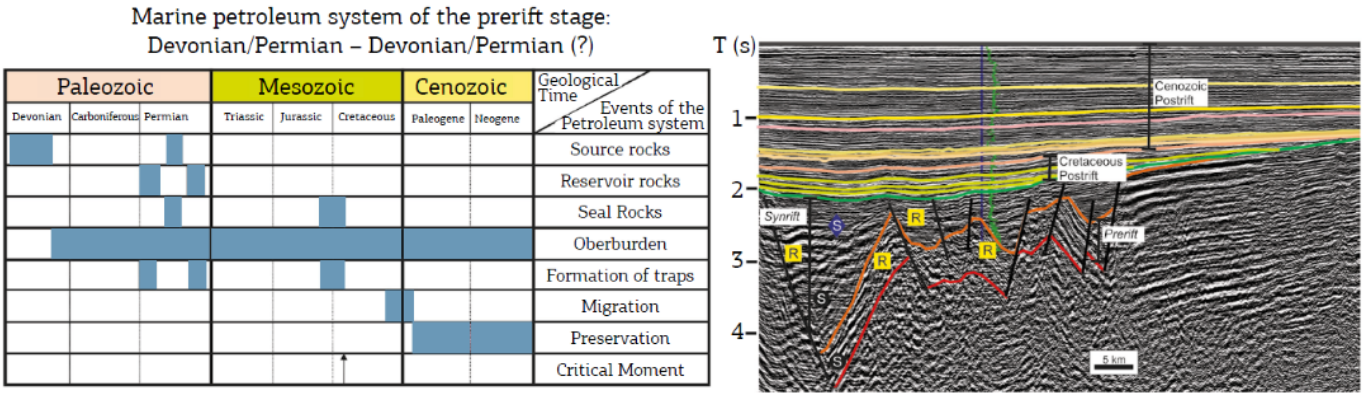

Fig. 5 – Chart of events and representative seismic section of the marine pre-rift petroleum system (Morales et al. 2017b)

B) Syn-rift lacustrine petroleum system (Fig. 6):

- Source Rocks: syn-rift Early Cretaceous lacustrine shales.
- Reservoirs: syn-rift Cretaceous alluvial conglomerates and sandstones, syn-rift lacustrine fans and fluvial-deltaic sandstones and post rift shelfal sandstones and basin floor fans.
- Seals: syn-rift lacustrine shales and volcanic rocks as well as post-rift regional marine shales of Paleocene age.

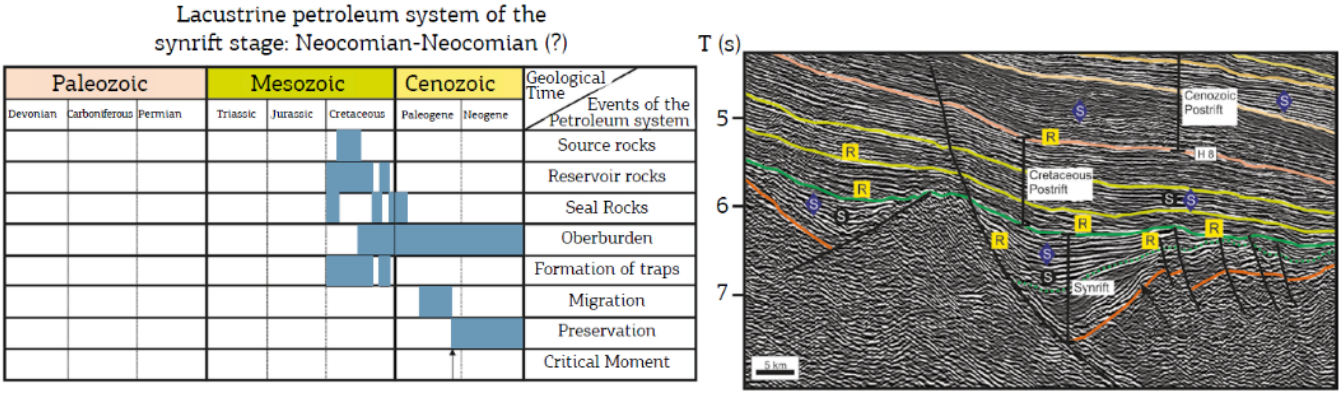

Fig. 6 – Chart of events and representative seismic section of the syn-rift lacustrine petroleum system (Morales et al. 2017b)

C) Cretaceous post-rift marine petroleum system (Fig. 7):

- Source Rocks: post-rift Aptian-Albian and Turonian shales.
- Reservoirs: post-rift Cretaceous basin floor fans, slope fans, lowstand wedges and shelf-edge deltas.
- Seals: post-rift regional marine shales of Paleocene-Eocene age as well as upper Cretaceous shales (depicted as blue diamonds in the seismic section of Fig. 7, but omitted in the chart of events).

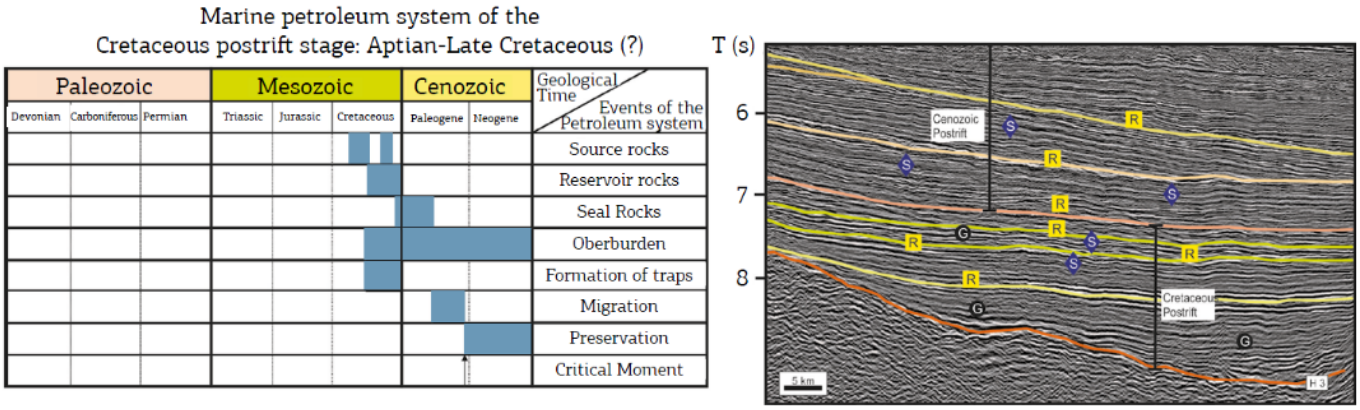

Fig. 7 – Chart of events and representative seismic section of the Cretaceous post-rift marine petroleum system (Morales et al. 2017b)

D) Cenozoic post-rift marine petroleum system (Fig. 8):

- Source Rocks: post-rift Aptian-Albian shales, Turonian shales and Paleocene-Eocene shales.
- Reservoirs: post-rift Paleogene and Neogene sandstones corresponding to basin floor fans, lowstand wedges and deltaic and shelfal deposits.
- Seals: post-rift regional marine shales of Paleogene and Neogene age.

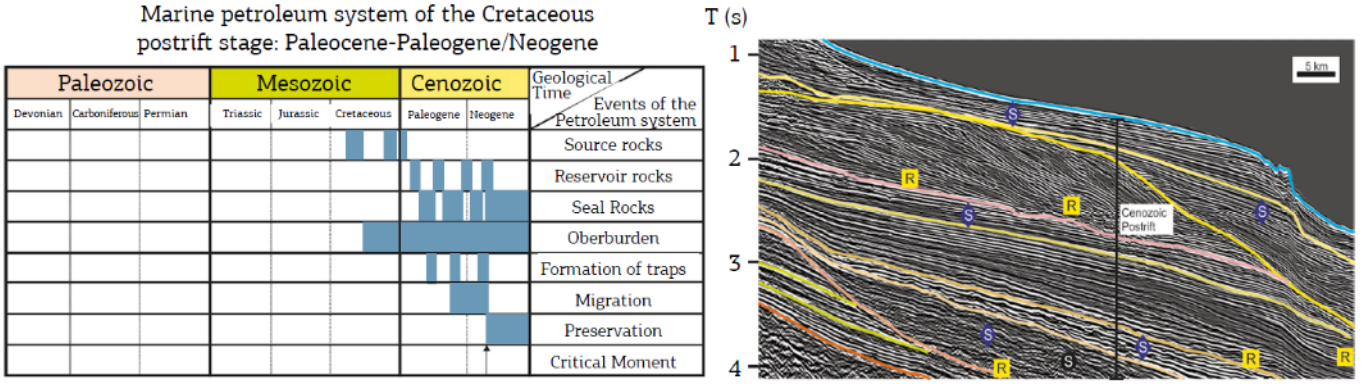

Fig. 8 – Chart of events and representative seismic section of the Cenozoic post-rift marine petroleum system (Morales et al. 2017b)

For the prospects analyzed in this report, based on their location within the stratigraphic column and the location of the interpreted source rocks, the posed petroleum system are (B), (C) and (D): syn-rift lacustrine petroleum system, Cretaceous post-rift marine petroleum system and Cenozoic post-rift marine petroleum system. Pre-rift rocks are not recognized in the studied areas; therefore the pre-rift marine petroleum system (A) is discarded.

4.4 – Seismic interpretation

In this study, the calculation of the GRV of each prospect relies on the interpretation of the turbidite bodies over 3D seismic. For that purpose, as well as for the generation of seismic amplitude maps and the calculation of GRV, the IHS® Kingdom® software package was used.

The interpretation of the different seismic datasets took into account the seismic response of various known turbidites from the South Atlantic region. In **Fig. 9** there is an example of the seismic response from the giant Brazilian Marlim oilfield. It has the peculiarity of presenting a decrease of seismic impedance (product of rock density and seismic velocity) at the top of the reservoir (TM in the figure for "Top Marlim"):

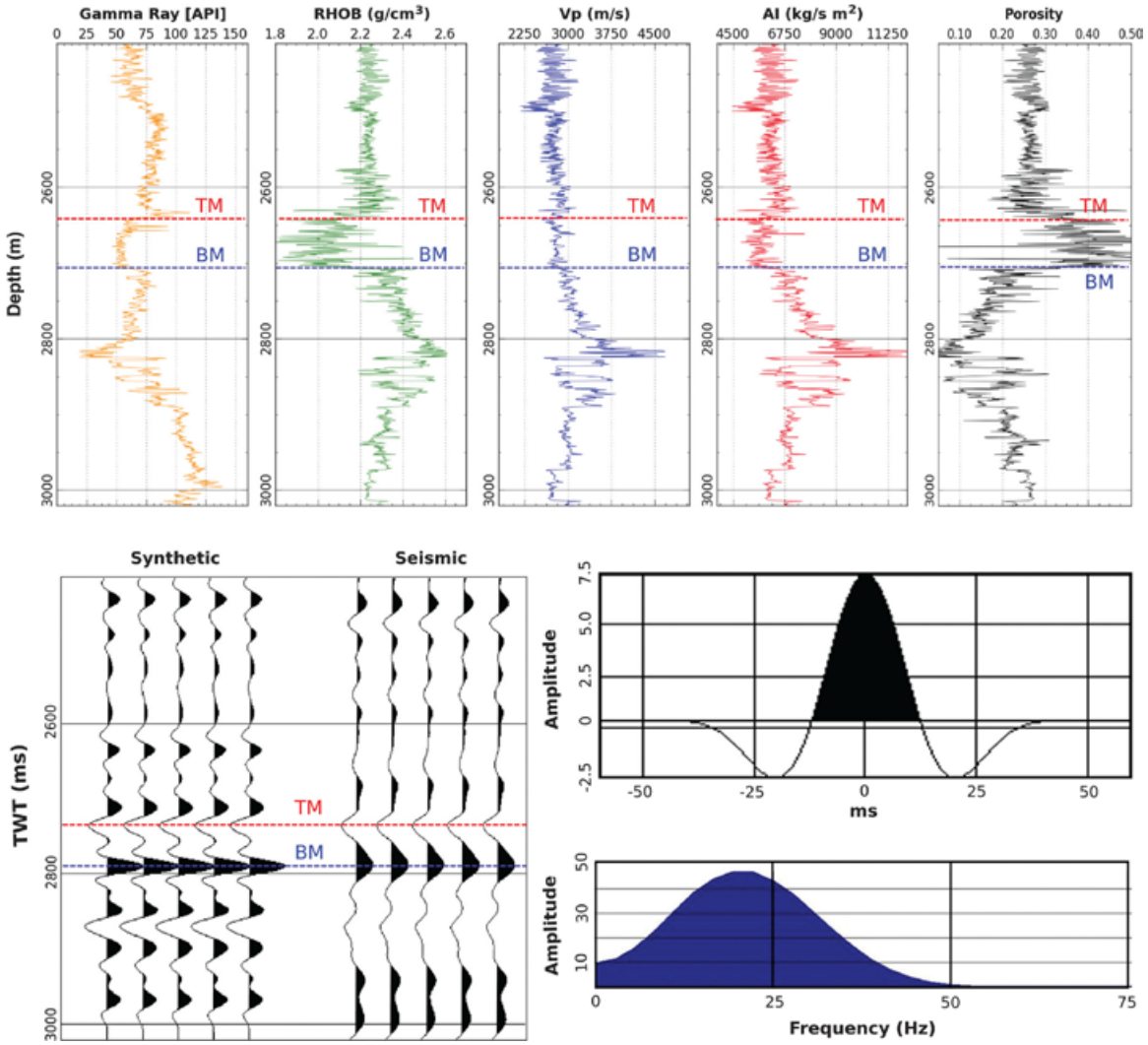

Fig. 9 – Well-logs and seismic response of Marlim (Nascimento et al. 2014)

The turbidite drilled by Total in the offshore of Uruguay in 2016 (RAYA well in Fig. 3), which resulted in a dry well, shares with Marlim, as well as with many others turbidites, a decrease of the acoustic impedance at its top.

Considering this property, besides the fact that the seismic dataset is zero phase and that it follows the SEG (Society of Exploration Geophysicists) standard polarity, then for a turbidite prospect, negative amplitudes are expected at the top of the reservoir and positive amplitudes

at the base (Brown 2011). This last fact is due to the increase in acoustic impedance in the transition from sandstone to shale when the seismic waves break through the base of the turbidite.

In **Fig. 10** there is an example of a seismic line across Marlim field. It can be seen that the top of the reservoir is represented by a reflector with negative amplitudes and its base by a reflector with positive amplitudes.

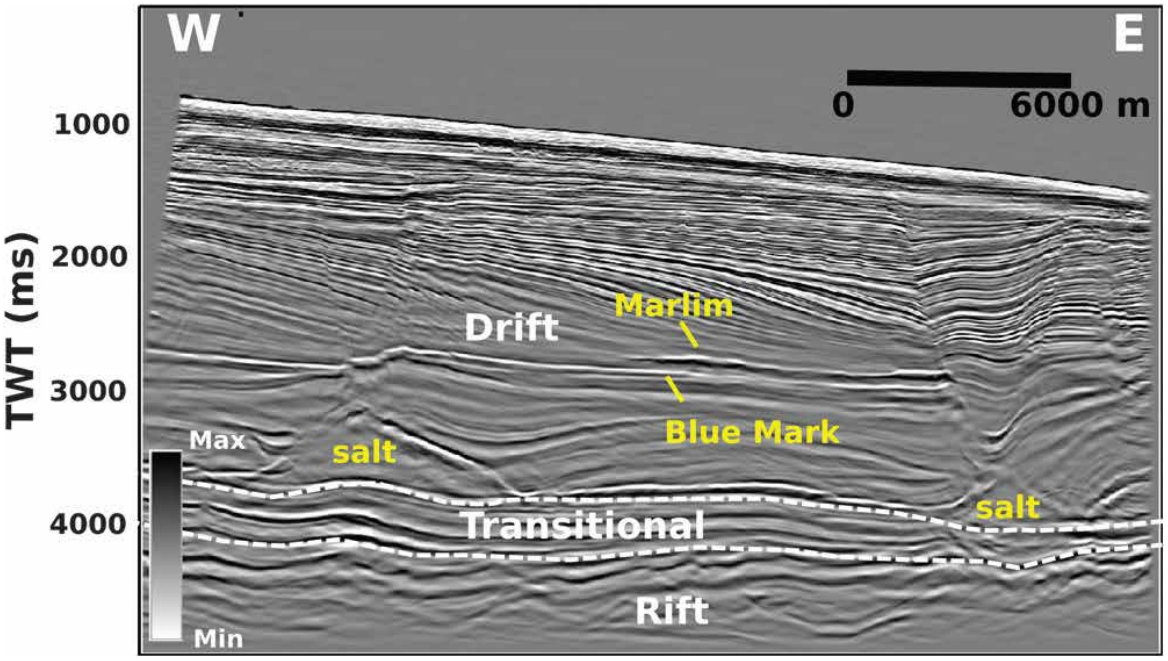

Fig. 10 – Seismic line through Marlim oilfield (Nascimento et al. 2014)

Once each potential prospect is recognized, the first step is to map the reflector that corresponds to its top (top horizon). For that purpose, a reflector with negative seismic amplitudes was followed using a user aided 2D automatic interpretation tool of IHS Kingdom (see **Fig. 26** as an example). This was executed approximately every 50 inlines and 50 crosslines (approximately one line every 625 meters in both directions, see **Fig. 11**) within the area of interest (AOI) of the prospect.

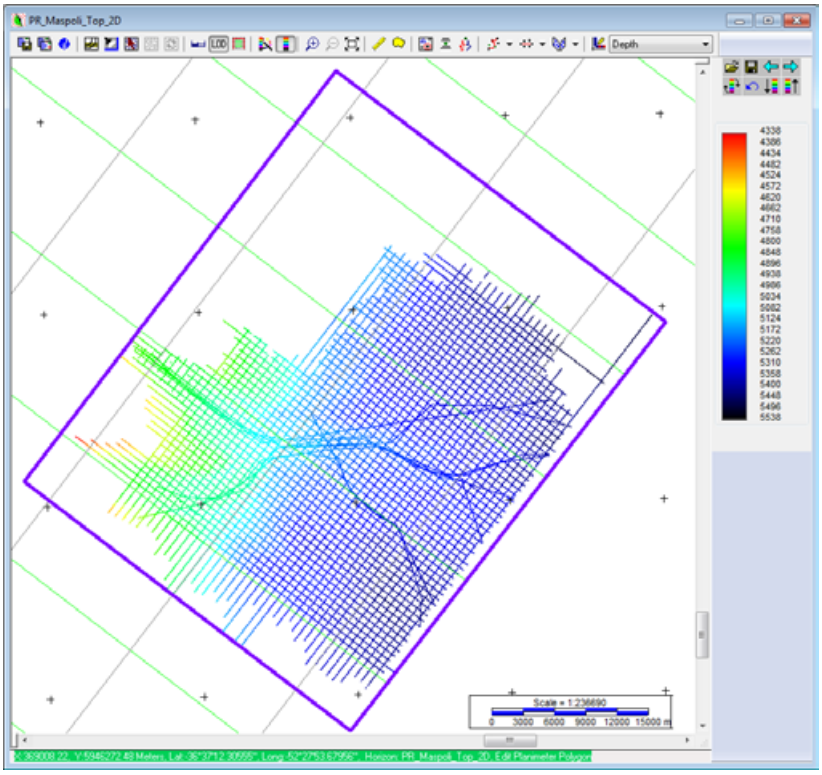

Fig. 11 – Example of 2D interpretation within the AOI of one prospect

After the 2D interpretation of inlines and crosslines was completed, an automatic 3D interpretation routine of IHS Kingdom was executed to expand the interpretation to the complete AOI of each prospect **(Fig. 12).**

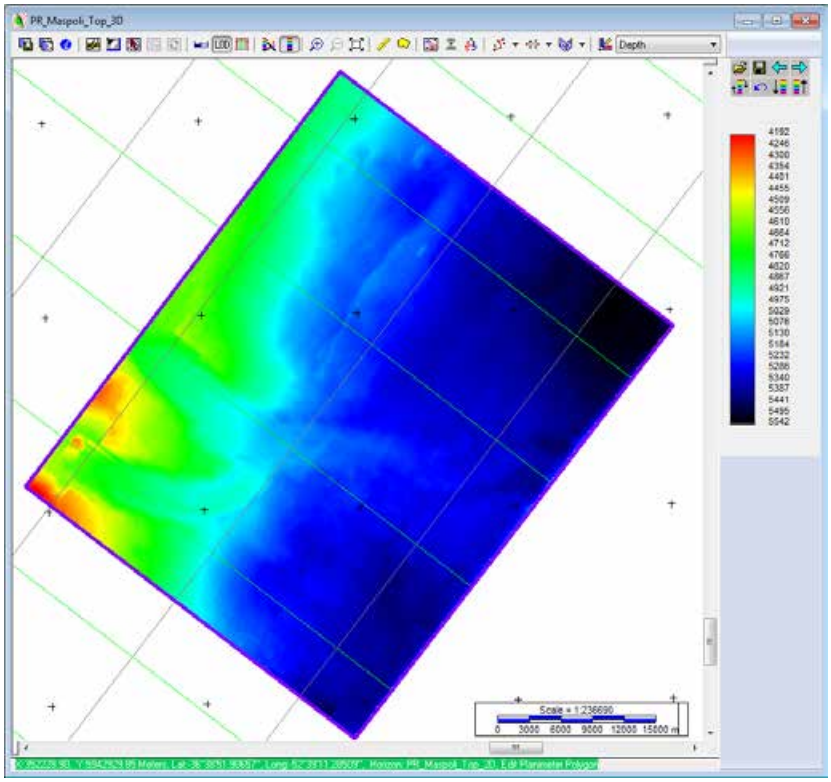

Fig. 12 – Example of 3D automatic interpretation within the AOI of one prospect

After the interpretation job of the top of the prospect was completed, then its base was interpreted. This enabled to close the potential reservoir volume and to proceed with the GRV calculation. At this step, a maximum extent polygon was created (P01 polygon). It considers the entire area where the potential turbidite was recognized, no matter what the seismic amplitudes are.

With the complete 3D interpretation of the top of the potential reservoir, a seismic amplitude map of that horizon was generated (see **Fig. 13**). This amplitude extraction map was used to recognize the areal extension of the turbidite body and thus to create two delimitation polygons. One of them, an optimistic case, which corresponds to an interpreted P10 extension of the prospect and the other, a conservative case, equivalent to a P90 area, which only encompasses the highest amplitudes **(Fig. 14).**

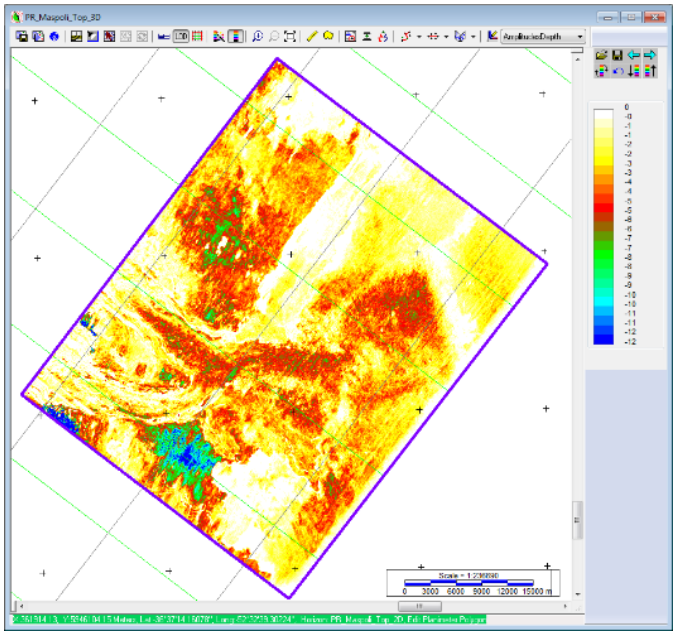

Fig. 13 – Example of a seismic amplitude map within the AOI of one prospect

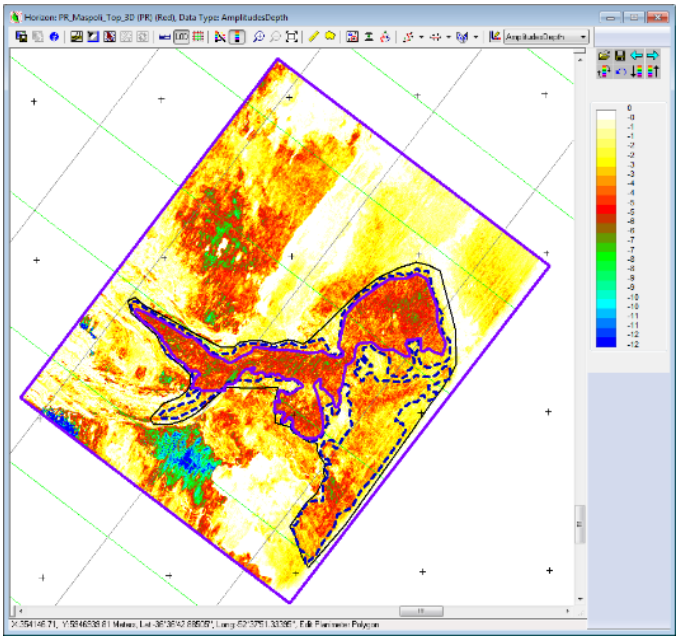

Fig. 14 – Example of a seismic amplitude map for one prospect with all its delimitation polygons

4.5 – Well data analysis

Besides the seismic analysis, a petrophysical evaluation of the offshore wells was carried out using the Interactive Petrophysics® (IP) software. This was done while I took the course "PETE608 Well Logging Methods", using an IP license available at the Texas A&M, accessed remotely through a Virtual Private Network.

The most significant results correspond to the analysis of the wireline logs from GAVIOTIN well; they are important because some gas indications can be deduced from them. There are two interesting Neutron-Density porosities crossovers within the Cretaceous sequence. The first one is located below 1808 m (Fig. 15, highlighted in red), which corresponds to the Cretaceous-Tertiary boundary, and the second one is located below 2150 m (Fig. 16, highlighted in red). In both cases, there is a shale interval at the top that act as a seal. Gas quantities are not significant due to the low bulk resistivity, that implies high water saturations, and also because the intervals that present the crossovers are not very thick. These indications support the generation, migration and trapping of gas. Latter fluid inclusion analyses proved also the generation and migration of oil (Tavella and Wright 1996; Soto et al. 2016).

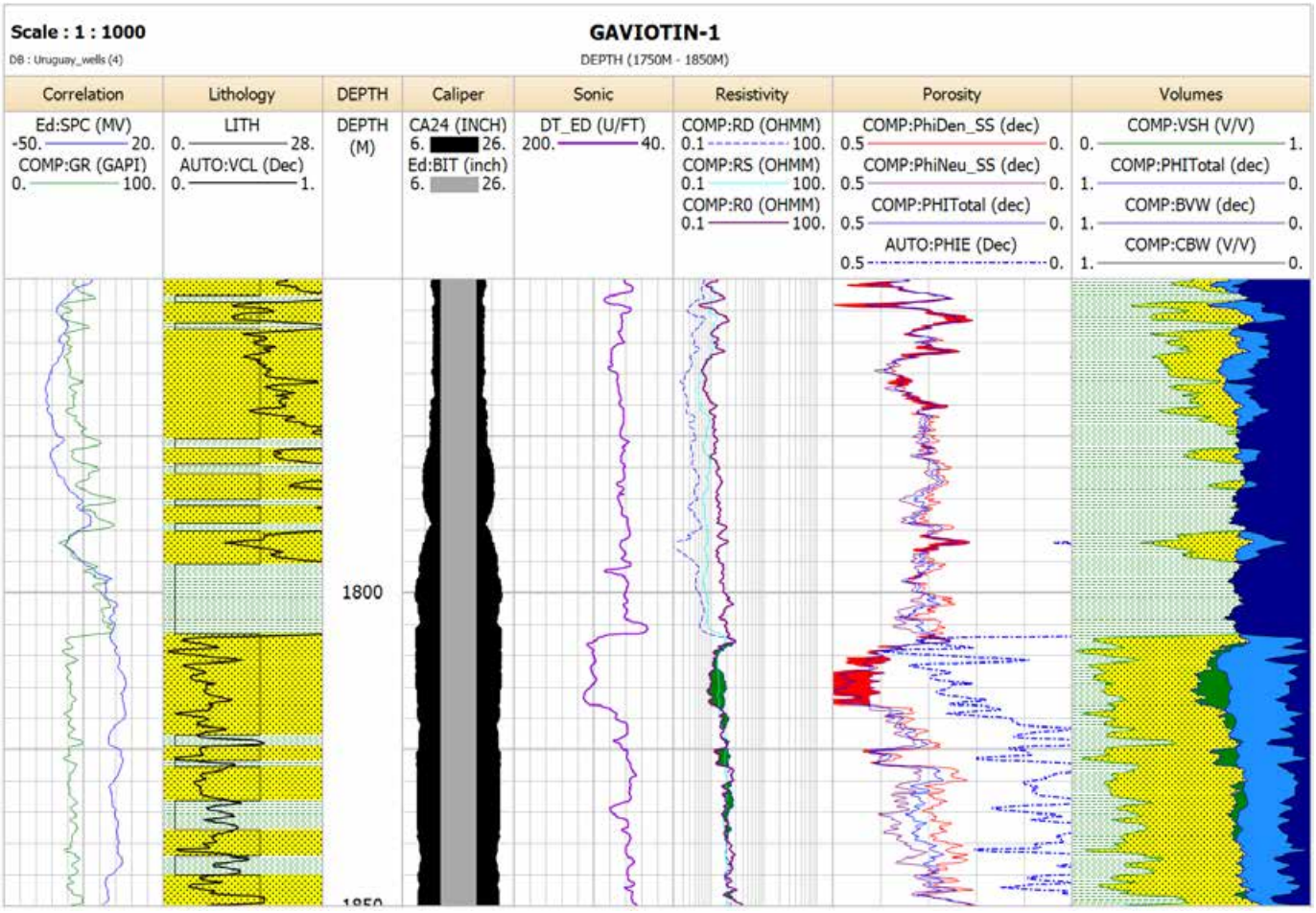

Fig. 15 – First Neutron-Density crossover at GAVIOTIN well

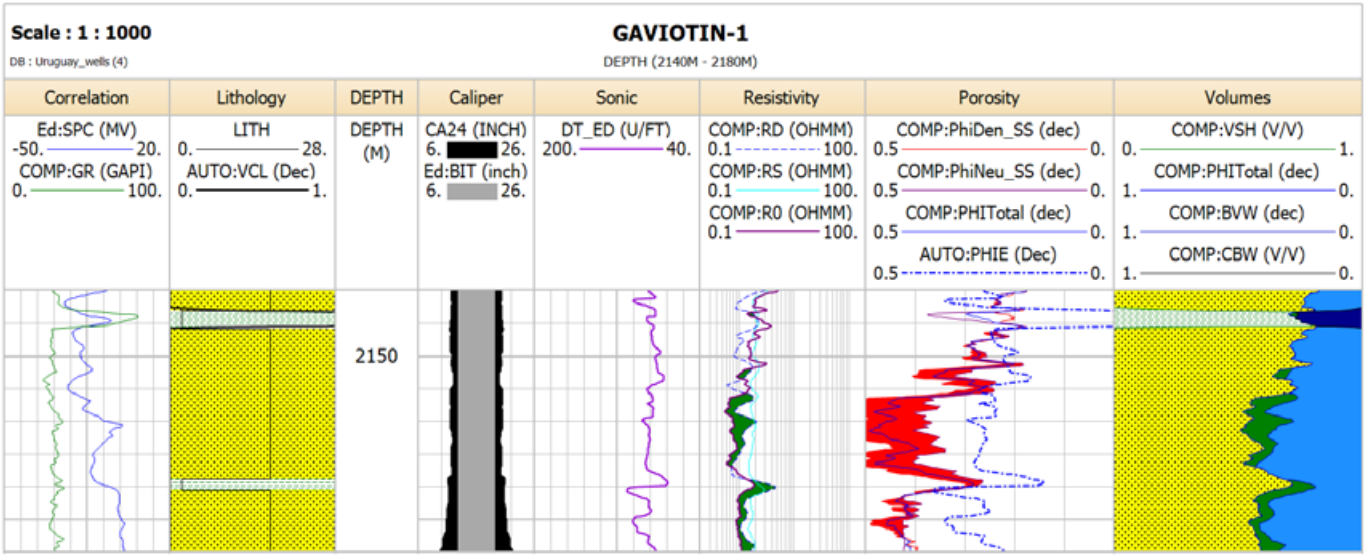

Fig. 16 – Second Neutron-Density crossover at GAVIOTIN well

5. Methodology used for EUR Analysis

5.1 – Volumetric EUR Analysis

To compute the oil EUR the volumetric formula (Wright 2015; Cronquist 2001) is used:

$$EUR_{oil} = \frac{7{,}758 * A * h * \frac{N}{G} * \varphi * (1 - S_w)}{B_{oi}} * RF = \frac{6.29 * GRV * \frac{N}{G} * \varphi * (1 - S_w)}{1{,}000{,}000 * B_{oi}} * RF$$

For the case of a black oil fluid, the associated gas EUR is calculated as:

$$EUR_{associated\_gas} = EUR_{oil} * GOR$$

To make the EUR analysis probabilistic a PDF has to be defined for every variable in the abovementioned formulae:

- ***GRV***: a maximum value is obtained directly from the entire volume interpreted in the seismic data, the P10 and P90 volumes are obtained from the analysis of the seismic amplitude anomalies. For this variable, a LogNormal distribution is chosen.
- ***N/G***: its PDF is chosen to be a BETA distribution and it is constructed from values obtained from the turbidite reservoirs previously analyzed.
- $\boldsymbol{\varphi}$ (Porosity): the PDF for this variable is defined as a BETA distribution which P10, P50 and P90 values are obtained from the publication of Ehrenberg and Nadeau (2005). This distribution is truncated at a value of 48% because porosities higher than this value are not possible for clastic rocks. The theoretical maximum porosity for a cubic packed rock is 47.64% (Graton and Fraser 1935).
- $\boldsymbol{S_w}$: the PDF for this variable is defined as a BETA distribution, and it is constructed from values obtained from the turbidite reservoirs previously analyzed.
- $\boldsymbol{RF}$: the PDF for this variable is defined as a BETA distribution; it is constructed from values obtained from the turbidite reservoirs previously analyzed. This distribution is

truncated at a value of 50% because recovery factors higher than this value are not expected.

- ***GOR***: the PDF for this variable is defined as a BETA distribution, and it is constructed from values obtained from the turbidite reservoirs previously analyzed. This distribution is truncated at a value of 2,000 scf/STB because for all the studied cases a "Black Oil" model is assumed.
- $\boldsymbol{B_{oi}}$: the PDF for this variable is defined as a BETA distribution. Its parameters are estimated using the Levitan and Murtha (1999) correlation for formation volume factor at the bubble point pressure and from the properties of the assumed fluid within the reservoir, the values of *GOR* and the estimation of reservoir temperature.

The distribution types chosen are justified by the facts that, GRV is well defined by a LogNormal distribution (Liner 2016), and BETA distributions are quite versatile and can approximate very well the most popular distributions like: Uniform, Triangular, Normal and Lognormal (Olea 2011). Moreover, the variables, which were fitted with different distributions, presented a better fit with the @Risk® BetaGeneral distribution (see **Fig. 17** to **Fig. 20** for further details).

All the volumetric probabilistic analyses are carried out in a Microsoft® Excel® spreadsheet, which runs the Palisade® @Risk add-in.

5.2 – Reservoir fluid

All the prospects analyzed in this project are assumed to contain a black oil fluid with the following properties:

$$30° \text{ API}$$
$$\gamma_g = 0.8 \text{ (air = 1)}$$
$$0 \leq GOR \leq 2{,}000 \text{ scf/STB}$$

This choice is supported by the fact that two independent fluid inclusions studies, which analyzed cuttings from LOBO and GAVIOTIN wells (see Fig. 3), encountered light oil inclusions of approximately 32° API (Tavella and Wright 1996; Soto et al. 2016).

Oil generation offshore Uruguay is also supported by source rock maturation models presented in Morales (2013).

5.3 – Gross rock volume

The calculation GRV was done using a specific tool of IHS Kingdom that calculates the GRV between two grids restricted to a delimitation area defined by a polygon.

A maximum extent polygon is created from the structural interpretation of the prospect. It comprises the entire area where the potential turbidite was recognized and it is the largest area where the turbidite may be present no matter what the seismic amplitudes are (P01 area).

Two new delimitation polygons are created from the amplitude map extracted at the top of the prospect. One of them is an optimistic case; it is an interpreted P10 extension of the prospect. The other is a conservative case and it corresponds to a P90 area that only encompasses the highest amplitudes observed.

With the grids of the top and the base of the prospect and the different restriction polygons, the maximum (P01), P10 and P90 values of GRV are deterministically calculated with IHS Kingdom.

5.4 – Net to Gross, Water Saturation, GOR and RF

For Net to Gross, water saturation, gas-oil ratio and Recovery Factor variables, probability density functions were found to fit the presented values within the database for the analyzed turbidite fields (Table 1). From that procedure, the following results were obtained and will be considered for the evaluation of every prospect:

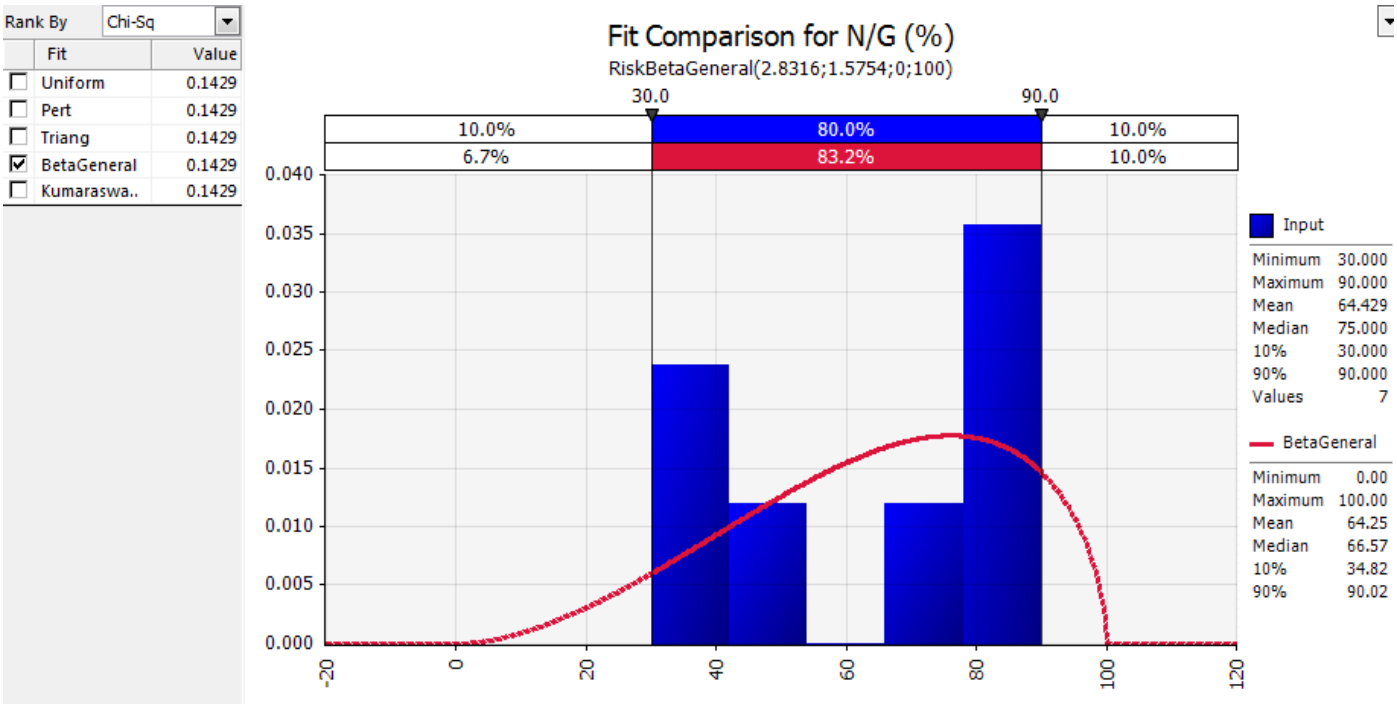

Fig. 17 – PDF for *N/G*

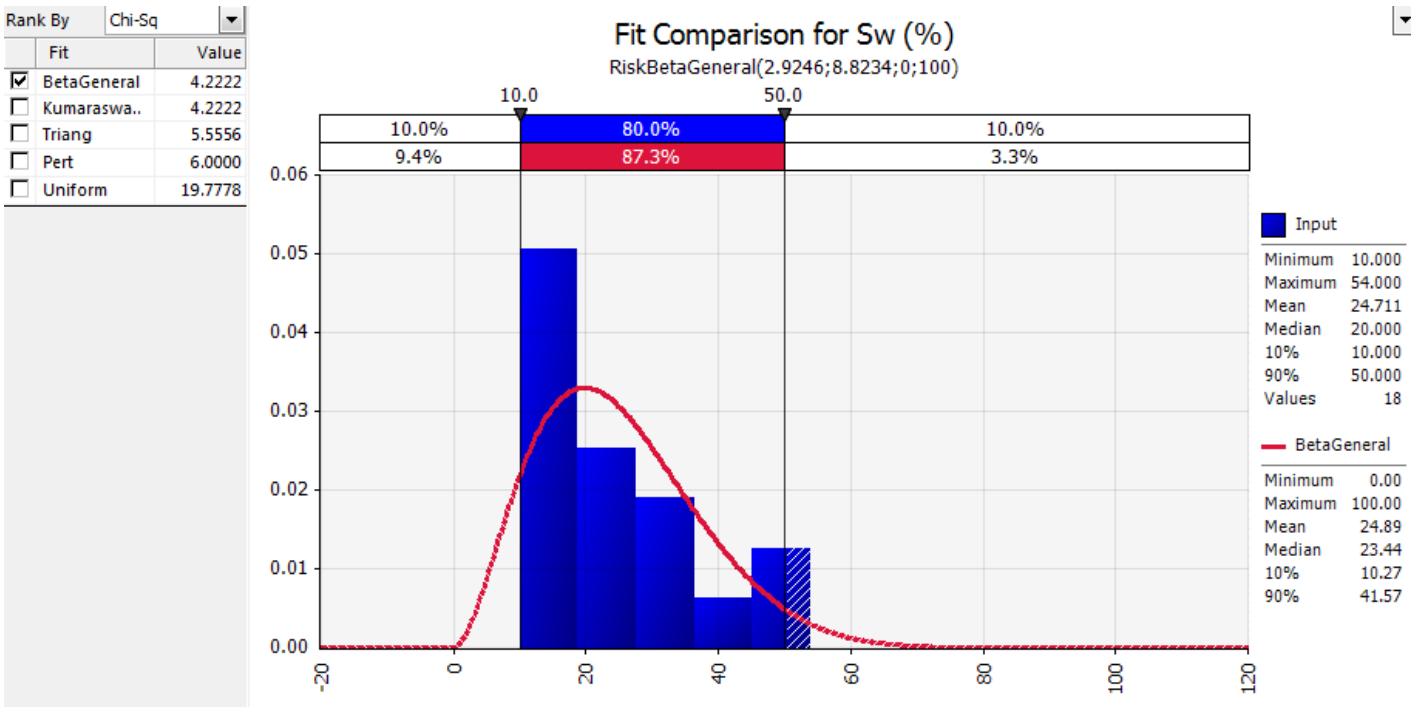

Fig. 18 – PDF for *Sw*

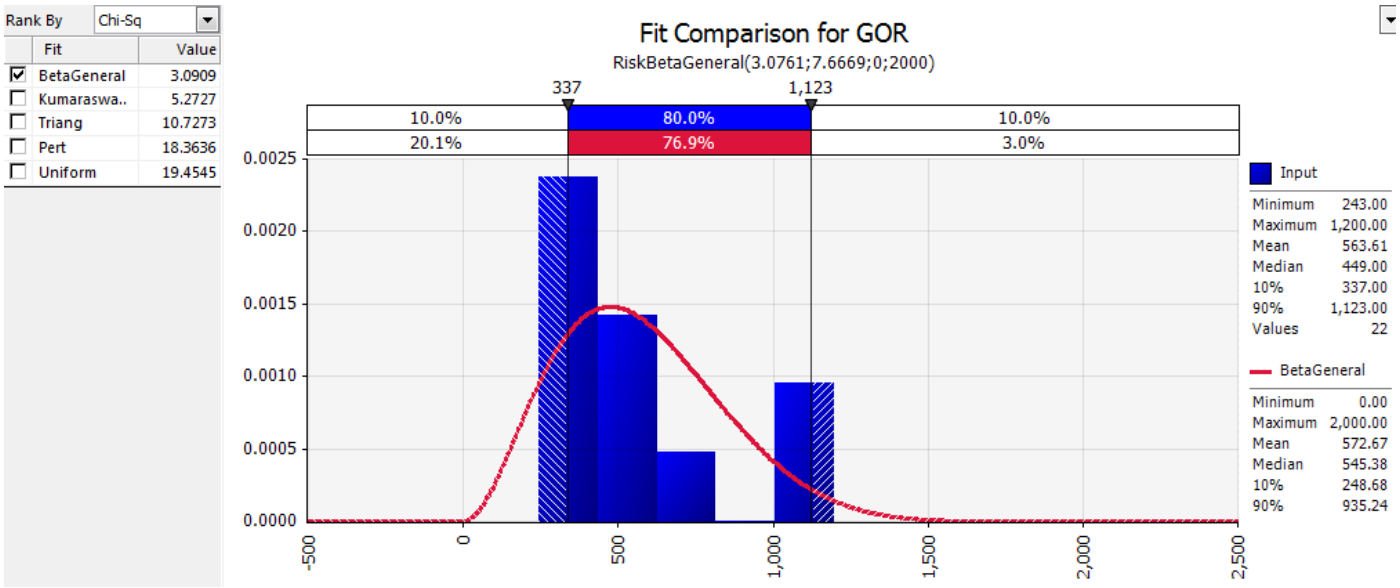

Fig. 19 – PDF for *GOR*

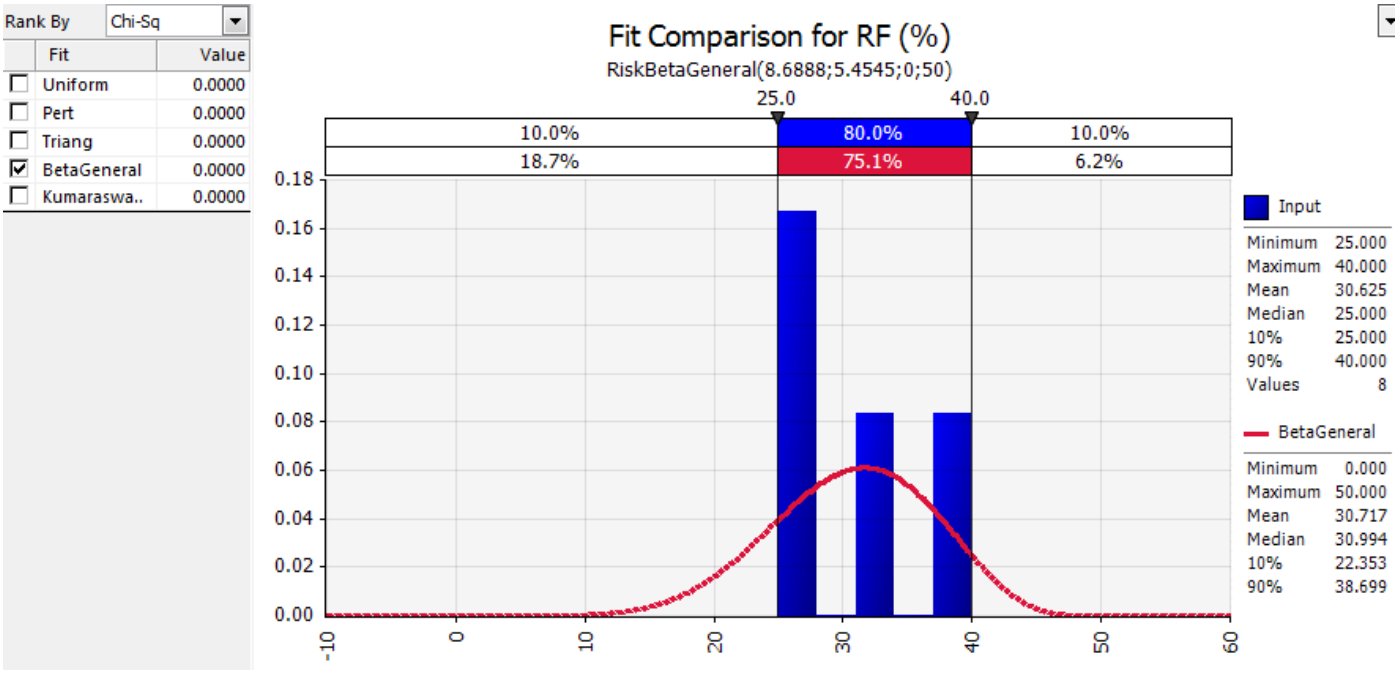

Fig. 20 – PDF for *RF*

This procedure leads to the following table **(Table 2),** which shows key values that are used for the evaluation of all the prospects studied in this project:

	Low Estimate	Best Estimate	High estimate
***N/G* (%)**	34.8	66.6	90.0
S_w (%)	10.3	23.4	41.6
***GOR* (scf/stb)**	248.7	545.4	935.2
***RF* (%)**	22.4	31.0	38.7

Table 2 – Key values for *N/G, Sw, GOR* and *RF*

5.5 – Formation volume factor

In order to define a realistic probability distribution function for the initial formation volume factor (B_{oi}) the following assumptions are made:

- T_{seabed} *is* obtained from the World Ocean Atlas 2013 (Locarnini et al. 2013) at the nearest available data point to each prospect.
- $\text{Geothermal Gradient} = 30\,°\text{C/km}$, which is the worldwide average temperature gradient.

Considering these two assumptions, the average reservoir temperature is estimated as:

$$T_r(°C) = T_{seabed} + 30\frac{°\text{C}}{\text{km}} * Sedimentary\ Overburden\ (\text{km})$$

- Oil gravity was assumed $30°\text{API} \Rightarrow \gamma_o = \frac{141.5}{121.5+30} \cong 0.93$

- Assuming $p_r > p_b$ and c_o negligible $\Rightarrow B_o = B_{ob} \Rightarrow$ applying Levitan and Murtha (1999) correlation for B_{ob}:

$$B_{ob} = 1 + 0.0005 * GOR * \left(\frac{\gamma_g}{\gamma_o}\right)^{0.25} + \frac{0.0004 * (T_r - 60)}{\gamma_o * \gamma_g} \cong B_o$$

Where T_r is reservoir temperature expressed in °F.

5.6 – Porosity

Several authors have analyzed the variation of rock porosity with burial depth (Ehrenberg and Nadeau 2005; Schmoker and Gautier 1988). With increasing burial depth, porosities tend to decrease due to the diagenetic processes that occurs (increase in pressure and temperature, amongst others). In order to create realistic porosity distributions the results from Ehrenberg and Nadeau (2005) for sandstones are considered as shown in **Fig. 21.**

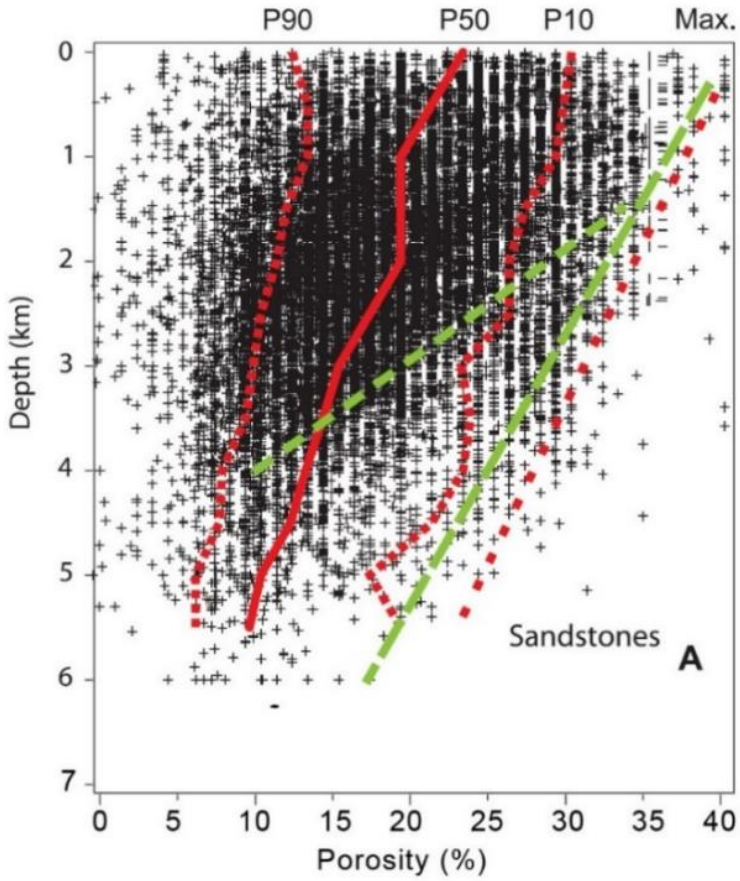

Fig. 21 – Variation of reservoir porosity with burial depth (Ehrenberg and Nadeau 2005)

Considering the P90, P50 and P10 average values, from the sandstones datasets they analyzed (Table 1 from their paper), the graph shown in **Fig. 22** is constructed.

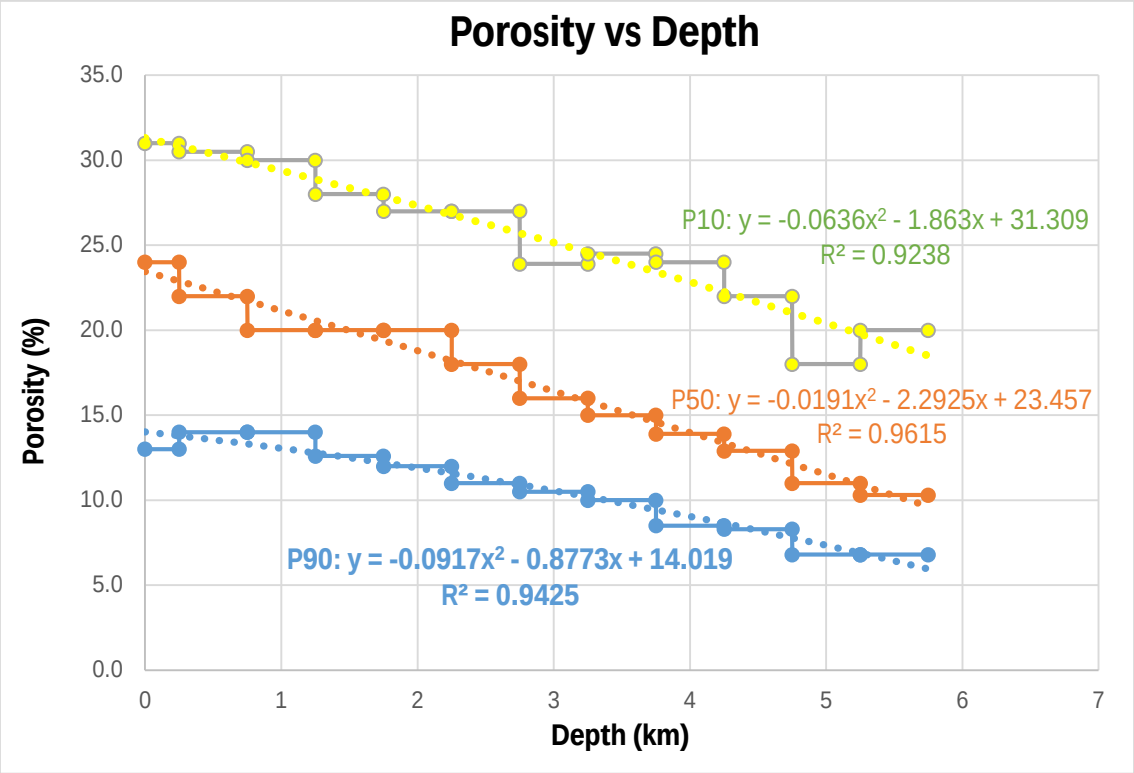

Fig. 22 – Porosity vs burial depth

Taking the second order polynomial approximation that best fits the points from the previous graph, it follows that:

$$\varphi_{P90} = -0.0917 \cdot x^2 - 0.8773 \cdot x + 14.019$$
$$\varphi_{P50} = -0.0191 \cdot x^2 - 2.2925 \cdot x + 23.457$$
$$\varphi_{P10} = -0.0636 \cdot x^2 - 1.863 \cdot x + 31.309$$

Where x is the sedimentary overburden in km.

The presented equations were validated against measured reservoir data from offshore Uruguay:

- The turbidite drilled by RAYA well has an average sedimentary overburden of approximately 2.210 km, therefore:

$$\varphi_{P90} = -0.0917 * (2.210)^2 - 0.8773 * (2.210) + 14.019 = 11.63\ \%$$
$$\varphi_{P50} = -0.0191 * (2.210)^2 - 2.2925 * (2.210) + 23.457 = 18.3\ \%$$
$$\varphi_{P10} = -0.0636 * (2.210)^2 - 1.863 * (2.210) + 31.309 = 26.88\ \%$$

  For this particular case, and considering that the drilled reservoir presented an average effective porosity ($PHIE$) equal to 24%, these equations leads to conservative results since the average porosity value is closer to the P10 percentile of the estimated porosity, however the average effective reservoir porosity does lie within the estimated porosity range.

- From the petrophysical analysis of GAVIOTIN well, and particularly for the intervals that present the gas effect on porosity (Fig. 15 and Fig. 16), the histogram of $PHIE$ shown in **Fig. 23** was created.

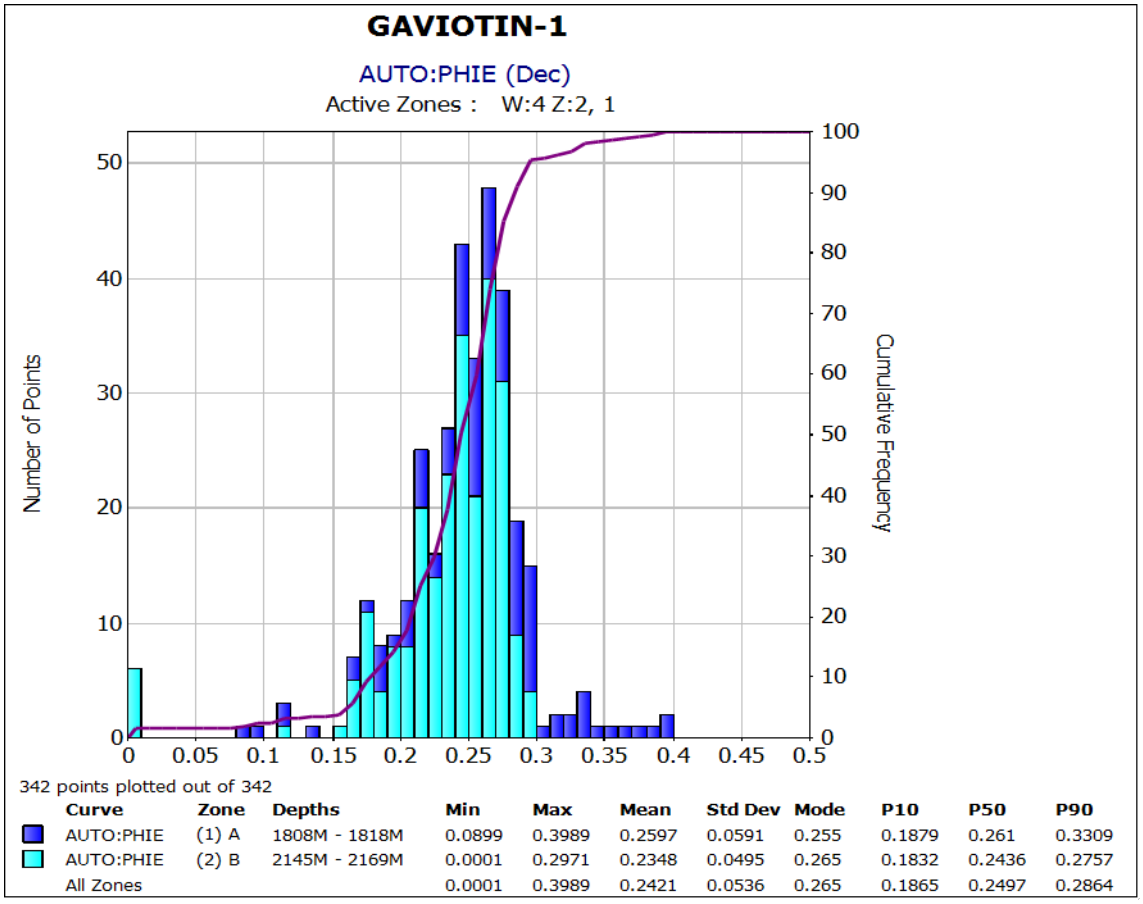

Curve	Zone	Depths	Min	Max	Mean	Std Dev	Mode	P10	P50	P90
AUTO:PHIE	(1) A	1808M - 1818M	0.0899	0.3989	0.2597	0.0591	0.255	0.1879	0.261	0.3309
AUTO:PHIE	(2) B	2145M - 2169M	0.0001	0.2971	0.2348	0.0495	0.265	0.1832	0.2436	0.2757
All Zones			0.0001	0.3989	0.2421	0.0536	0.265	0.1865	0.2497	0.2864

Fig. 23 – GAVIOTIN Effective Porosity histogram

In this well, the seabed is at 81.4 m, therefore the sedimentary overburden of the analyzed intervals are 1.727 km and 2.069 km.

In the first interval (zone A in Fig. 23) the estimated porosity range using the proposed correlation is:

$$\varphi_{P90} = -0.0917 * (1.727)^2 - 0.8773 * (1.727) + 14.019 = 12.23\ \%$$
$$\varphi_{P50} = -0.0191 * (1.727)^2 - 2.2925 * (1.727) + 23.457 = 19.44\ \%$$
$$\varphi_{P10} = -0.0636 * (1.727)^2 - 1.863 * (1.727) + 31.309 = 27.9\ \%$$

In the second interval (zone B in Fig. 23) the estimated porosity range using the proposed correlation is:

$$\varphi_{P90} = -0.0917 * (2.069)^2 - 0.8773 * (2.069) + 14.019 = 11.81\ \%$$
$$\varphi_{P50} = -0.0191 * (2.069)^2 - 2.2925 * (2.069) + 23.457 = 18.63\ \%$$
$$\varphi_{P10} = -0.0636 * (2.069)^2 - 1.863 * (2.069) + 31.309 = 27.18\ \%$$

In these two reservoir intervals of GAVIOTIN, the effective porosity range (presented at the legend of Fig. 23) mostly lies between the best estimate and the optimist values, therefore the presented equations can be used for the identified reservoirs in this well and they even cover more pessimistic scenarios.

6. Probabilistic Volumetric Analysis

In this section, the probabilistic volumetric analysis for the five potential turbidites is presented. The interpreted maximum extension of each prospect is shown, as a reference, in **Fig. 24.**

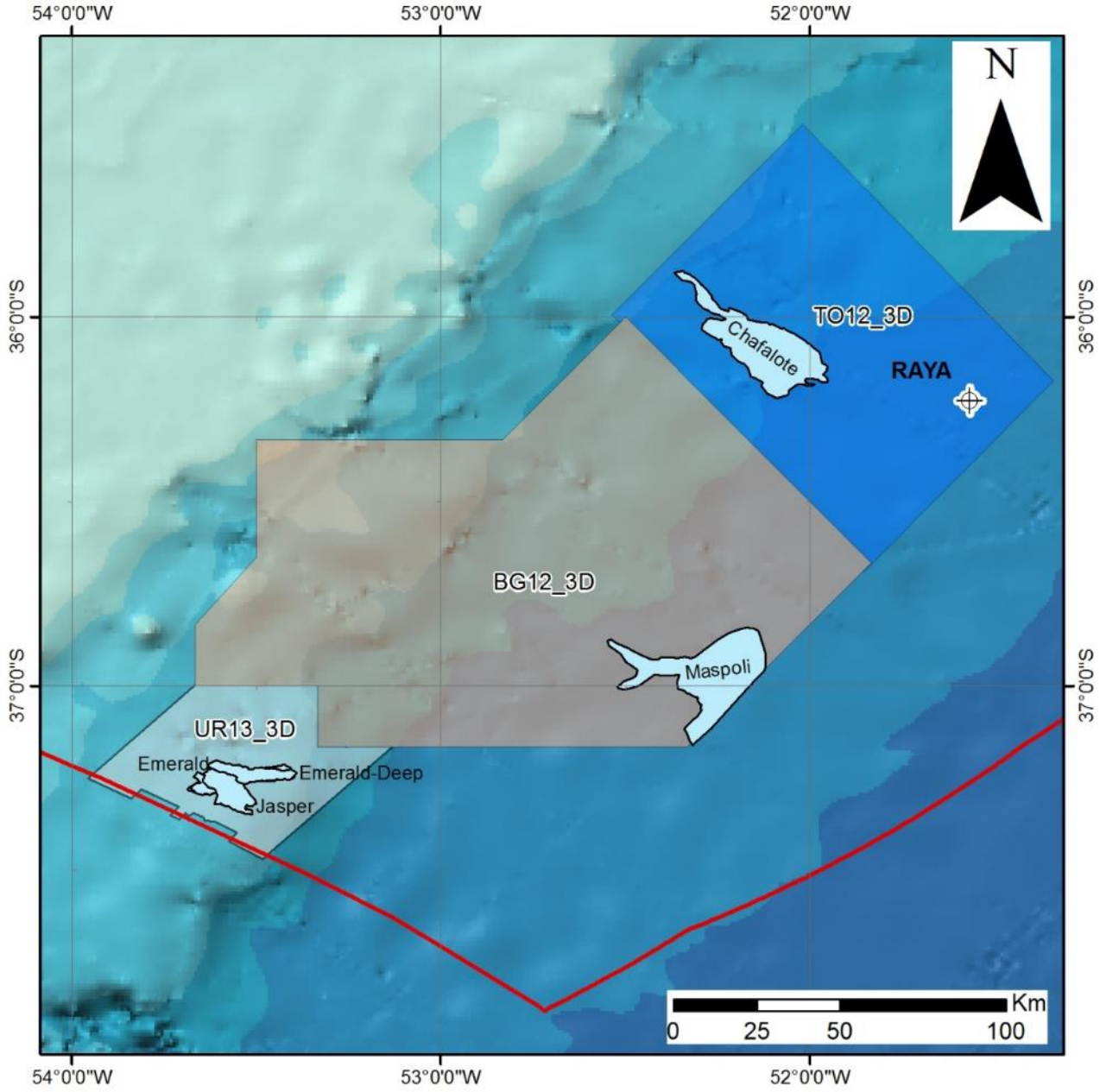

Fig. 24 – Location map of the analyzed potential turbidites

6.1 – Analysis of Prospect 1 - Chafalote

Prospect Name: Chafalote

Seismic Survey Used: TO12_3D

Source Rock: Marine Aptian shales

Reservoir: Upper Albian turbidites

Seal: Cenomanian-Turonian shales

Trap: Combined stratigraphic-structural trap with an updip sealing fault

Migration: through faults connecting the source rock with the reservoir

6.1.1 – Interpretation of 3D seismic data

For this prospect approximately 1,770 km^2 of a 7,200 km^2 Pre-Stack Depth Migrated (PSDM) 3D seismic survey (TO12_3D survey shown in Fig. 3) were interpreted.

The structural map at top of the prospect, overlaid with a polygon that depicts its interpreted maximum extension, is shown in **Fig. 25.**

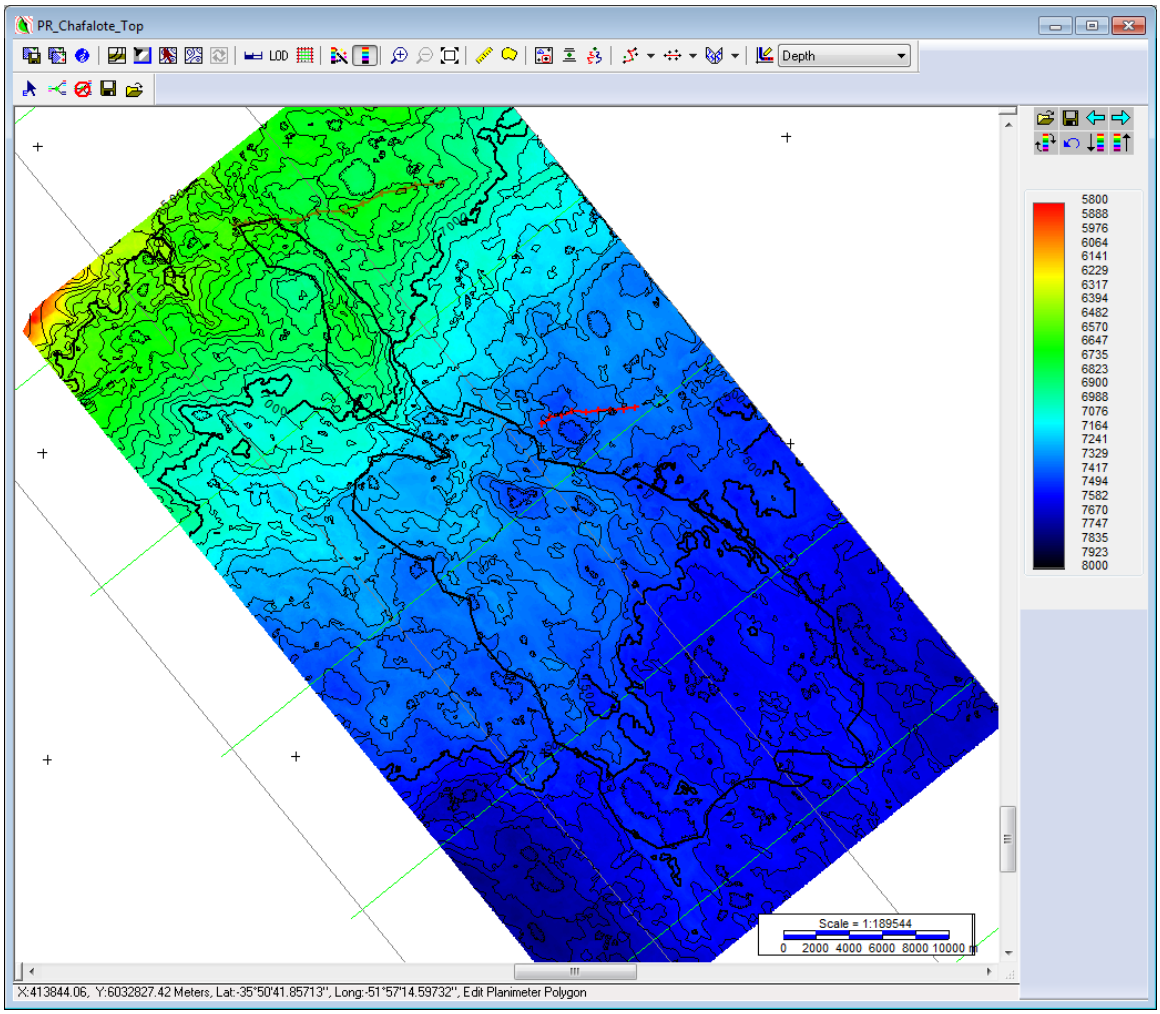

Fig. 25 – Structural map at the top of Chafalote

An arbitrary seismic line along Chafalote is shown in **Fig. 26.** The green horizon depicts the top of the prospect and the pink horizon its base.

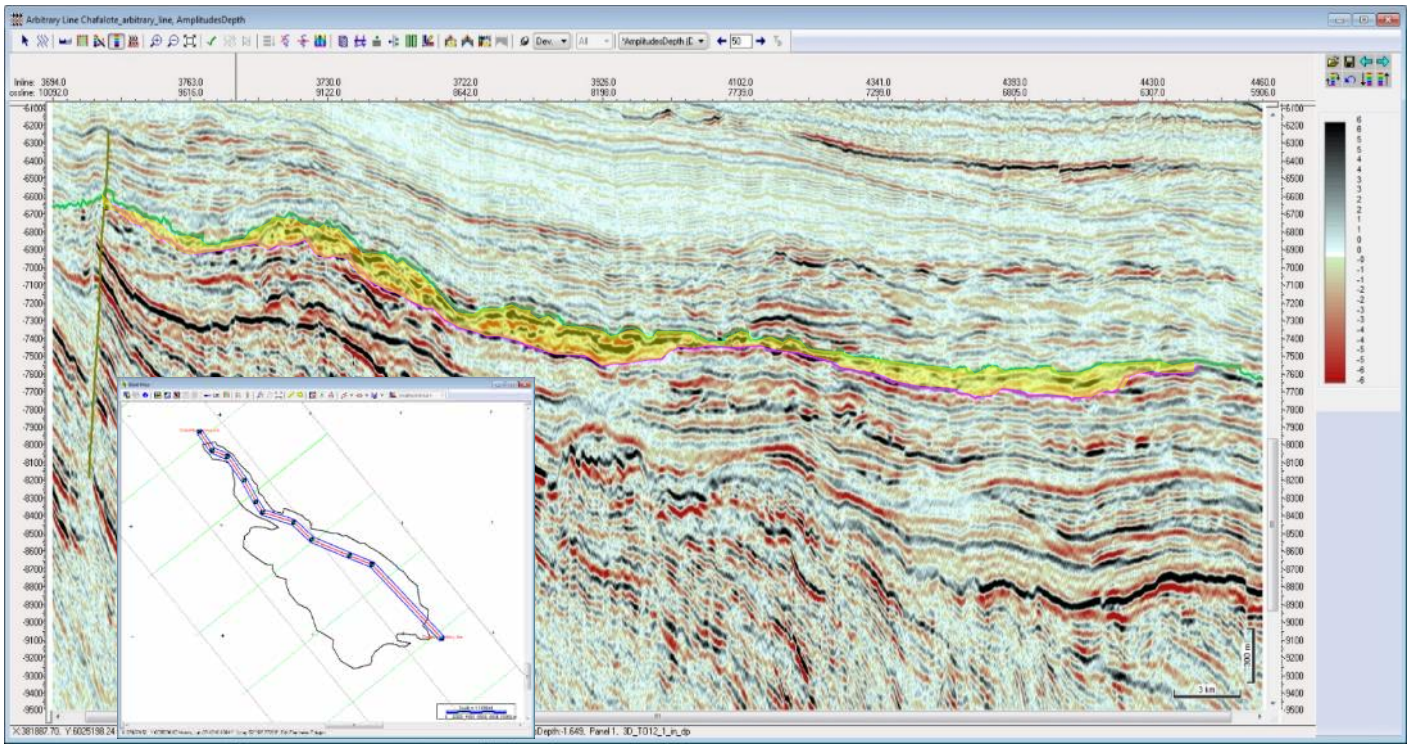

Fig. 26 – Arbitrary line along Chafalote (courtesy of ANCAP)

The lobular shape of Chafalote, seen in the perpendicular direction, is shown in **Fig. 27.**

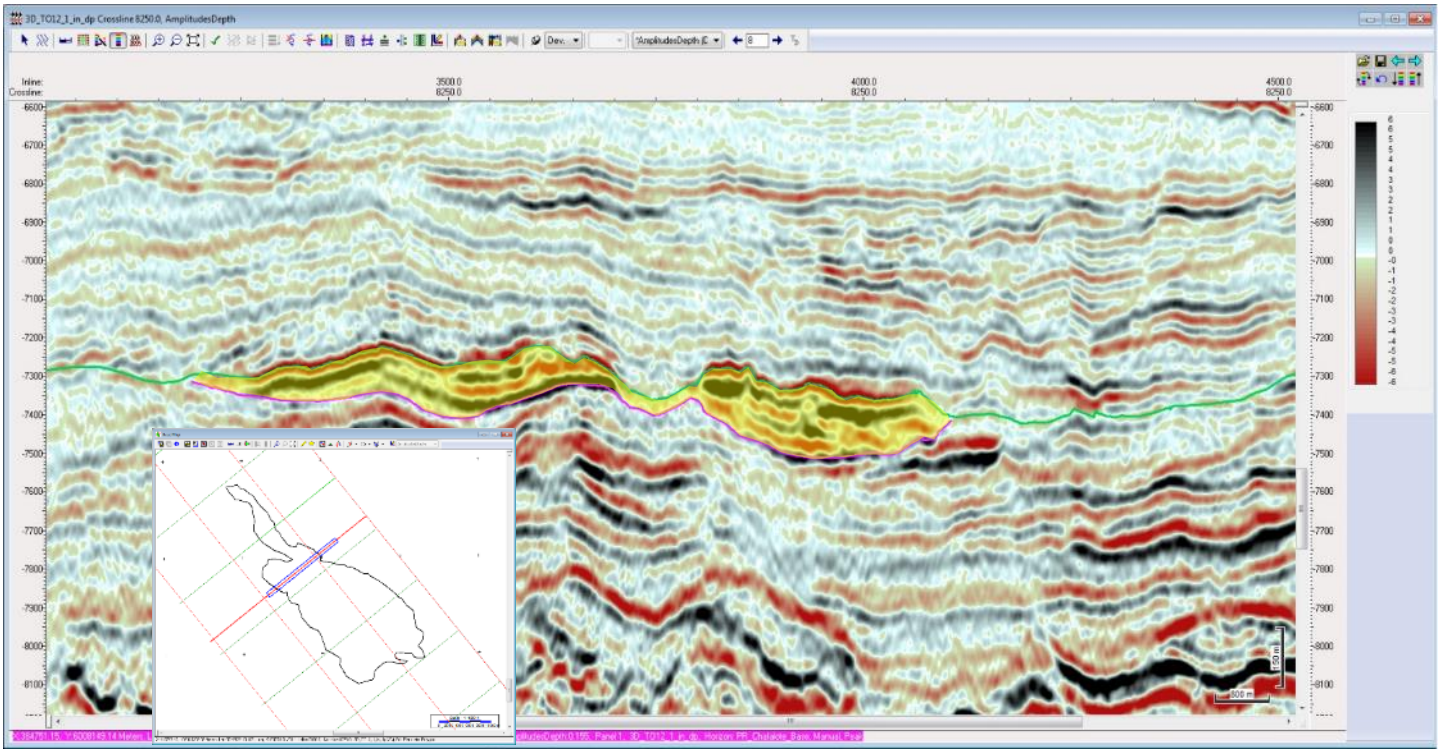

Fig. 27 – Crossline across Chafalote (courtesy of ANCAP)

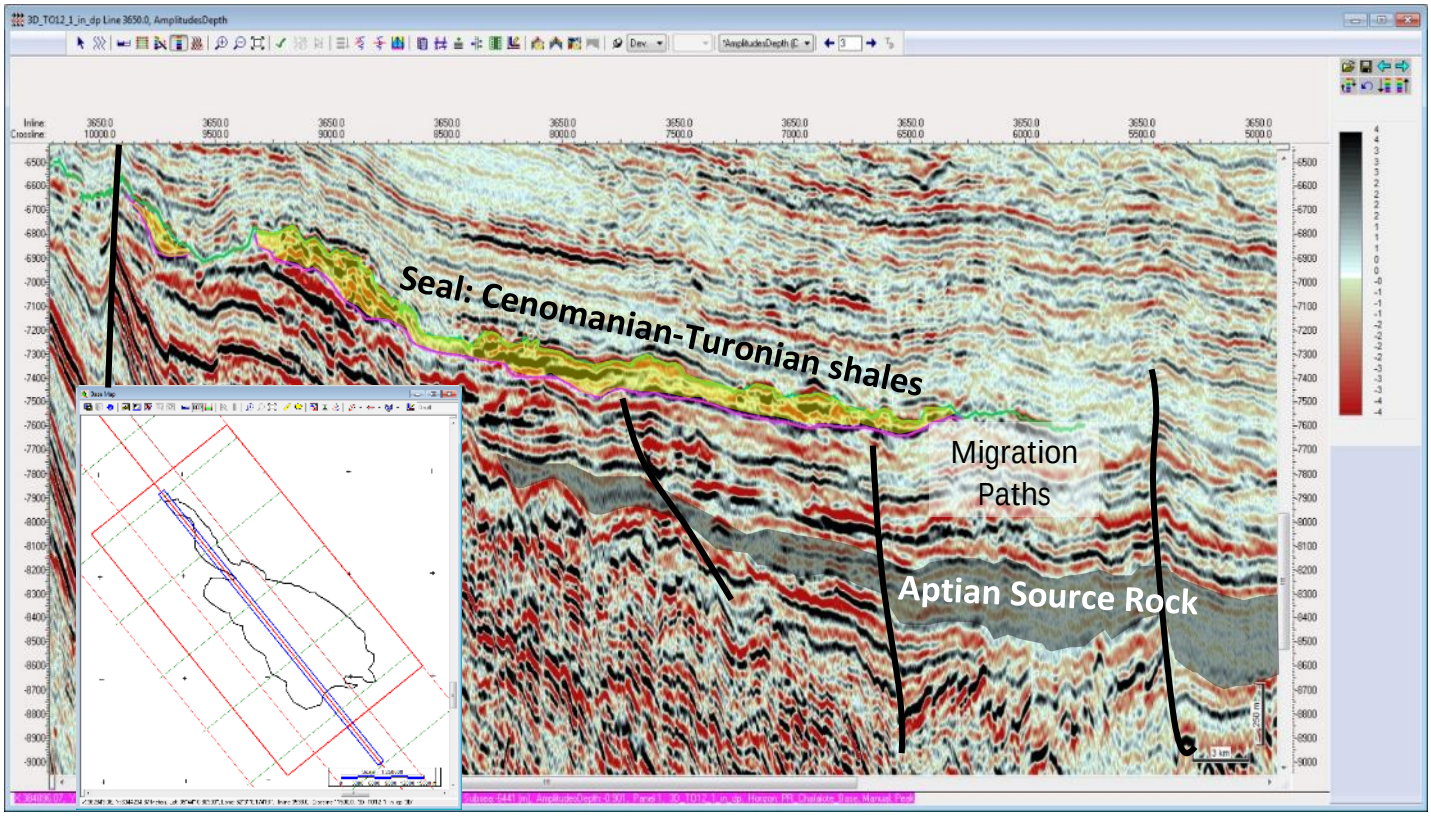

Fig. 28 – Inline along Chafalote with interpreted petroleum system elements (courtesy of ANCAP)

Fig. 29 shows the seismic amplitude map at the top of the prospect overlaid with the contours of the structural map from Fig. 25 and the defined delimitation polygon that accounts for its maximum extension.

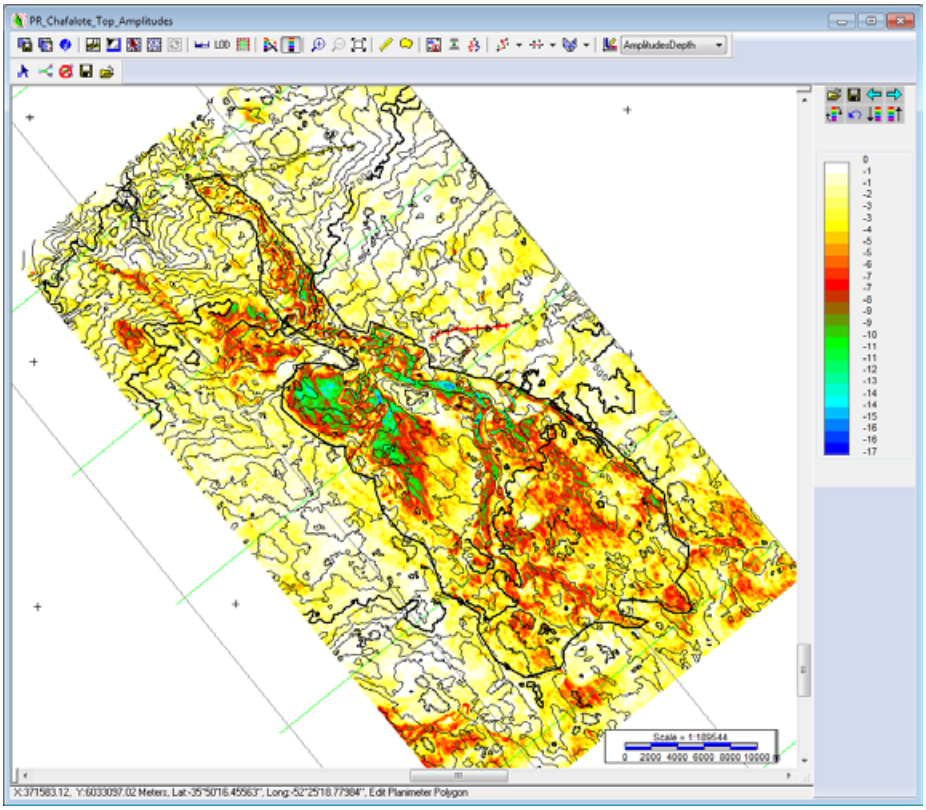

Fig. 29 – Amplitude map of Chafalote

Fig. 30 shows the seismic amplitude map at the top of the prospect with its defined P10 delimitation polygon.

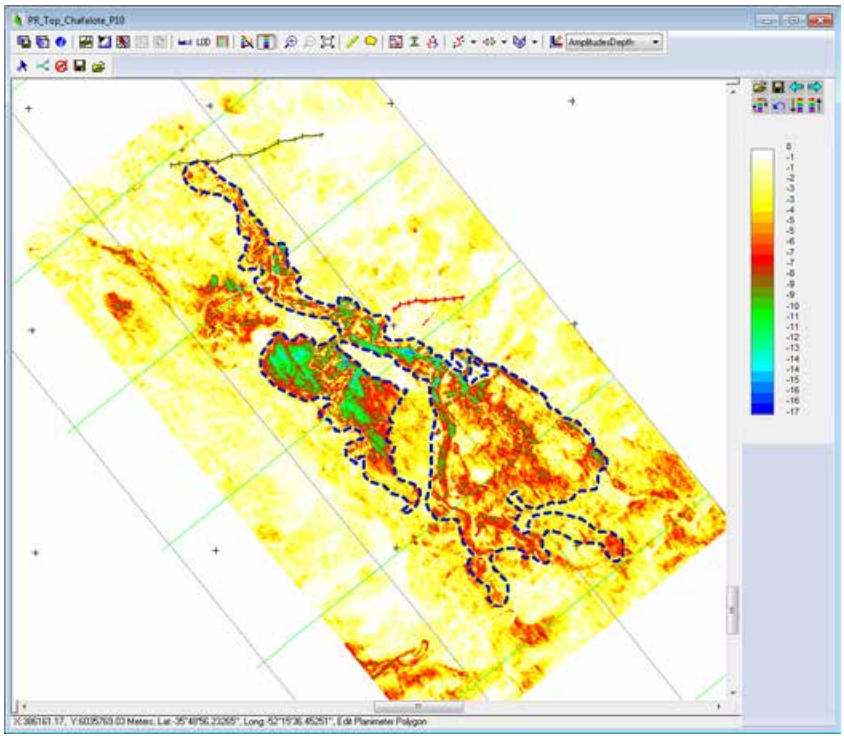

Fig. 30 – Amplitude map of Chafalote with P10 polygon overlaid

Finally, **Fig. 31** shows the seismic amplitude map at the top of the prospect, but with a delimitation polygon that accounts for its P90 extension:

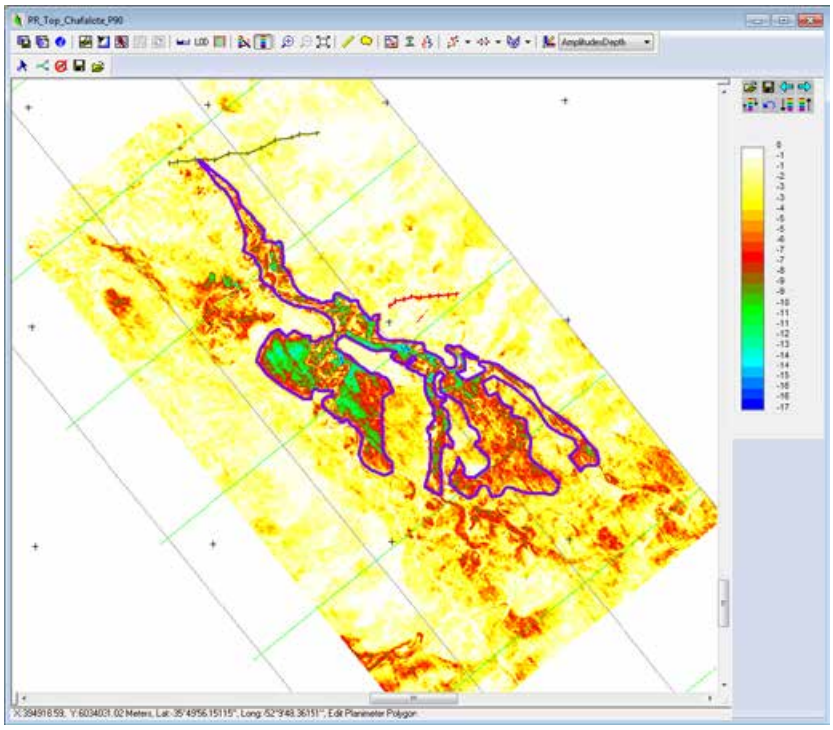

Fig. 31 – Amplitude map of Chafalote with P90 polygon overlaid

The delimitation polygons shown were used to restrict the volumetric calculation in order to get estimated values of a maximum (P01), an optimistic (P10) and a conservative (P90) GRV.

From the interpretation of the seabed in the seismic data, it follows that this potential turbidite lies between a minimum and a maximum water depth of 2,100 m and 3,050 m, respectively **(Fig. 32).**

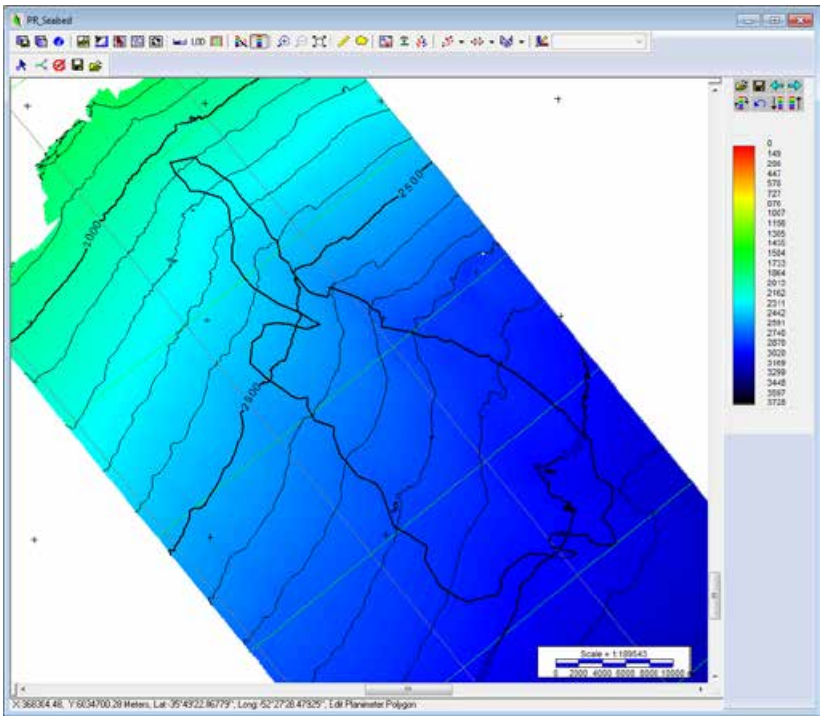

Fig. 32 – Seabed map at Chafalote area of study

The sedimentary overburden is determined by subtracting the seabed grid with the grid that corresponds to the top of the prospect. In this case, this results in an overburden between 4,351 m to 4,827 m **(Fig. 33),** therefore, an average sedimentary overburden of 4587.5 m was assumed for reservoir and oil properties estimation (porosity and B_{oi}).

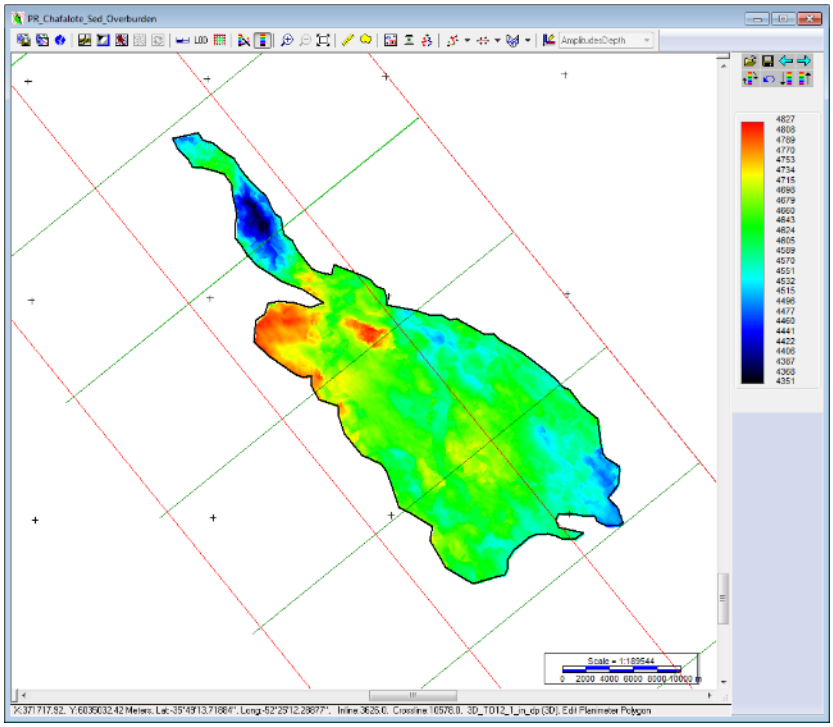

Fig. 33 – Sedimentary overburden map at Chafalote

6.1.2 – Estimation of Oil Formation Volume Factor

In order to define a realistic probability distribution for the initial oil formation volume factor (B_{oi}) the following assumptions were made:

- $T_{seabed} = 2.53\ ℃$, this temperature is obtained from the World Ocean Atlas (2013) at a point with coordinates: 52.12W, 36.13S.

- Geothermal Gradient = $30\ ℃/\text{km}$, which is the worldwide average temperature gradient.

Considering these two assumptions, the estimated average reservoir temperature is:

$$T_r = T_{seabed} + 30\frac{℃}{\text{km}} * 4.5875\ \text{km} = 140.2\ ℃ = 284.36\ °\text{F}$$

- Oil gravity was assumed 30°API ⇒ $\gamma_o = \frac{141.5}{121.5+30} \cong 0.93$

- Assuming $p_r > p_b$ and c_o negligible ⇒ $B_o \cong B_{ob}$ ⇒ applying Levitan and Murtha (1999) correlation for B_{ob}:

$$B_{oi} \cong B_{ob} = 1 + 0.0005 * GOR * \left(\frac{\gamma_g}{\gamma_o}\right)^{0.25} + \frac{0.0004 * (T_r - 60)}{\gamma_o * \gamma_g}$$

Where T_r is reservoir temperature in °F.

For the case GOR=0 scf/STB then:

$$B_{oi} \cong 1 + 0.0005 * 0 * \left(\frac{0.8}{0.93}\right)^{0.25} + \frac{0.0004 * (284.36 - 60)}{0.93 * 0.8} = 1.12\ \text{RB/STB}$$

Finally, applying the same equation for the rest of the cases (see Table 2 for GOR values):

- GOR=248.7 scf/STB ⇒ $B_{oi} \cong 1.24\ \text{RB/STB}$
- GOR=545.4 scf/STB ⇒ $B_{oi} \cong 1.38\ \text{RB/STB}$
- GOR=935.2 scf/STB ⇒ $B_{oi} \cong 1.57\ \text{RB/STB}$
- GOR=2,000 scf/STB ⇒ $B_{oi} \cong 2.08\ \text{RB/STB}$

These values are used to define Chafalote PDF for oil formation volume factor.

6.1.3 – Estimation of Porosity

For the case of Chafalote, which is approximately beneath 4.5875 km of sediments, the porosity values obtained through the equations derived from Ehrenberg and Nadeau (2005) analysis give the following results:

$$\varphi_{P90} = -0.0917 * (4.5875)^2 - 0.8773 * (4.5875) + 14.019 = 7.9\%$$

$$\varphi_{P50} = -0.0191 * (4.5875)^2 - 2.2925 * (4.5875) + 23.457 = 12.5\%$$

$$\varphi_{P10} = -0.0636 * (4.5875)^2 - 1.863 * (4.5875) + 31.309 = 21.9\ \%$$

These values are used to define Chafalote PDF for porosity.

6.1.4 – Computation of Gross Rock Volume

The GRV reports created by IHS Kingdom, using the surfaces interpreted for the top and base of Chafalote and the three different restriction polygons, are as follows:

- Maximum Case:

```
Volumetric Model:          Single Structure
Grid:      PR_Chafalote_Top
Polygons Used:   PR_Chafalote_P01
Lower Contact:   PR_Chafalote_Base

Polygon PR_Chafalote_P01
-------------------------------------------------
Polygon Area:     453.7202    10^6 M2
Polygon Area within the Grid(s):     449.2216    10^6 M2
Gross Volume:     39,353.6395    10^6 M3
```

- Optimistic Case:

```
Volumetric Model:          Single Structure
Grid:      PR_Chafalote_Top
Polygons Used:   PR_Chafalote_P10
Lower Contact:   PR_Chafalote_Base

Polygon PR_Chafalote_P10
-------------------------------------------------
Polygon Area:     310.8917    10^6 M2
Polygon Area within the Grid(s):     310.6296    10^6 M2
Gross Volume:     28,809.0334    10^6 M3
```

- Conservative Case

```
Volumetric Model:          Single Structure
Grid:      PR_Chafalote_Top
Polygons Used:   PR_Chafalote_P90
Lower Contact:   PR_Chafalote_Base

Polygon PR_Chafalote_P90
-------------------------------------------------
Polygon Area:     178.2285    10^6 M2
Polygon Area within the Grid(s):     178.1721    10^6 M2
Gross Volume:     17,798.0803    10^6 M3
```

This variable, GRV, is defined as a LogNormal distribution, therefore three parameters are required in @Risk for its definition: P10, P50 and P90 values. The P50 value is calculated, as a function of the P10 and P90 values using the formula: $\mathrm{P50} = \mathrm{e}^{(\mathrm{LN(P90)+LN(P10)})/2}$ (Wright 2015).

For the case of Chafalote, this results in a P50 value for *GRV* = 22,643,884,159 m^3.

6.1.5 – Inputs used for the probabilistic analysis of Chafalote

A summary of the inputs used for the probabilistic volumetric analysis of Chafalote, based on the previous results, is shown in **Table 3.**

Parameter	MIN	Low Estimate	Best Estimate	High Estimate	MAX	Distr. Type
GRV (m^3)	0	17,798,080,300	22,643,884,159	28,809,033,400	39,353,639,500	LogNormal
N/G (%)	0	34.8%	66.6%	90%	100%	Beta
Phi (%)	0	7.9%	12.5%	21.9%	48%	Beta
S_w (%)	0	10.3%	23.4%	41.6%	100%	Beta
GOR (scf/STB)	0	248.7	545.4	935.2	2,000	Beta
B_{oi} (RB/STB)	1.12	1.24	1.38	1.57	2.08	Beta
RF (%)	0	22.4%	31%	38.7%	50%	Beta

Table 3 – Reservoir and fluid properties used for the volumetric analysis of Chafalote

The following figures (**Fig. 34** to **Fig. 40**) show the detail of the input distributions defined in @Risk and its simulation results:

- Gross Rock Volume:

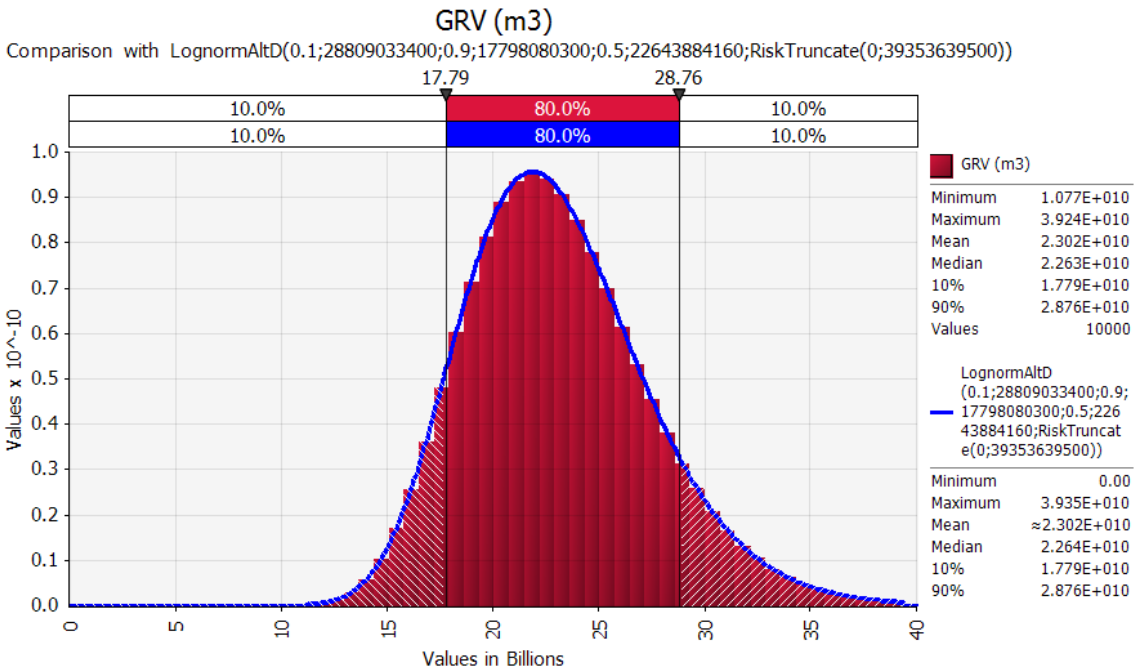

Fig. 34 – *GRV* distribution of Chafalote

- Net to Gross:

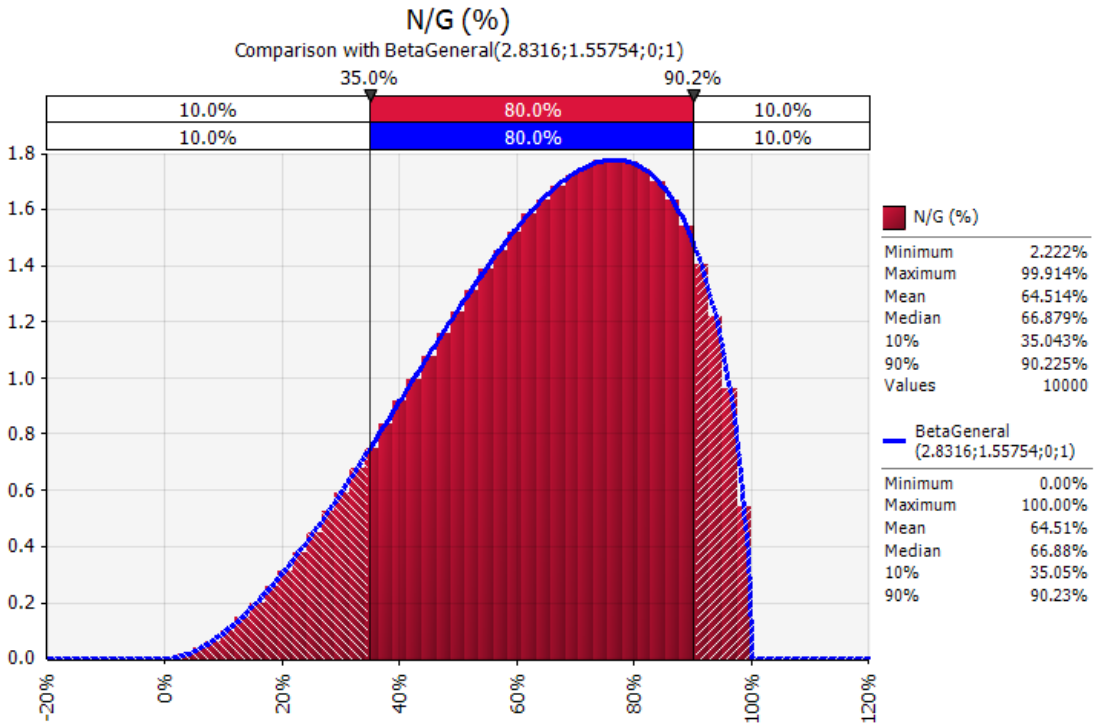

Fig. 35 – *N/G* distribution at Chafalote

- Porosity:

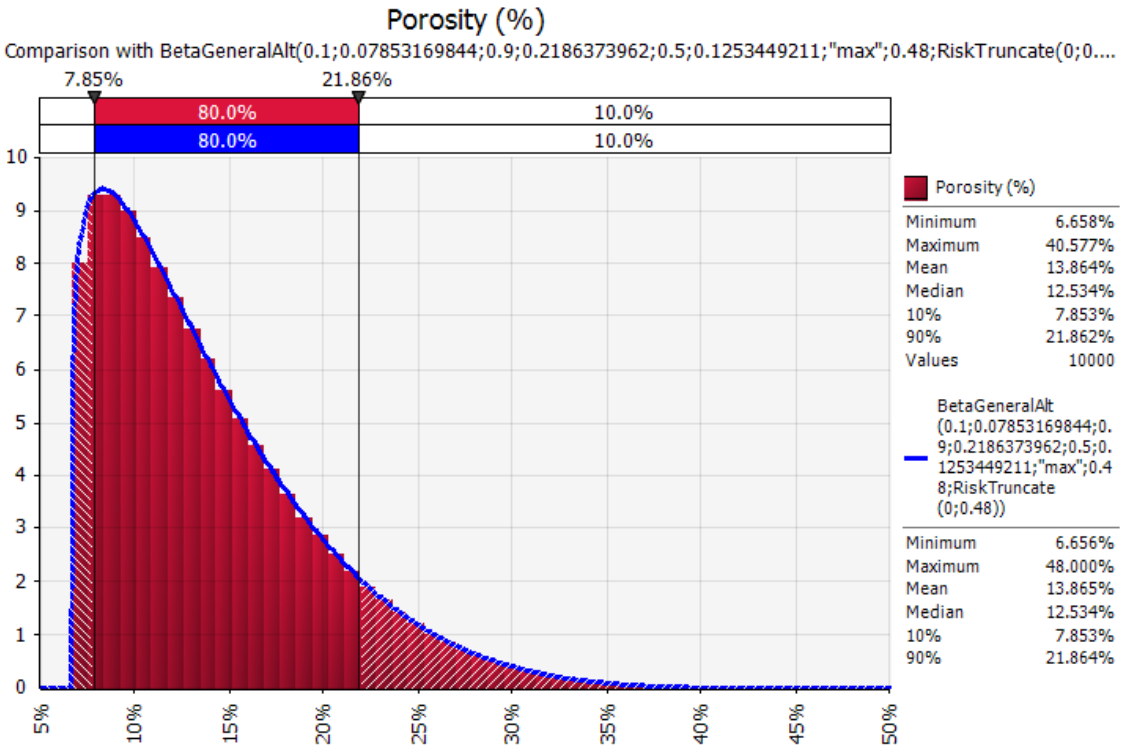

Fig. 36 – Porosity distribution at Chafalote

- Water Saturation:

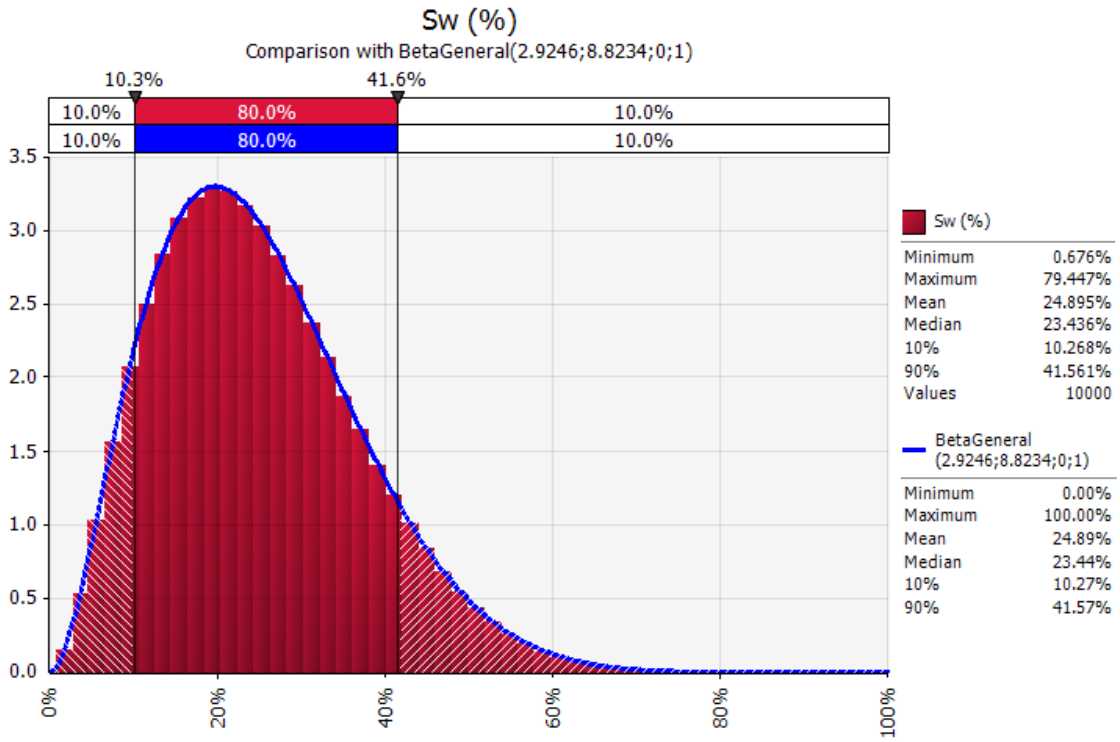

Fig. 37 – *Sw* distribution at Chafalote

- Gas/Oil Ratio:

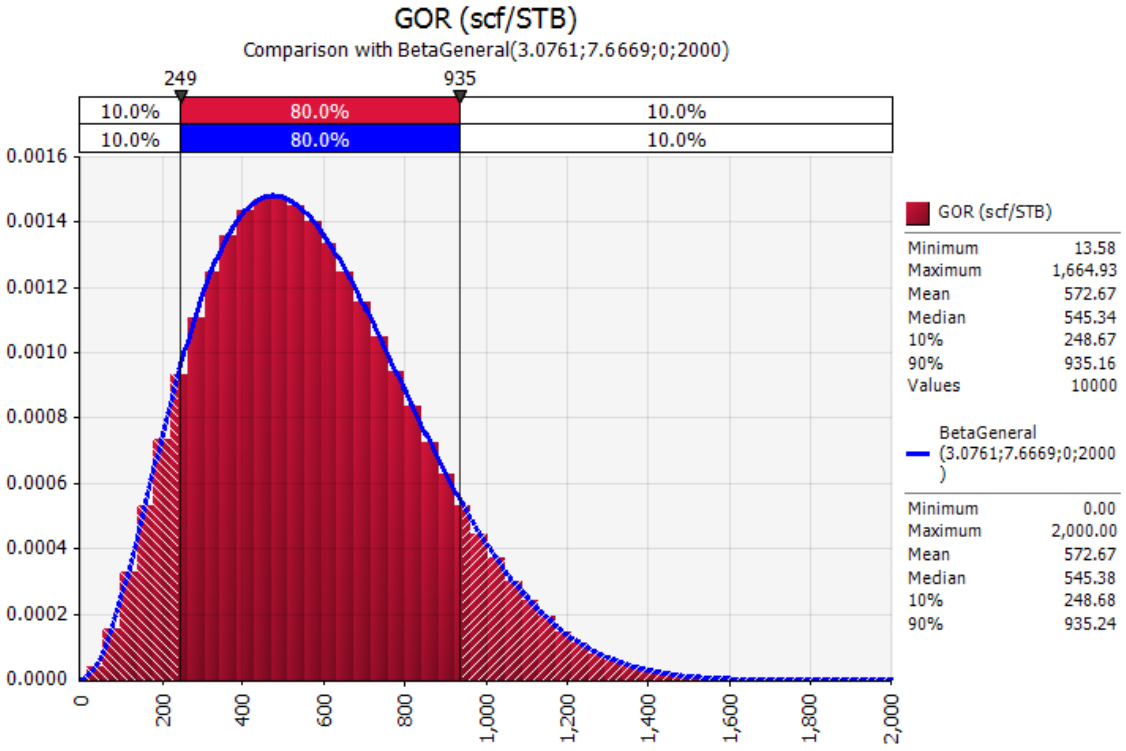

Fig. 38 – *GOR* distribution at Chafalote

- Initial formation volume factor:

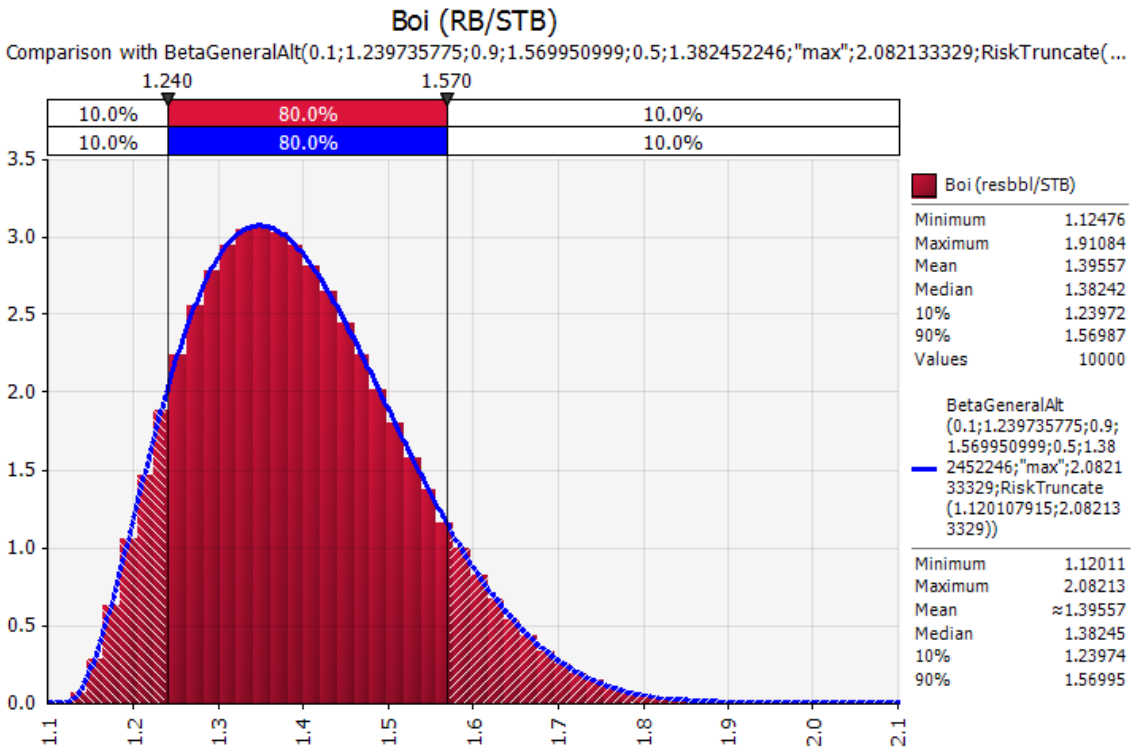

Fig. 39 – *Boi* distribution at Chafalote

- Recovery Factor:

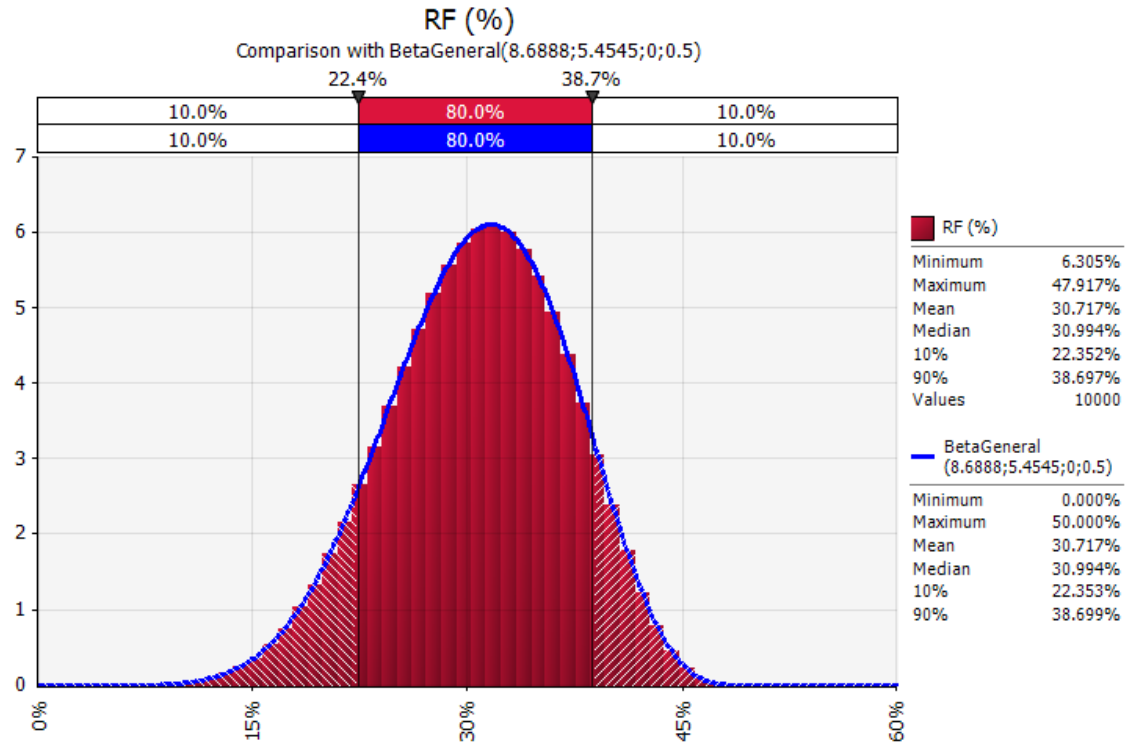

Fig. 40 – *RF* distribution at Chafalote

6.1.6 – Results of the probabilistic analysis for Chafalote

After all the inputs were set, and the output defined as the oil EUR then an @Risk simulation of 10,000 iterations was run using Latin Hypercube sampling. **Fig. 41** and **Fig. 42** show the resulting EUR distribution graphs for oil and associated gas, respectively:

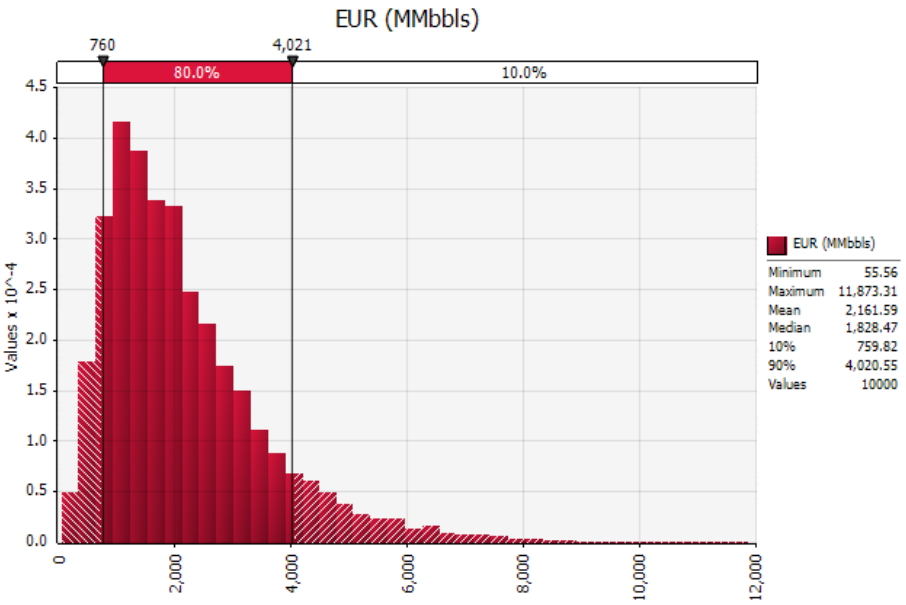

Fig. 41 – Chafalote Oil EUR

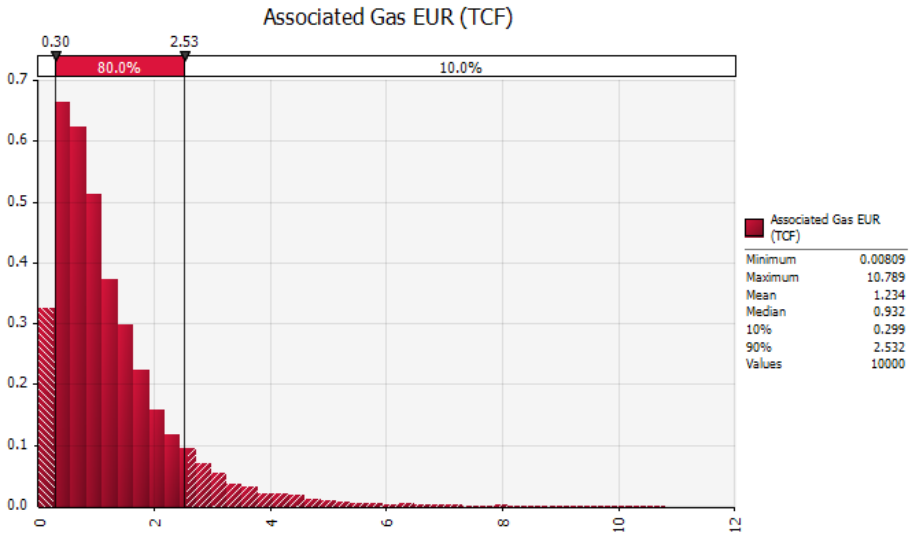

Fig. 42 – Chafalote Associated Gas EUR

According to the Petroleum Resources Management System (SPE 2007), for this study case, the calculated resources can be classified as "Prospective Resources" and categorized as follows:

	Oil	Associated Gas
Low estimate Prospective Resources:	759.821 MMbbls	0.299 TCF
Best estimate Prospective Resources:	1,828.472 MMbbls	0.932 TCF
High estimate Prospective Resources:	4,020.547 MMbbls	2.532 TCF

Table 4 – Estimation of Chafalote Prospective Resources

Sensibility Analysis

A tornado chart with the relative influence of the main variables on the oil EUR for this prospect is shown in **Fig. 43.**

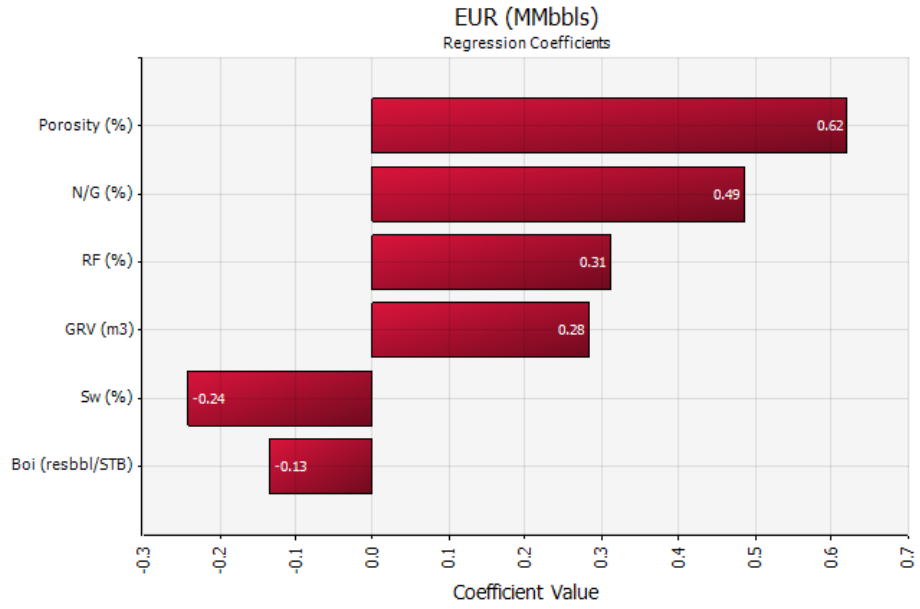

Fig. 43 – Tornado chart for Chafalote Oil EUR

Fig. 44 shows a tornado chart with the relative influence of the main variables on the associated gas EUR for this prospect.

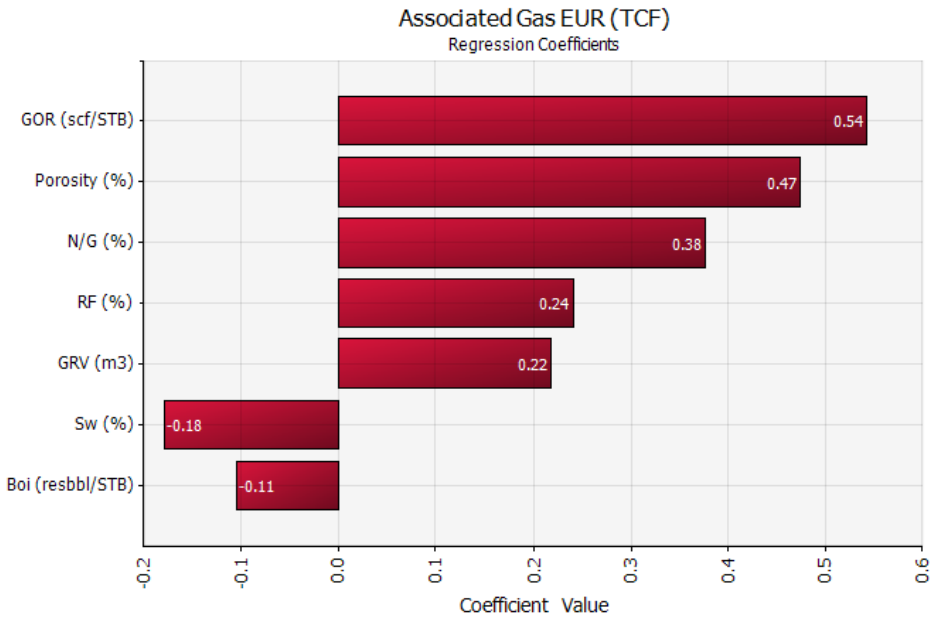

Fig. 44 – Tornado chart for Chafalote Associated Gas EUR

From these tornado charts, it can be concluded that porosity and N/G are the parameters which oil EUR is most sensible to. On the other hand, for associated gas EUR, GOR is the most sensible parameter.
With the presented methodology for GRV calculation, and particularly for this prospect, the uncertainty in this variable is reduced, therefore GRV it is not the input that has the greatest influence on the EUR calculation.

6.2 – Analysis of Prospect 2 - Maspoli

Prospect Name: Maspoli

Seismic Survey Used: BG12_3D

Potential Source Rocks: Marine Aptian shales

Reservoir: Oligocene turbidites

Seal: Regional Miocene shales

Trap: Stratigraphic, with updip reservoir pinch out into feeder canyons

Migration: through faults connecting the source rock with the reservoir

6.2.1 – Interpretation of 3D seismic data

For this prospect approximately 1,967 km^2 of a 13,235 km^2 PSDM 3D seismic survey (BG12_3D survey shown in Fig. 3) were interpreted.

The structural map at top of the prospect, overlaid with a polygon that depicts its interpreted maximum extension, is shown in **Fig. 45.**

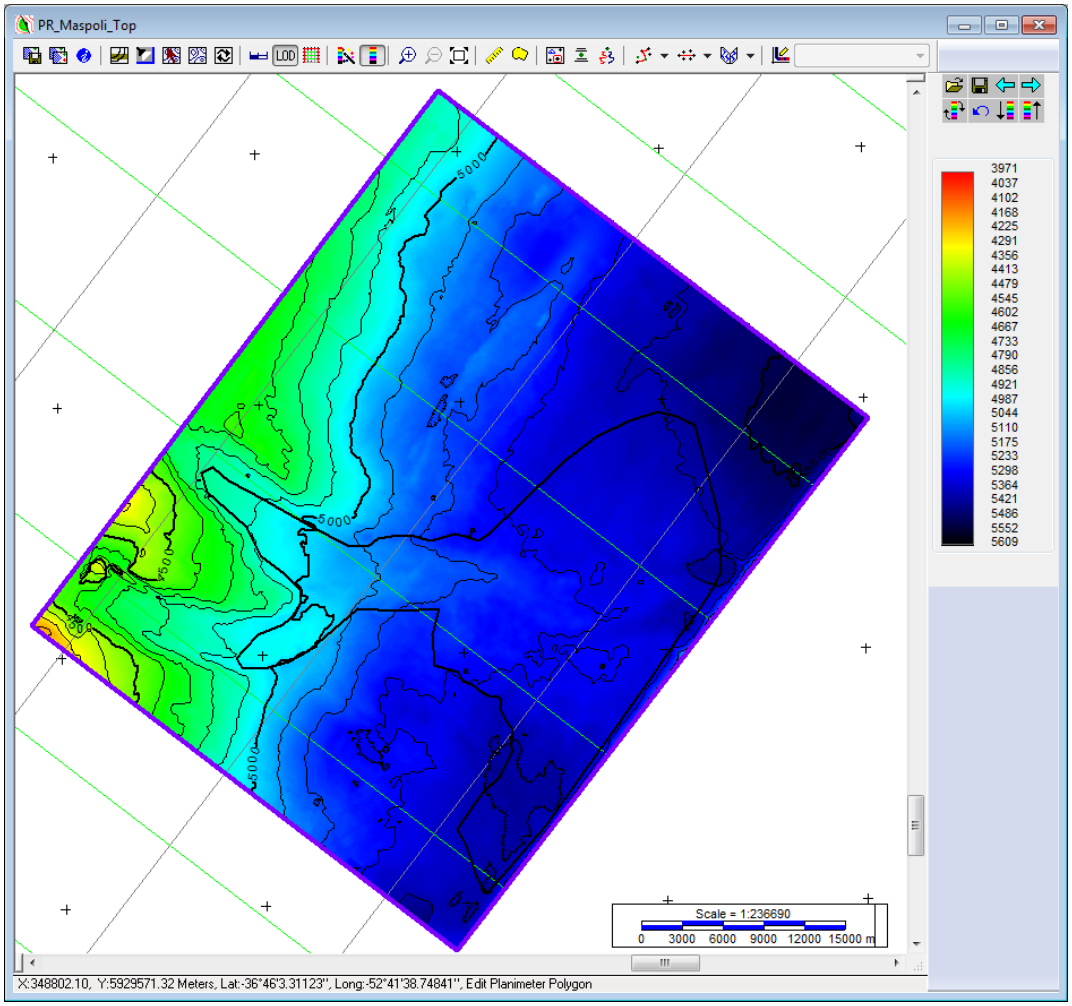

Fig. 45 – Structural map at the top of Maspoli

An arbitrary seismic line through Maspoli is shown in **Fig. 46.** The green horizon depicts the top of the prospect and the pink horizon its base.

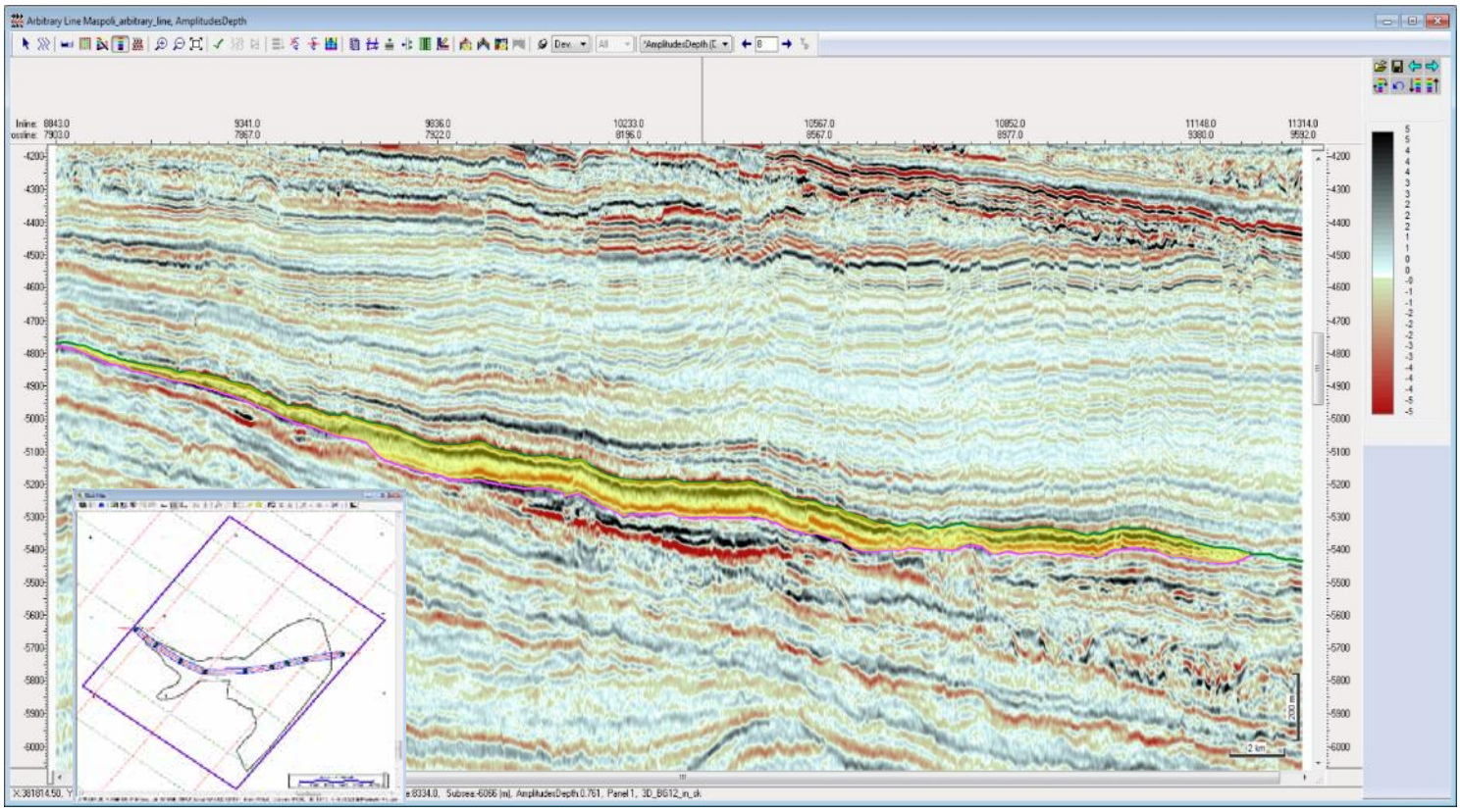

Fig. 46 – Arbitrary line along Maspoli (courtesy of ANCAP)

The lobular shape of Maspoli, seen in the perpendicular direction, is shown in **Fig. 47.**

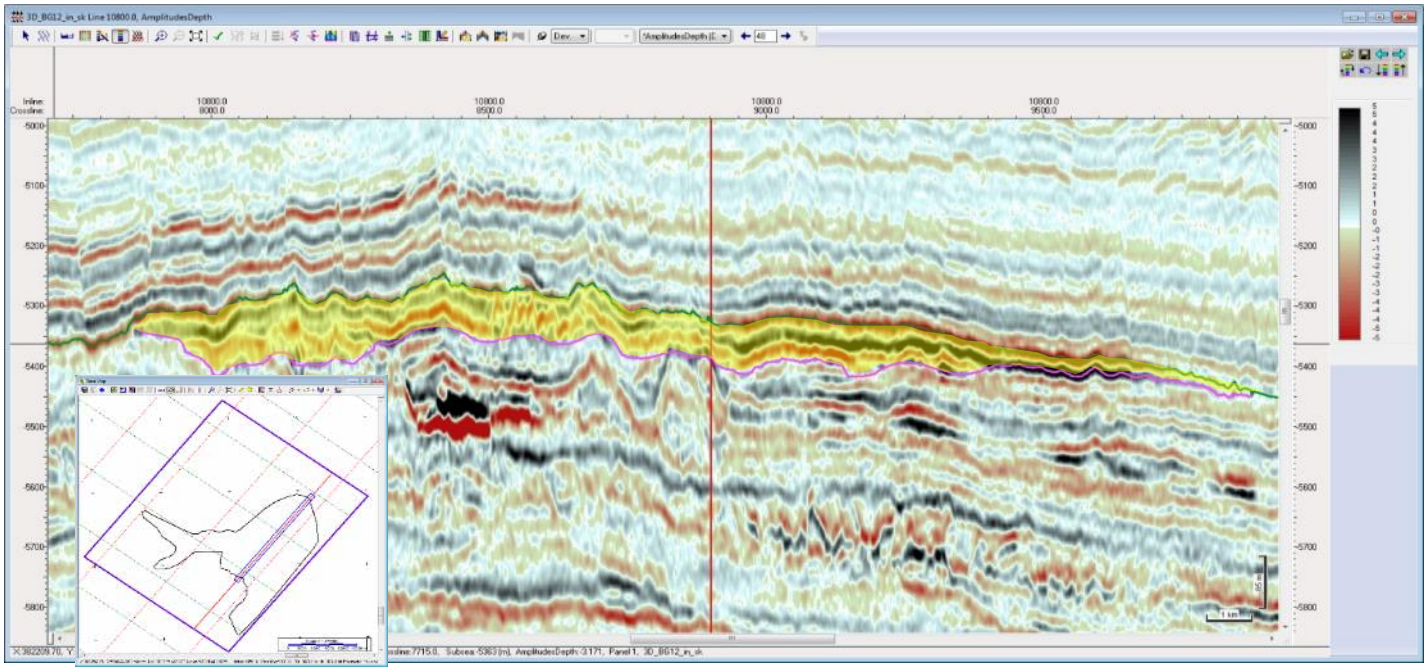

Fig. 47 – Inline across Maspoli (courtesy of ANCAP)

Fig. 48 shows the different elements of the proposed petroleum system for the case of Maspoli.

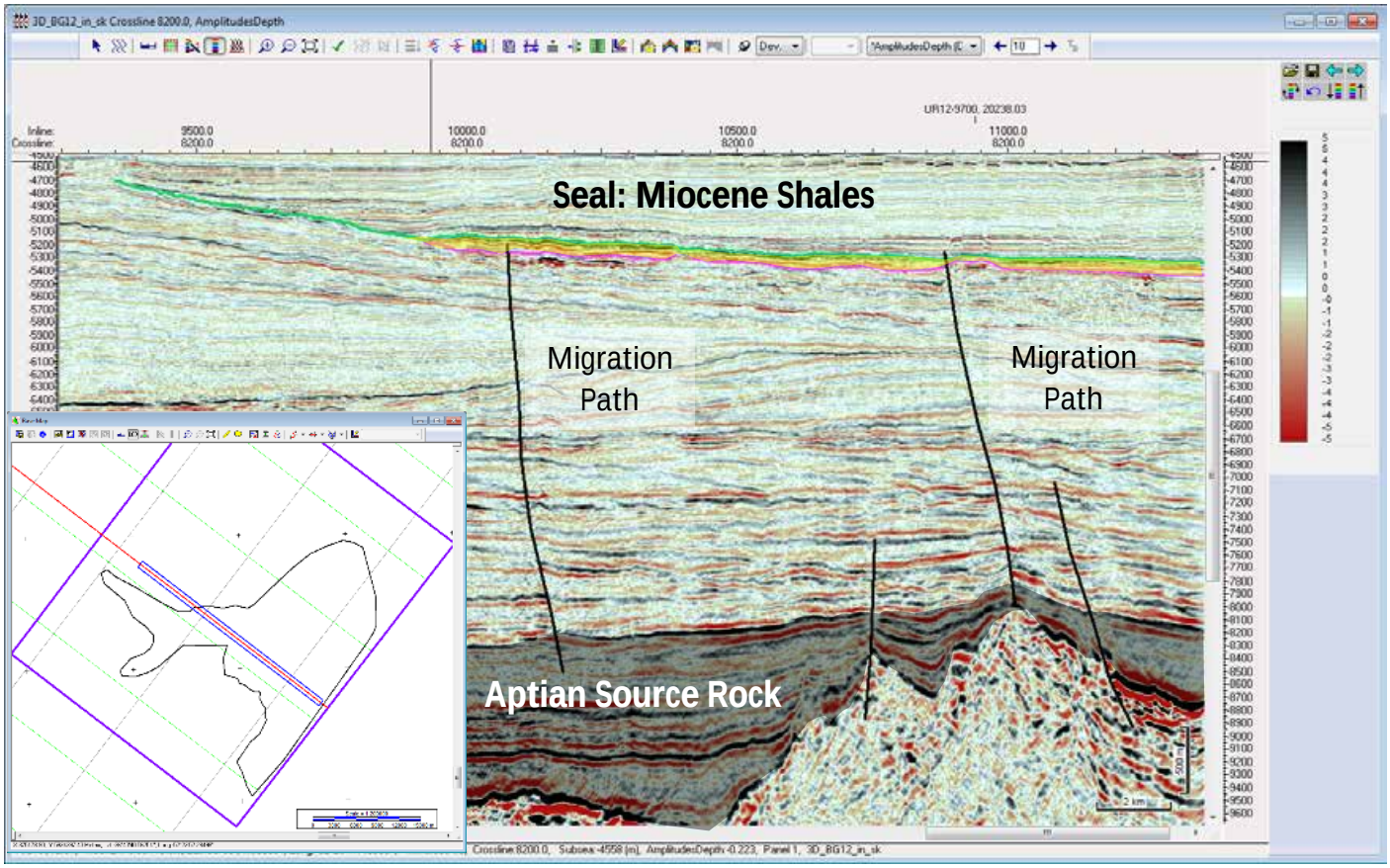

Fig. 48 – Crossline along Maspoli with interpreted petroleum system elements (courtesy of ANCAP)

Fig. 49 shows the seismic amplitude map at the top of the prospect, overlaid with, the contours of the structural map from Fig. 45 and the defined delimitation polygon that accounts for its maximum extension.

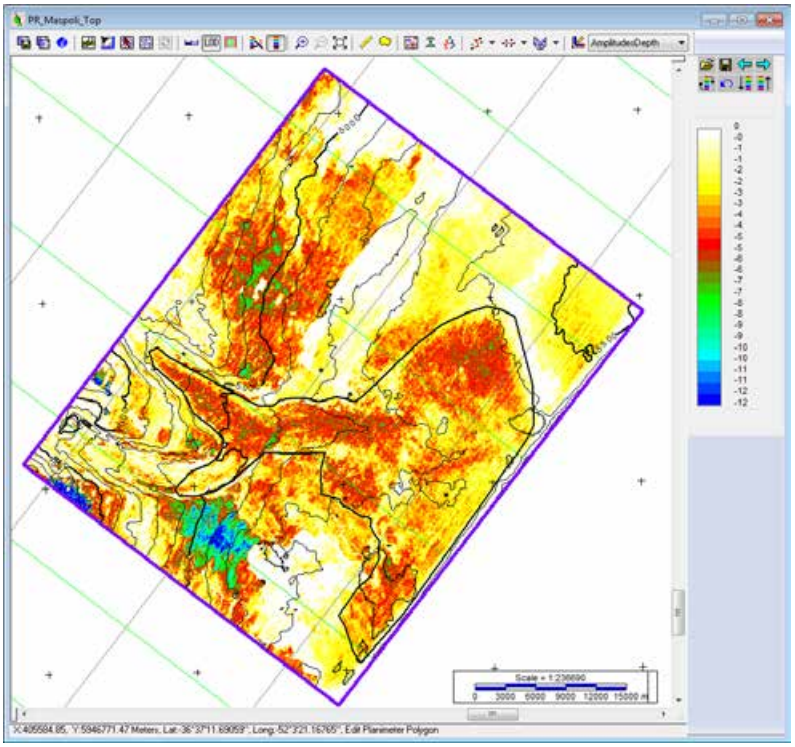

Fig. 49 – Amplitude map of Maspoli

Fig. 50 shows the seismic amplitude map at the top of the prospect with its defined P10 delimitation polygon.

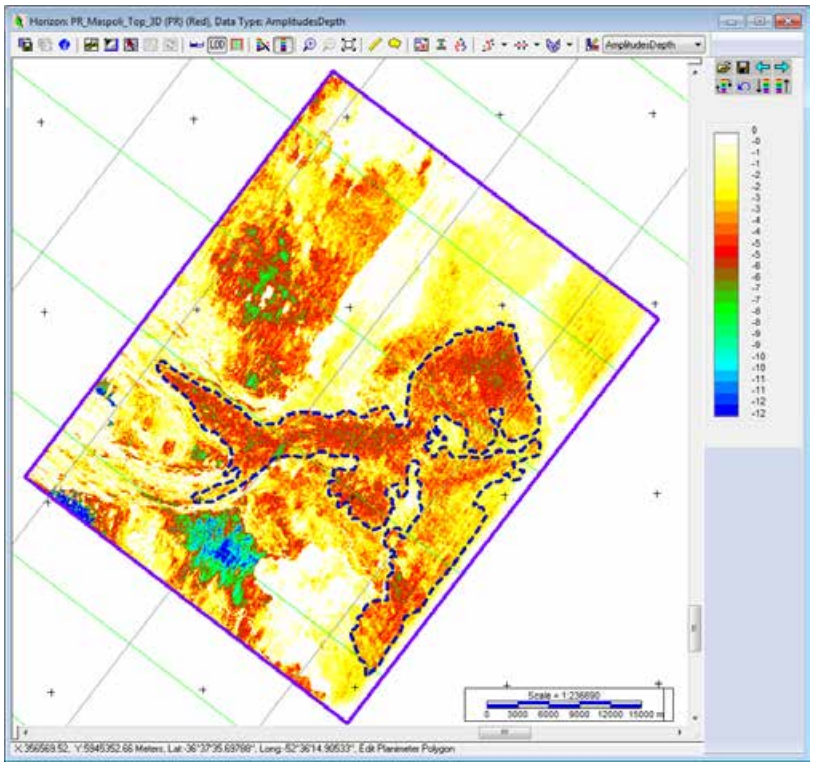

Fig. 50 – Amplitude map of Maspoli with P10 polygon overlaid

Finally, **Fig. 51** shows the seismic amplitude map at the top of the prospect, but with a delimitation polygon showing its P90 extension:

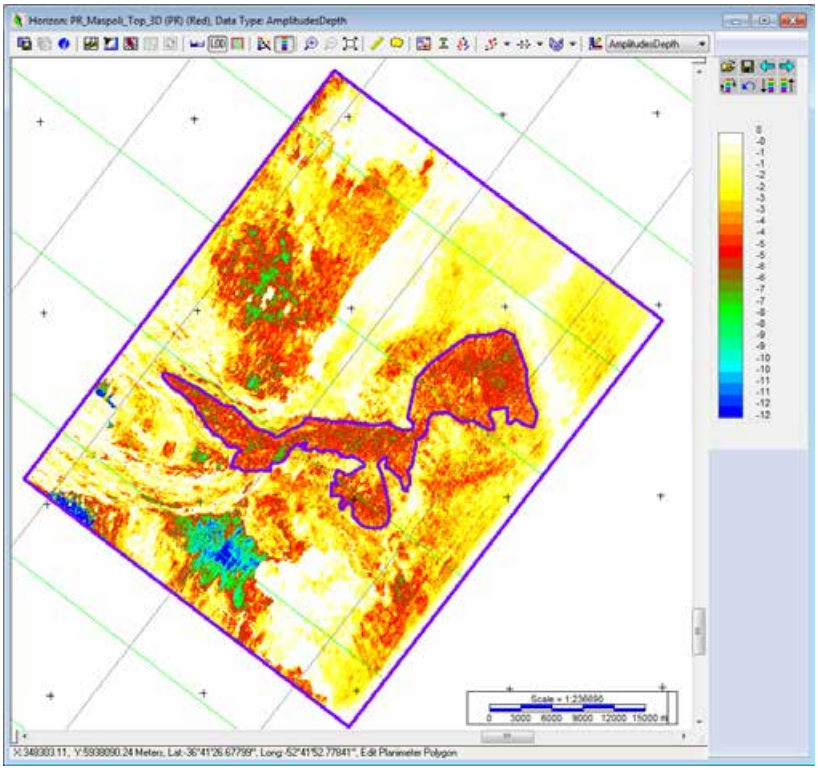

Fig. 51 – Amplitude map of Maspoli with P90 polygon overlaid

The delimitation polygons shown in this study were used to restrict the volumetric calculation in order to get estimated values of a maximum, an optimistic (P10) and a conservative (P90) GRV.

From the interpretation of the seabed in the seismic data, it follows that this potential turbidite lies between a minimum and a maximum water depth of 3,100 m and 3,550 m, respectively **(Fig. 52).**

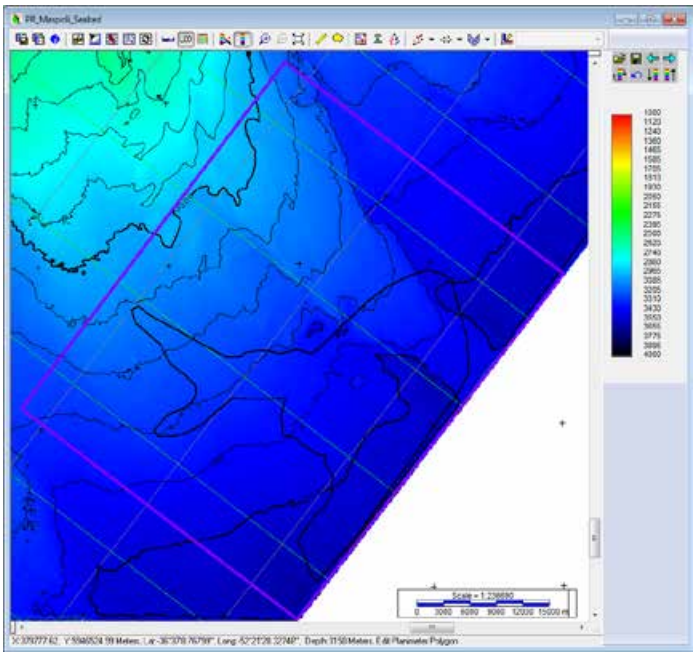

Fig. 52 – Seabed map at Maspoli area of study

The sedimentary overburden is determined by subtracting the seabed grid with the grid that corresponds to the top of the prospect. In this case, this results in an overburden between 1,610 m to 2,064 m **(Fig. 53),** therefore, an average sedimentary overburden of 1,837 m was assumed for reservoir and oil properties estimation (porosity and B_{oi}).

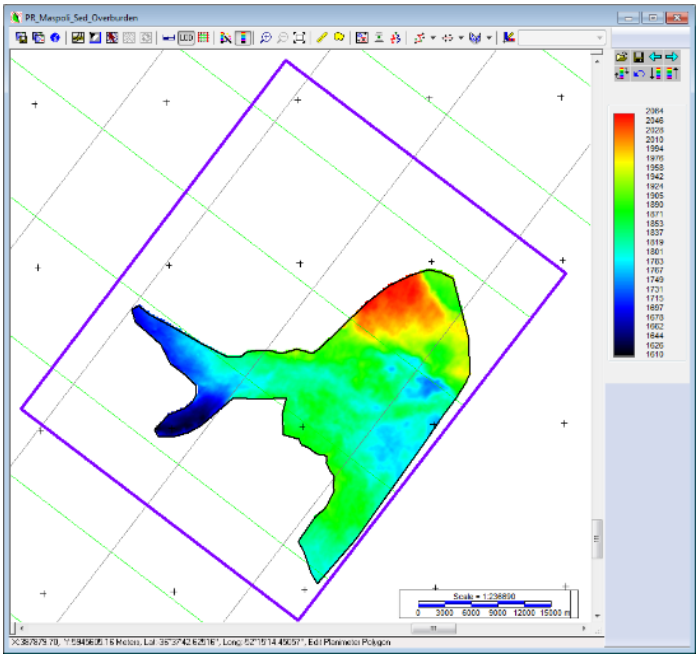

Fig. 53 – Sedimentary overburden map at Maspoli

6.2.2 – Estimation of Oil Formation Volume Factor

In order to define a realistic probability distribution function for the initial formation volume factor (B_{oi}) the following assumptions were made:

- $T_{seabed} = 1.29\ ^{\circ}\text{C}$, this temperature is obtained from the World Ocean Atlas (2013) at a point with coordinates: 52.38W, 36.88S.

- Geothermal Gradient = $30\ ^{\circ}\text{C/km}$, which is the worldwide average temperature gradient.

Considering these two assumptions, the estimated average reservoir temperature is:

$$T_r = T_{seabed} + 30\frac{^{\circ}\text{C}}{\text{km}} * 1.837\ \text{km} = 56.40\ ^{\circ}\text{C} = 133.52\ ^{\circ}\text{F}$$

- Oil gravity was assumed 30°API $\Rightarrow \gamma_o = \frac{141.5}{121.5+30} \cong 0.93$

- Assuming $p_r > p_b$ and c_o negligible $\Rightarrow B_{oi} \cong B_{ob} \Rightarrow$ applying Levitan and Murtha (1999) correlation for B_{ob}:

$$B_{oi} \cong B_{ob} = 1 + 0.0005 * GOR * \left(\frac{\gamma_g}{\gamma_o}\right)^{0.25} + \frac{0.0004 * (T_r - 60)}{\gamma_o * \gamma_g}$$

Where T_r is reservoir temperature in °F.

For the case GOR=0 scf/STB then:

$$B_{oi} \cong 1 + 0.0005 * 0 * \left(\frac{0.8}{0.93}\right)^{0.25} + \frac{0.0004 * (133.52 - 60)}{0.93 * 0.8} = 1.04\ \text{RB/STB}$$

Finally, applying the same equation for the rest of the cases (see Table 2 for GOR values):

- GOR=248.7 scf/STB $\Rightarrow B_{oi} \cong 1.16\ \text{RB/STB}$
- GOR=545.4 scf/STB $\Rightarrow B_{oi} \cong 1.30\ \text{RB/STB}$
- GOR=935.2 scf/STB $\Rightarrow B_{oi} \cong 1.49\ \text{RB/STB}$
- GOR=2,000 scf/STB $\Rightarrow B_{oi} \cong 2.00\ \text{RB/STB}$

These values are used to define Maspoli PDF for oil formation volume factor.

6.2.3 – Estimation of Porosity

For the case of Maspoli, which is approximately beneath 1.837 km of sediments, the porosity values obtained through the equations derived from Ehrenberg and Nadeau (2005) analysis give the following results:

$$\varphi_{P90} = -0.0917 * (1.837)^2 - 0.8773 * (1.837) + 14.019 = 11.9\%$$

$$\varphi_{P50} = -0.0191 * (1.837)^2 - 2.2925 * (1.837) + 23.457 = 19.2\%$$

$$\varphi_{P10} = -0.0636 * (1.837)^2 - 1.863 * (1.837) + 31.309 = 28.1\ \%$$

These values are used to define Maspoli PDF for porosity.

6.2.4 – Computation of Gross Rock Volume

The GRV reports created by IHS Kingdom, using the surfaces interpreted for the top and base of Maspoli and the three different restriction polygons, are as follows:

- Maximum Case:

```
Volumetric Model:          Single Structure
Grid:      PR_Maspoli_Top
Polygons Used:   PR_Maspoli_P01
Lower Contact:   PR_Maspoli_Base

Polygon PR_Maspoli_P01
-----------------------------------------------
Polygon Area:     498.1183    10^6 M2
Polygon Area within the Grid(s):     493.9338    10^6 M2
Gross Volume:     32,061.6758    10^6 M3
```

- Optimistic Case:

```
Volumetric Model:          Single Structure
Grid:      PR_Maspoli_Top
Polygons Used:   PR_Maspoli_P10
Lower Contact:   PR_Maspoli_Base

Polygon PR_Maspoli_P10
-----------------------------------------------
Polygon Area:     374.4949    10^6 M2
Polygon Area within the Grid(s):     374.0291    10^6 M2
Gross Volume:     25,554.2292    10^6 M3
```

- Conservative Case

```
Volumetric Model:          Single Structure
Grid:      PR_Maspoli_Top
Polygons Used:   PR_Maspoli_P90
Lower Contact:   PR_Maspoli_Base

Polygon PR_Maspoli_P90
-----------------------------------------------
Polygon Area:     181.6707    10^6 M2
Polygon Area within the Grid(s):     181.6274    10^6 M2
Gross Volume:     12,455.6600    10^6 M3
```

This variable, GRV, is defined as a LogNormal distribution, therefore three parameters are required in @Risk for its definition: P10, P50 and P90 values. The P50 value is calculated, as a function of the P10 and P90 values using the formula: $\mathrm{P50} = \mathrm{e}^{(\mathrm{LN(P90)+LN(P10)})/2}$ (Wright 2015).

For the case of Maspoli, this results in a P50 value for *GRV* = 17,840,818,100 m^3.

6.2.5 – Inputs used for the probabilistic analysis of Maspoli

A summary of the inputs used for the probabilistic volumetric analysis of Maspoli, based on the previous results, is shown in **Table 5.**

Parameter	MIN	Low Estimate	Best Estimate	High Estimate	MAX	Distr. Type
GRV (m^3)	0	12,455,660,000	17,840,818,100	25,554,229,200	32,061,675,800	LogNormal
N/G (%)	0	34.8%	66.6%	90%	100%	Beta
Phi (%)	0	11.9%	19.2%	28.1%	48%	Beta
S_w (%)	0	10.3%	23.4%	41.6%	100%	Beta
GOR (scf/STB)	0	248.7	545.4	935.2	2,000	Beta
B_{oi} (RB/STB)	1.04	1.16	1.31	1.49	2.00	Beta
RF (%)	0	22.4%	31%	38.7%	50%	Beta

Table 5 – Reservoir and fluid properties used for the volumetric analysis of Maspoli

The following figures (**Fig. 54** to **Fig. 60**) show the detail of the input distributions defined in @Risk and its simulation results:

- Gross Rock Volume:

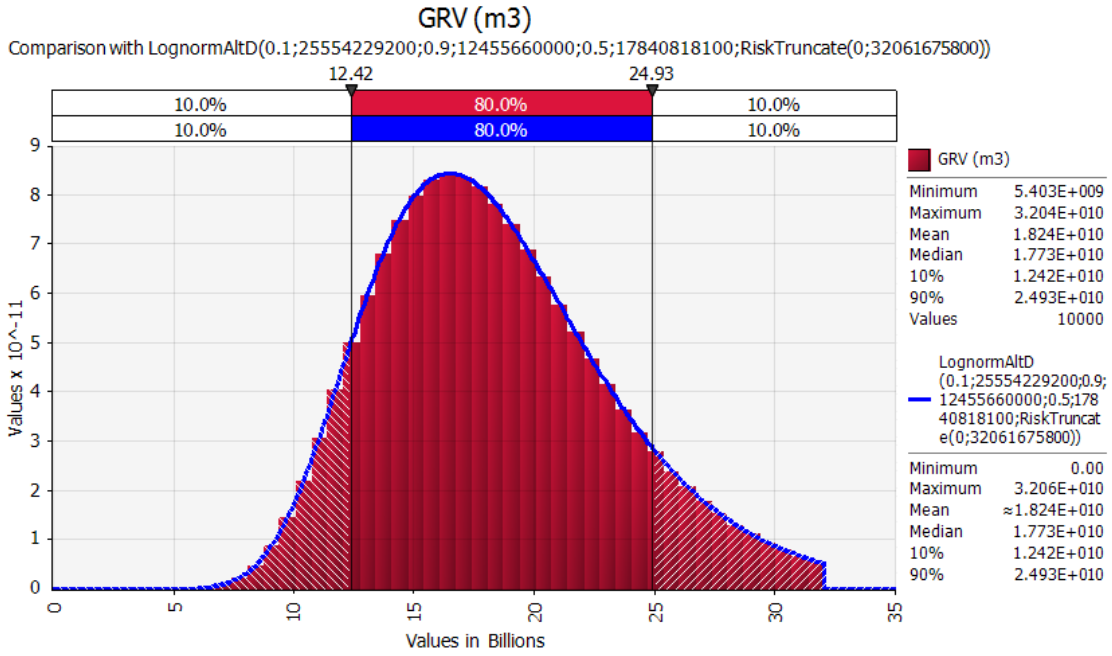

Fig. 54 – *GRV* distribution of Maspoli

- Net to Gross:

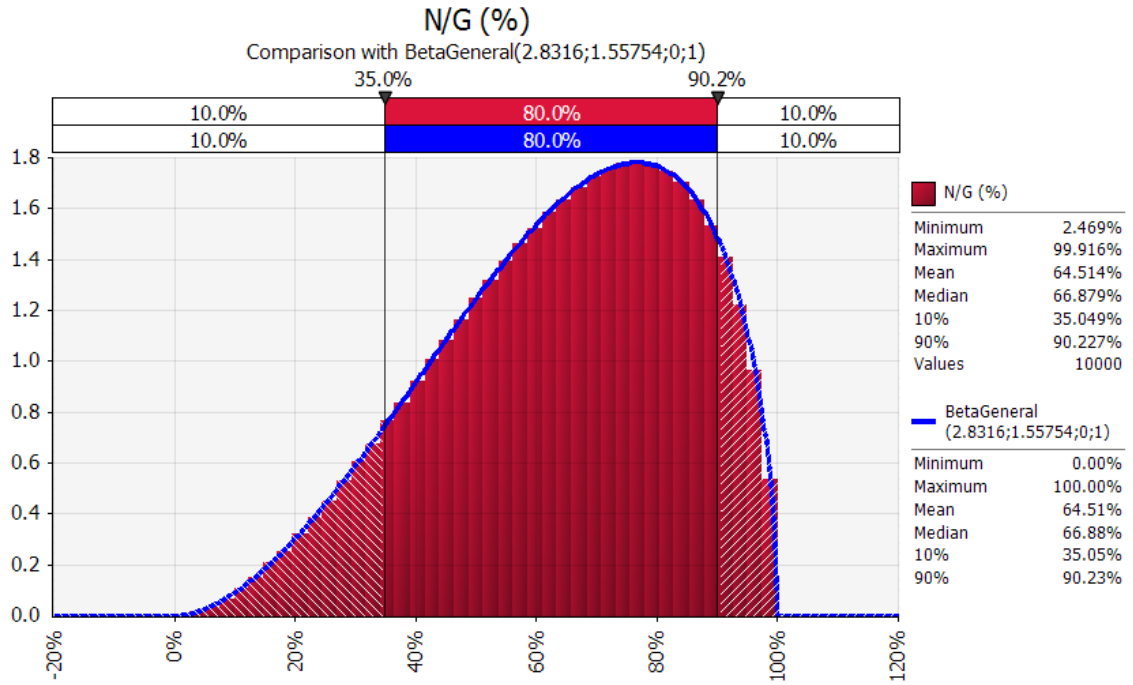

Fig. 55 – *N/G* distribution at Maspoli

- Porosity:

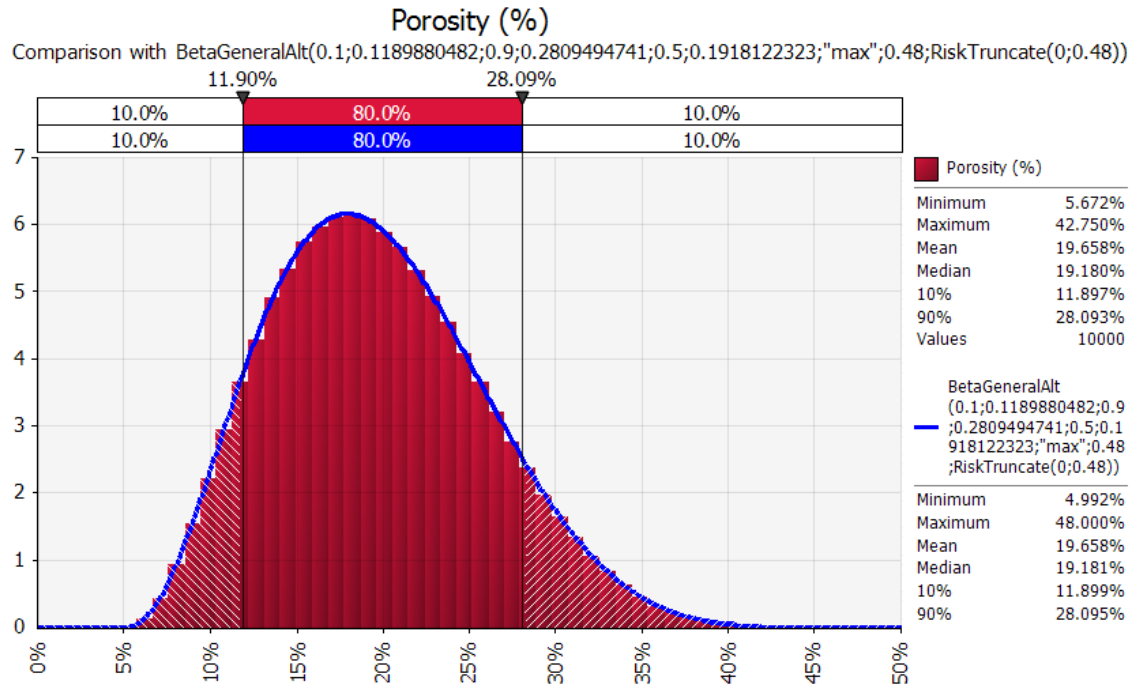

Fig. 56 – Porosity distribution at Maspoli

- Water Saturation:

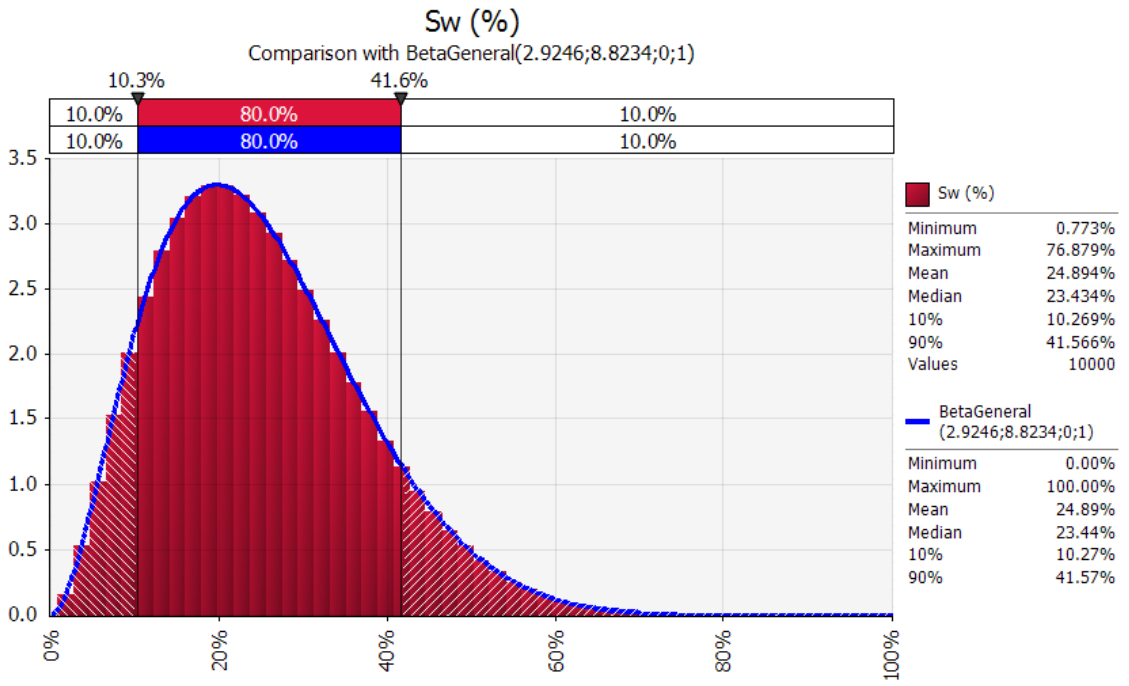

Fig. 57 – *Sw* distribution at Maspoli

- Gas/Oil Ratio:

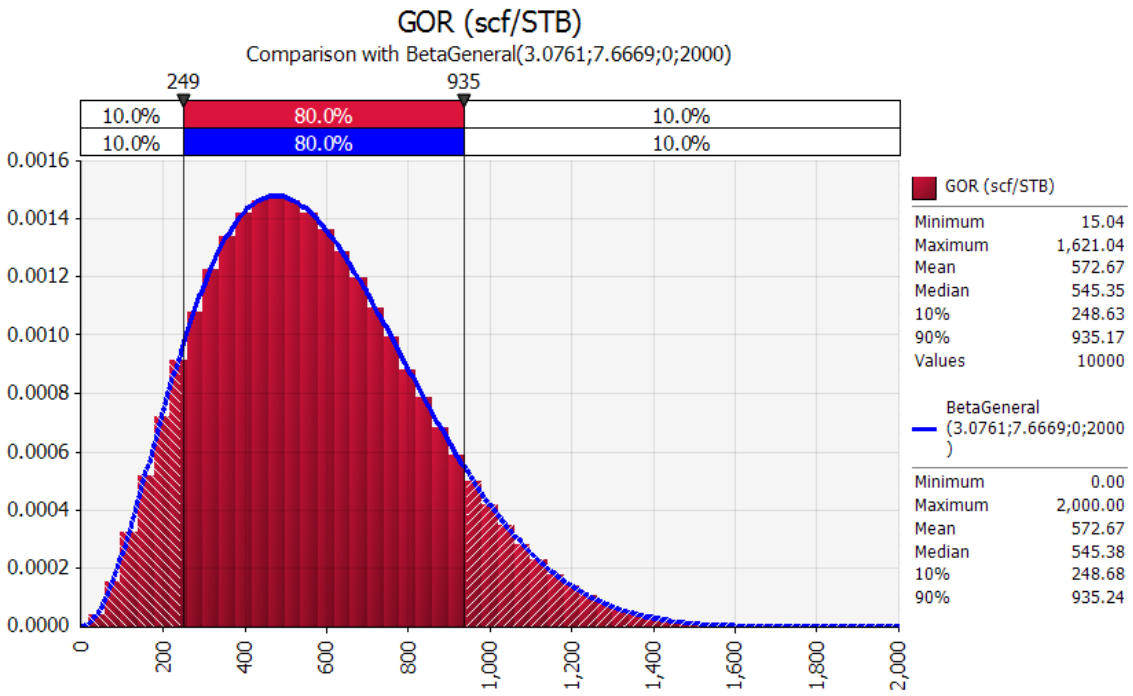

Fig. 58 – *GOR* distribution at Maspoli

- Initial formation volume factor:

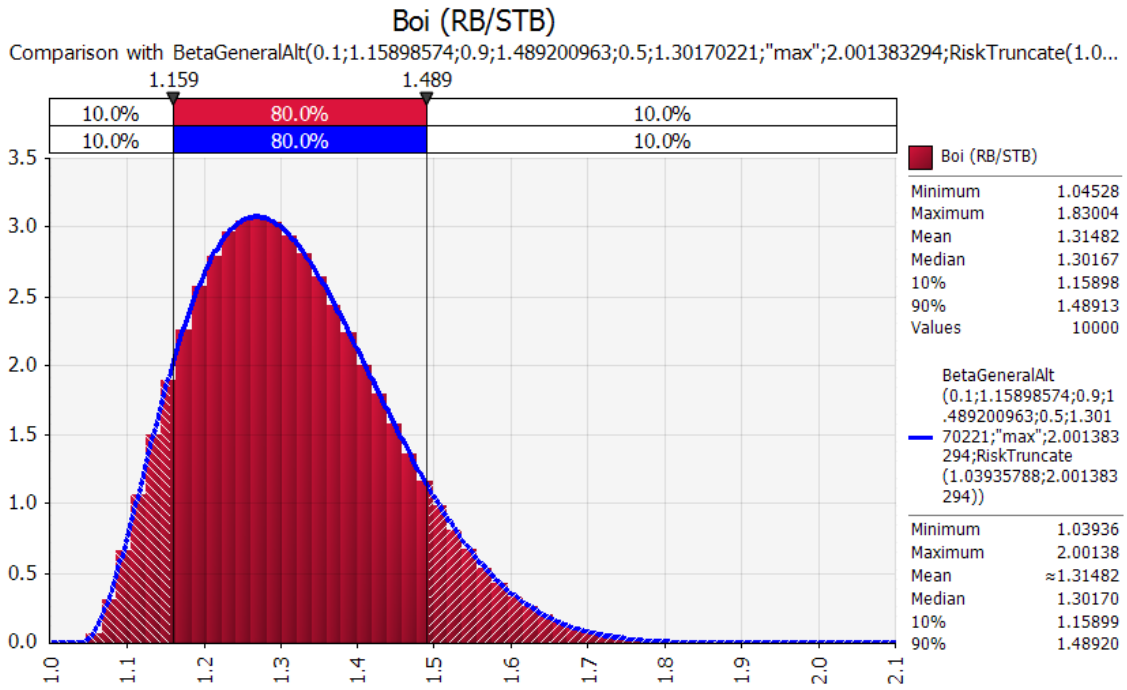

Fig. 59 – *Boi* distribution at Maspoli

- Recovery Factor:

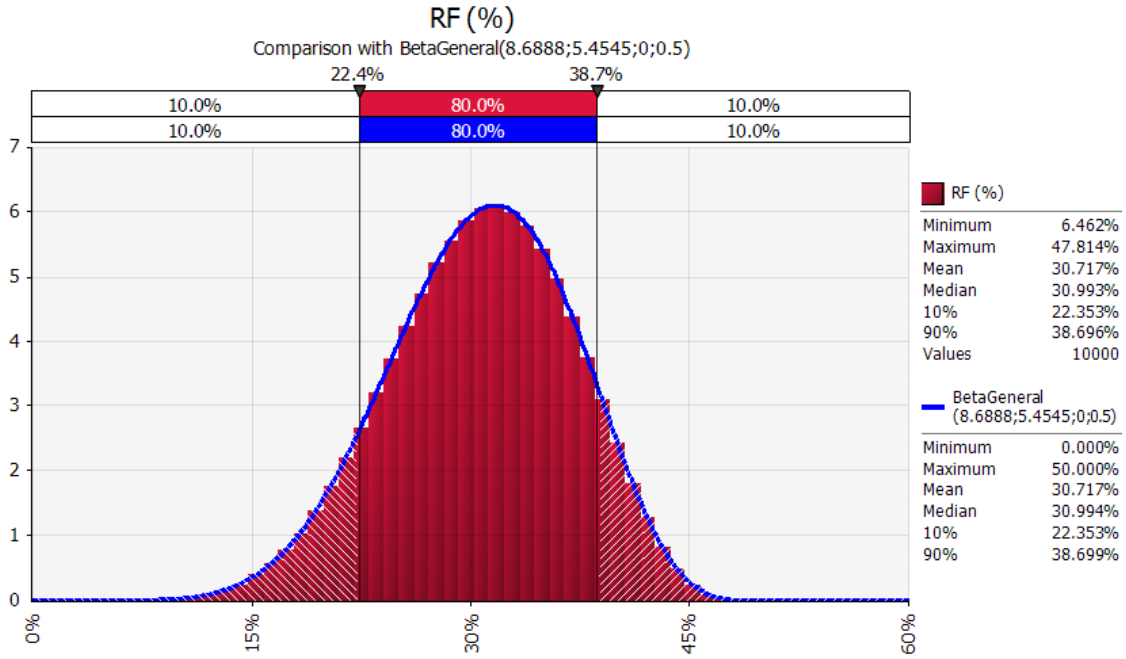

Fig. 60 – *RF* distribution at Maspoli

6.2.6 – Results of the probabilistic analysis for Maspoli

After all the inputs were set, and the output defined as the oil EUR then an @Risk simulation of 10,000 iterations was run using Latin Hypercube sampling. **Fig. 61** and **Fig. 62** show the resulting EUR distribution graphs for oil and associated gas, respectively:

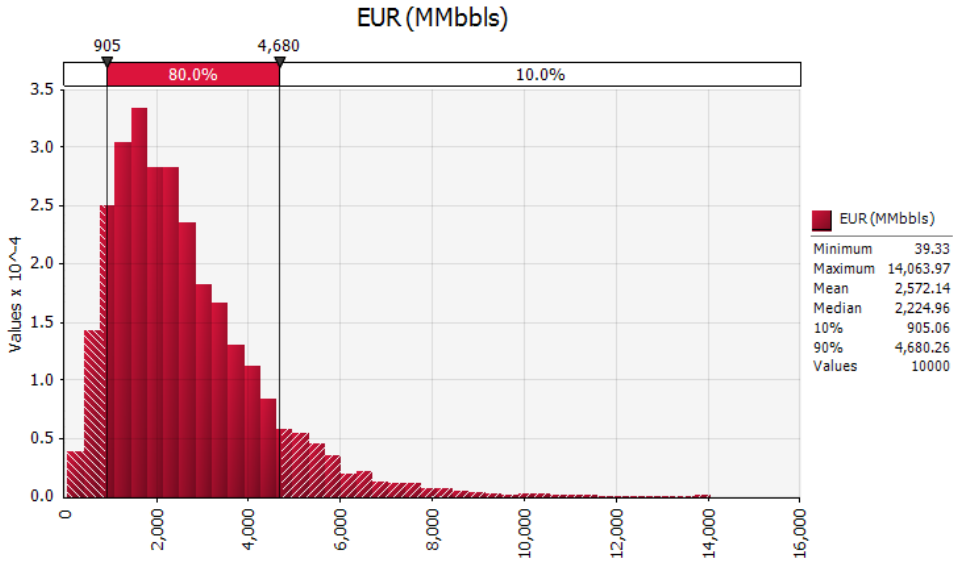

Fig. 61 – Maspoli Oil EUR

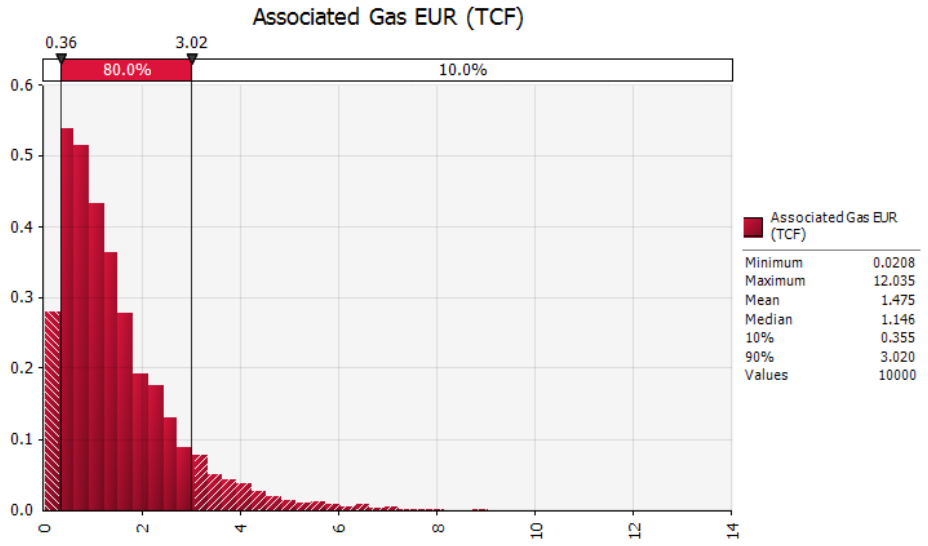

Fig. 62 – Maspoli Associated Gas EUR

According to the Petroleum Resources Management System (SPE 2007), for this study case, the calculated resources can be classified as "Prospective Resources" and categorized as follows:

	Oil	Associated Gas
Low estimate Prospective Resources:	905.062 MMbbls	0.355 TCF
Best estimate Prospective Resources:	2,224.964 MMbbls	1.146 TCF
High estimate Prospective Resources:	4,680.260 MMbbls	3.020 TCF

Table 6 – Estimation of Maspoli Prospective Resources

Sensibility Analysis

A tornado chart with the relative influence of the main variables on the oil EUR for this prospect is shown in **Fig. 63.**

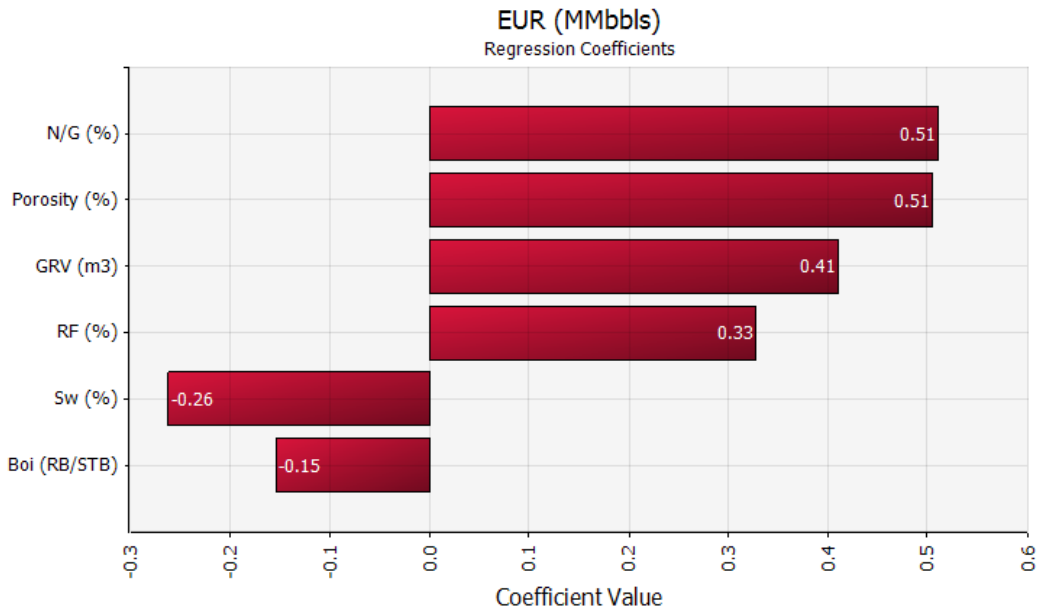

Fig. 63 – Tornado chart for Maspoli Oil EUR

Fig. 64 shows a tornado chart with the relative influence of the main variables on the associated gas EUR for this prospect.

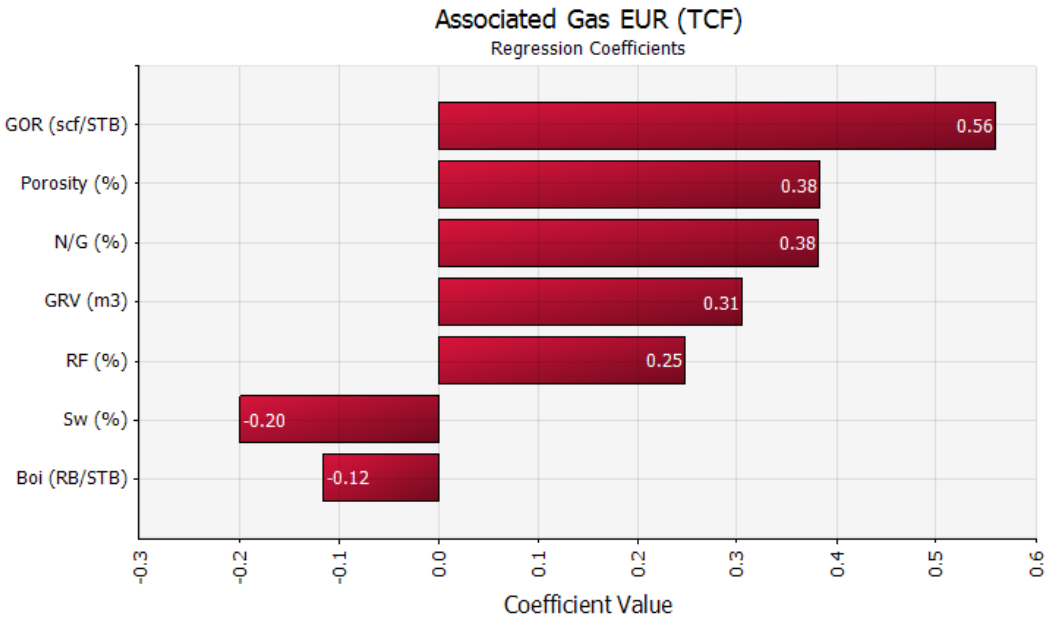

Fig. 64 – Tornado chart for Maspoli Associated Gas EUR

From these tornado charts, it can be concluded that N/G and porosity are the parameters which oil EUR is most sensible to. On the other hand, for associated gas EUR, GOR is the most sensible parameter.
With the presented methodology for GRV calculation, and particularly for this prospect, the uncertainty in this variable is reduced therefore it is not the input that has the greatest influence on the EUR calculation.

6.3 – Analysis of Prospect 3 – Jasper

Prospect Name: Jasper

Seismic Survey Used: UR13_3D

Source Rock: Marine Aptian shales

Reservoir: Confined Santonian-Campanian turbidites

Seal: Campanian-Maastrichtian shales

Trap: Combined stratigraphic-structural trap with an updip sealing fault

Migration: through faults connecting the source rock with the reservoir

6.3.1 – Interpretation of 3D seismic data

For this prospect approximately 263 km^2 of a 2,076 km^2 Pre-Stack Time Migrated (PSTM), converted to depth, 3D seismic survey (UR13_3D survey shown in Fig. 3) were interpreted.

The structural map at top of the prospect, overlaid with a polygon that depicts its interpreted maximum extension, is shown in **Fig. 65.**

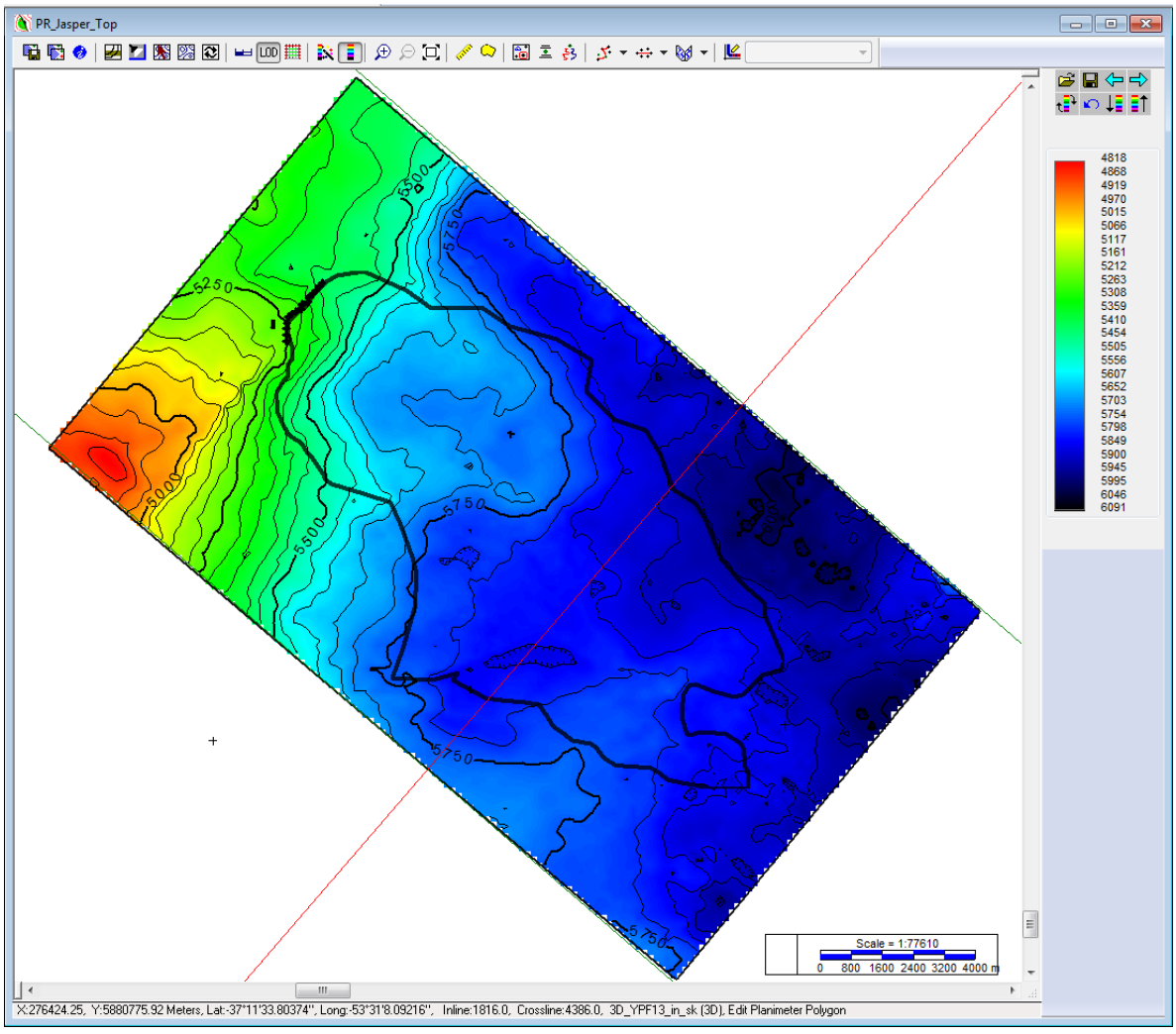

Fig. 65 – Structural map at the top of Jasper

An arbitrary seismic line through Jasper is shown in **Fig. 66.** The green horizon depicts the top of the prospect and the pink horizon its base.

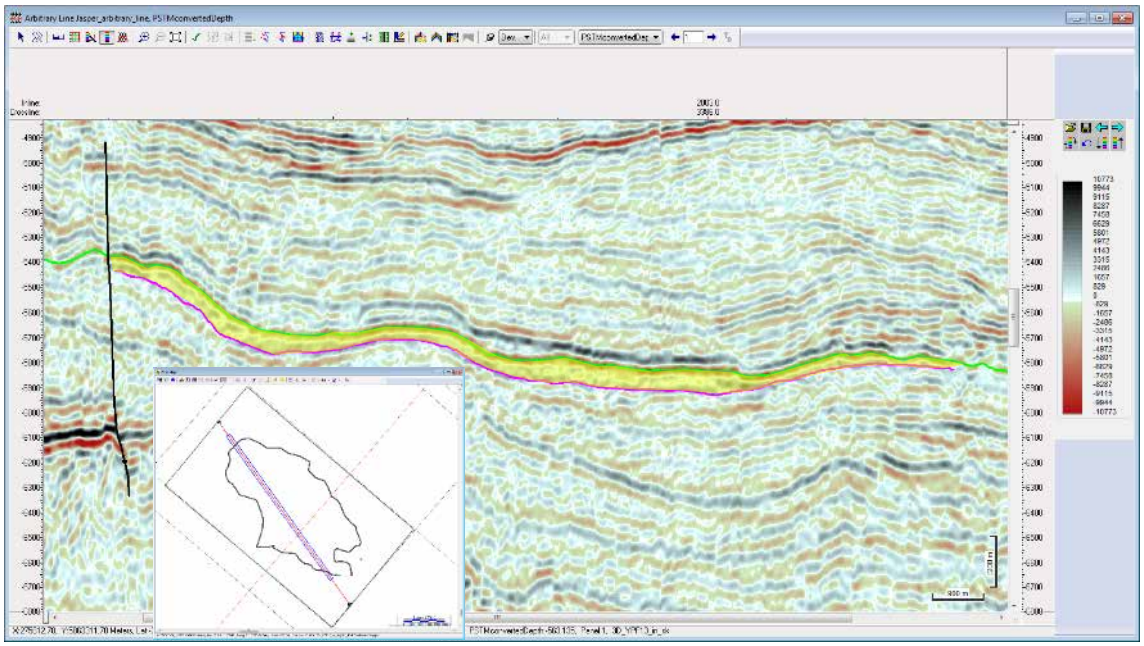

Fig. 66 – Arbitrary line along Jasper (courtesy of ANCAP)

The lobular shape of Jasper, seen in the perpendicular direction, is shown in **Fig. 67.**

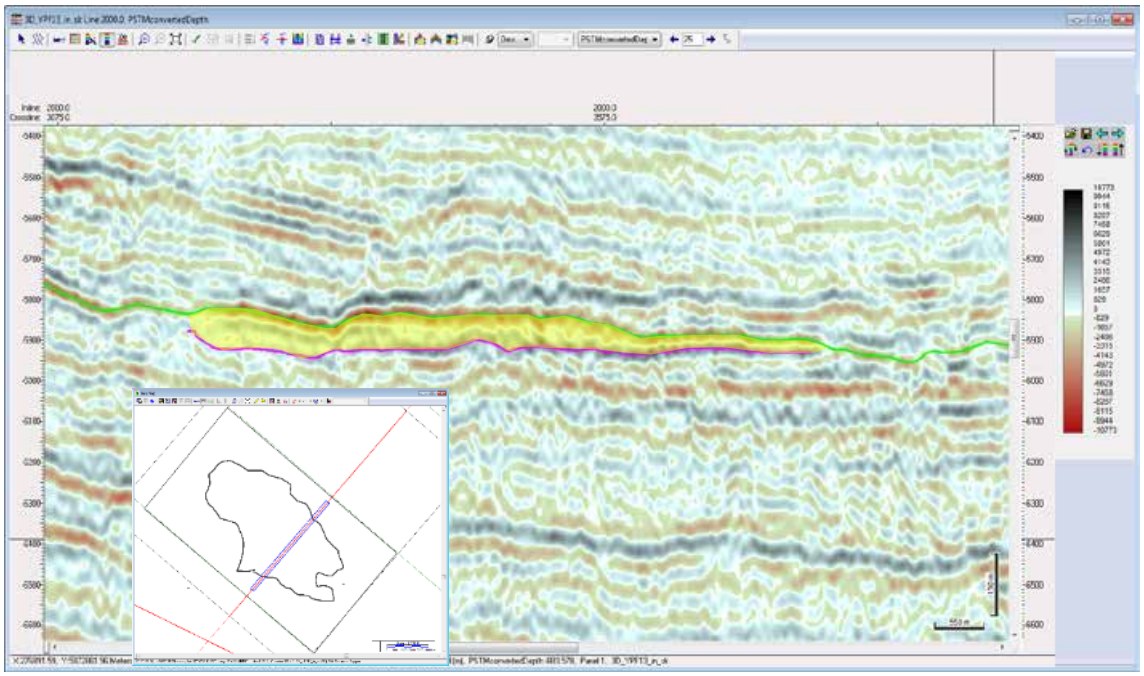

Fig. 67 – Inline across Jasper (courtesy of ANCAP)

Fig. 68 shows the different elements of the proposed petroleum system for the case of Jasper.

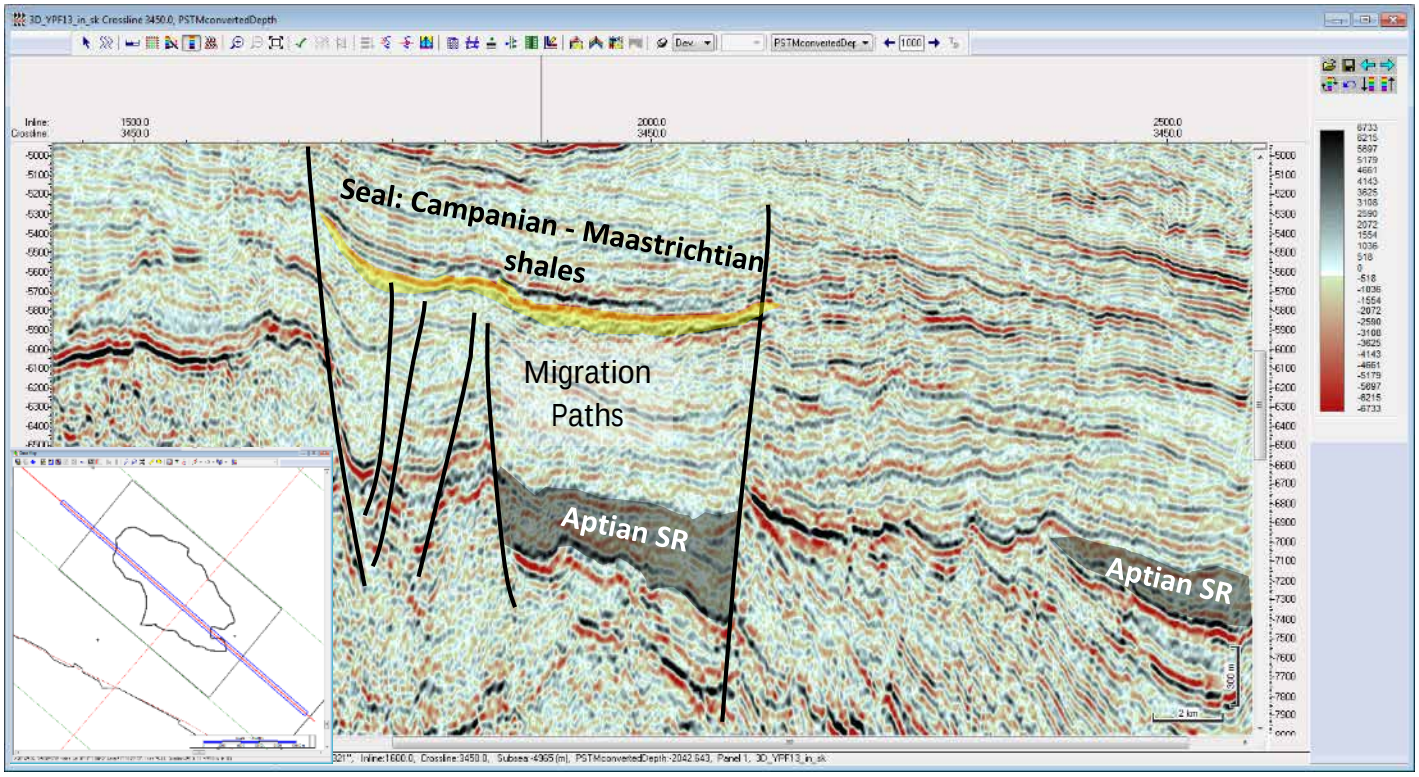

Fig. 68 – Crossline along Jasper with interpreted petroleum system elements (courtesy of ANCAP)

Fig. 69 shows the seismic amplitude map at the top of the prospect, overlaid with, the contours of the structural map from Fig. 65 and the defined delimitation polygon that accounts for its maximum extension.

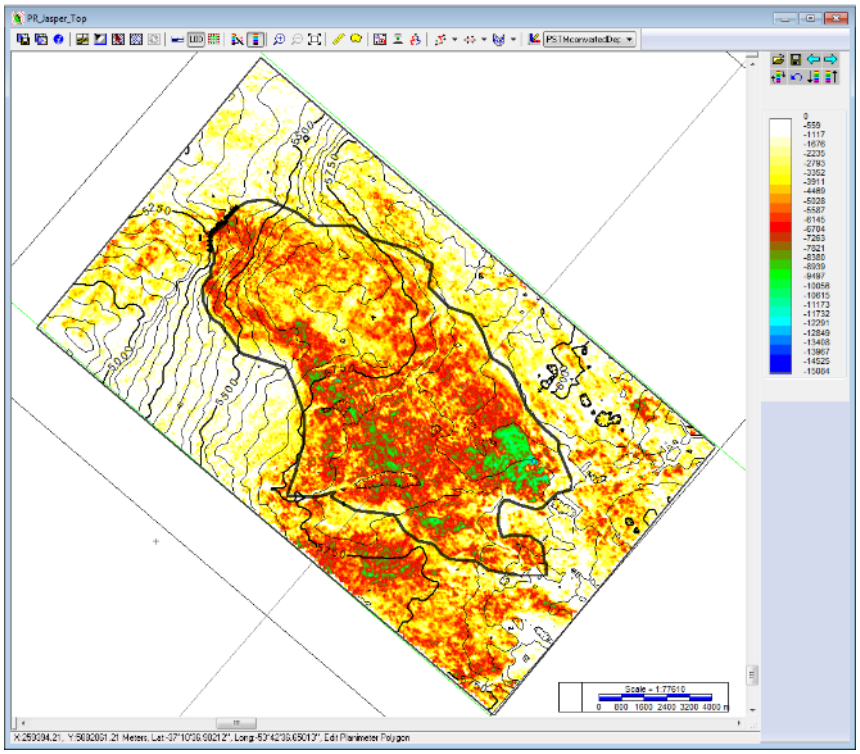

Fig. 69 – Amplitude map of Jasper

Fig. 70 shows the seismic amplitude map at the top of the prospect with its defined P10 delimitation polygon.

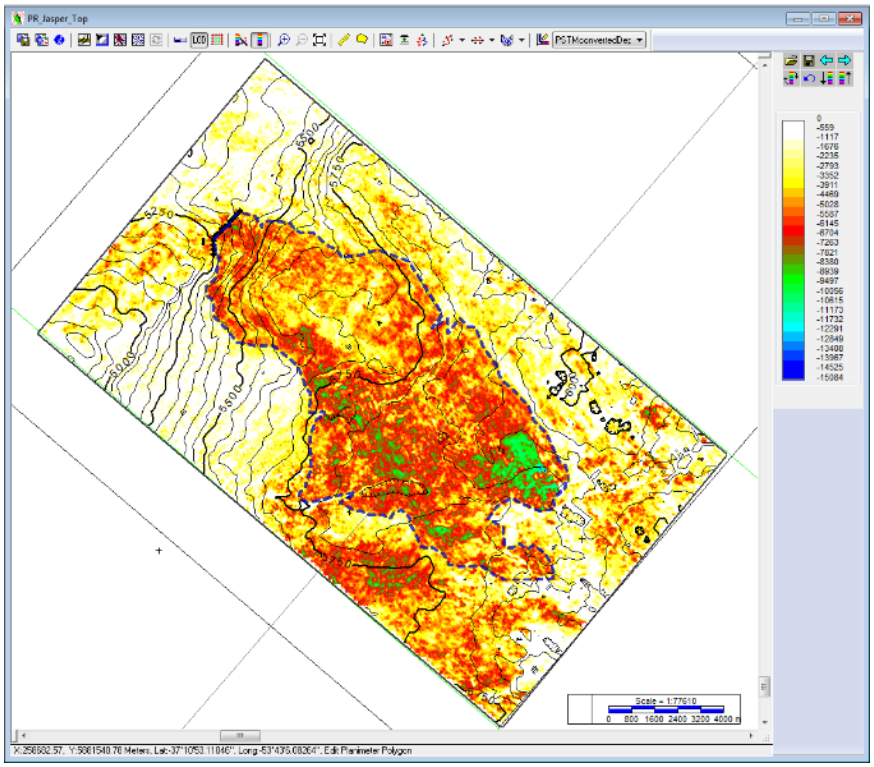

Fig. 70 – Amplitude map of Jasper with P10 polygon overlaid

Finally, **Fig. 71** shows the seismic amplitude map at the top of the prospect, but with a delimitation polygon showing its P90 extension:

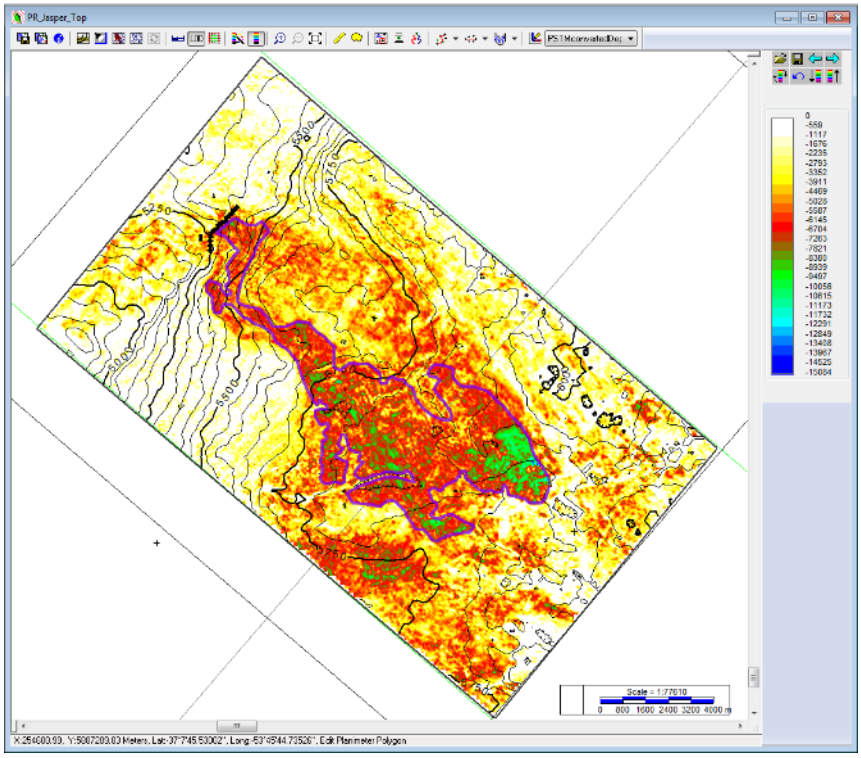

Fig. 71 – Amplitude map of Jasper with P90 polygon overlaid

The delimitation polygons shown in this study were used to restrict the volumetric calculation in order to get estimated values of a maximum, an optimistic (P10) and a conservative (P90) GRV.

From the interpretation of the seabed in the seismic data, it follows that this potential turbidite lies between a minimum and a maximum water depth of 1,250 m and 1,400 m, respectively **(Fig. 72).**

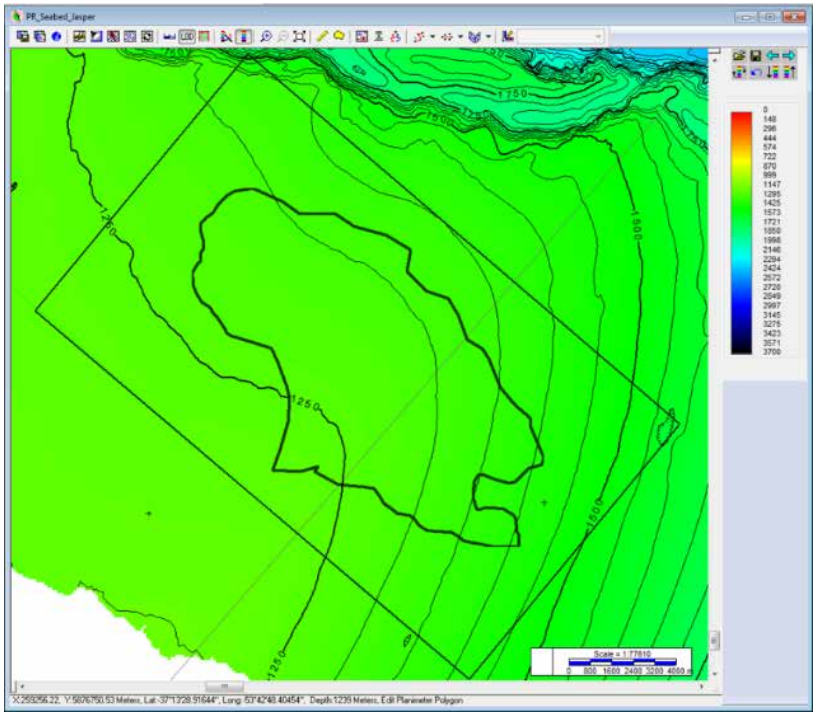

Fig. 72 – Seabed map at Jasper area of study

The sedimentary overburden is determined by subtracting the seabed grid with the grid that corresponds to the top of the prospect. In this case, this results in an overburden between 3,980 m to 4,614 m **(Fig. 73),** therefore, an average sedimentary overburden of 4,297 m was assumed for reservoir and oil properties estimation (porosity and B_{oi}).

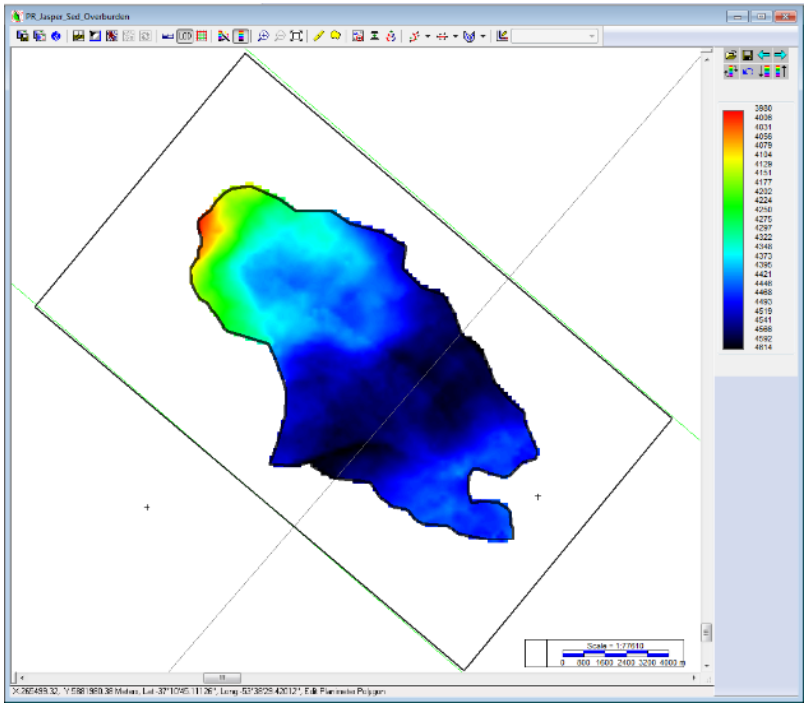

Fig. 73 – Sedimentary overburden at Jasper

6.3.2 – Estimation of Oil Formation Volume Factor

In order to define a realistic probability distribution function for the initial formation volume factor (B_{oi}) the following assumptions were made:

- $T_{seabed} = 2.957\ ^{\circ}\text{C}$, this temperature is obtained from the World Ocean Atlas (2013) at a point with coordinates: 53.63W, 37.38S.

- Geothermal Gradient = $30\ ^{\circ}\text{C/km}$, which is the worldwide average temperature gradient.

Considering these two assumptions, the estimated average reservoir temperature is:

$$T_r = T_{seabed} + 30\frac{^{\circ}\text{C}}{\text{km}} * 4.297\ \text{km} = 131.87\ ^{\circ}\text{C} = 269.36\ ^{\circ}\text{F}$$

- Oil gravity was assumed 30°API $\Rightarrow \gamma_o = \frac{141.5}{121.5+30} \cong 0.93$

- Assuming $p_r > p_b$ and c_o negligible $\Rightarrow B_{oi} \cong B_{ob} \Rightarrow$ applying Levitan and Murtha (1999) correlation for B_{ob}:

$$B_{oi} \cong B_{ob} = 1 + 0.0005 * GOR * \left(\frac{\gamma_g}{\gamma_o}\right)^{0.25} + \frac{0.0004 * (T_r - 60)}{\gamma_o * \gamma_g}$$

Where T_r is reservoir temperature in °F.

For the case GOR=0 scf/STB then:

$$B_{oi} \cong 1 + 0.0005 * 0 * \left(\frac{0.8}{0.93}\right)^{0.25} + \frac{0.0004 * (269.36 - 60)}{0.93 * 0.8} = 1.11\ \text{RB/STB}$$

Finally, applying the same equation for the rest of the cases (see Table 2 for GOR values):

- GOR=248.7 scf/STB $\Rightarrow B_{oi} \cong 1.23\ \text{RB/STB}$
- GOR=545.4 scf/STB $\Rightarrow B_{oi} \cong 1.37\ \text{RB/STB}$
- GOR=935.2 scf/STB $\Rightarrow B_{oi} \cong 1.56\ \text{RB/STB}$
- GOR=2,000 scf/STB $\Rightarrow B_{oi} \cong 2.07\ \text{RB/STB}$

These values are used to define Jasper PDF for oil formation volume factor.

6.3.3 – Estimation of Porosity

For the case of Jasper, which is approximately beneath 4.297 km of sediments, the porosity values obtained through the equations derived from Ehrenberg and Nadeau (2005) analysis give the following results:

$$\varphi_{P90} = -0.0917 * (4.297)^2 - 0.8773 * (4.297) + 14.019 = 8.3\%$$

$$\varphi_{P50} = -0.0191 * (4.297)^2 - 2.2925 * (4.297) + 23.457 = 13.3\%$$

$$\varphi_{P10} = -0.0636 * (4.297)^2 - 1.863 * (4.297) + 31.309 = 22.7\ \%$$

These values are used to define Jasper PDF for porosity.

6.3.4 – Computation of Gross Rock Volume

The GRV reports created by IHS Kingdom, using the surfaces interpreted for the top and base of Jasper and the three different restriction polygons, are as follows:

- Maximum Case:

```
Volumetric Model:          Single Structure
Grid:      PR_Jasper_Top
Polygons Used:   PR_Jasper_P01
Lower Contact:   PR_Jasper_Base

Polygon PR_Jasper_P01
-------------------------------------------------
Polygon Area:     92.6735    10^6 M2
Polygon Area within the Grid(s):     90.0186    10^6 M2
Gross Volume:     4,727.9823    10^6 M3
```

- Optimistic Case:

```
Volumetric Model:          Single Structure
Grid:      PR_Jasper_Top
Polygons Used:   PR_Jasper_P10
Lower Contact:   PR_Jasper_Base

Polygon PR_Jasper_P10
-------------------------------------------------
Polygon Area:     80.5924    10^6 M2
Polygon Area within the Grid(s):     80.1581    10^6 M2
Gross Volume:     4,354.5728    10^6 M3
```

- Conservative Case

```
Volumetric Model:          Single Structure
Grid:      PR_Jasper_Top
Polygons Used:   PR_Jasper_P90
Lower Contact:   PR_Jasper_Base

Polygon PR_Jasper_P90
-------------------------------------------------
Polygon Area:     35.5193    10^6 M2
Polygon Area within the Grid(s):     35.4982    10^6 M2
Gross Volume:     2,205.5293    10^6 M3
```

This variable, GRV, is defined as a LogNormal distribution, therefore three parameters are required in @Risk for its definition: P10, P50 and P90 values. The P50 value is calculated, as a function of the P10 and P90 values using the formula: $\mathrm{P50} = \mathrm{e}^{(\mathrm{LN(P90)+LN(P10)})/2}$ (Wright 2015).

For the case of Jasper, this results in a P50 value for *GRV* = 3,099,054,356 m^3.

6.3.5 – Inputs used for the probabilistic analysis of Jasper

A summary of the inputs used for the probabilistic volumetric analysis of Jasper, based on the previous results, is shown in **Table 7.**

Parameter	MIN	Low Estimate	Best Estimate	High Estimate	MAX	Distr. Type
GRV (m^3)	0	2,205,529,300	3,099,054,356	4,354,572,800	4,727,982,300	LogNormal
N/G (%)	0	34.8%	66.6%	90%	100%	Beta
Phi (%)	0	8.3%	13.3%	22.7%	48%	Beta
S_w (%)	0	10.3%	23.4%	41.6%	100%	Beta
GOR (scf/STB)	0	248.7	545.4	935.2	2,000	Beta
B_{oi} (RB/STB)	1.11	1.23	1.37	1.56	2.07	Beta
RF (%)	0	22.4%	31%	38.7%	50%	Beta

Table 7 – Reservoir and fluid properties used for the volumetric analysis of Jasper

The following figures (**Fig. 74** to **Fig. 80**) show the detail of the input distributions defined in @Risk and its simulation results:

- Gross Rock Volume:

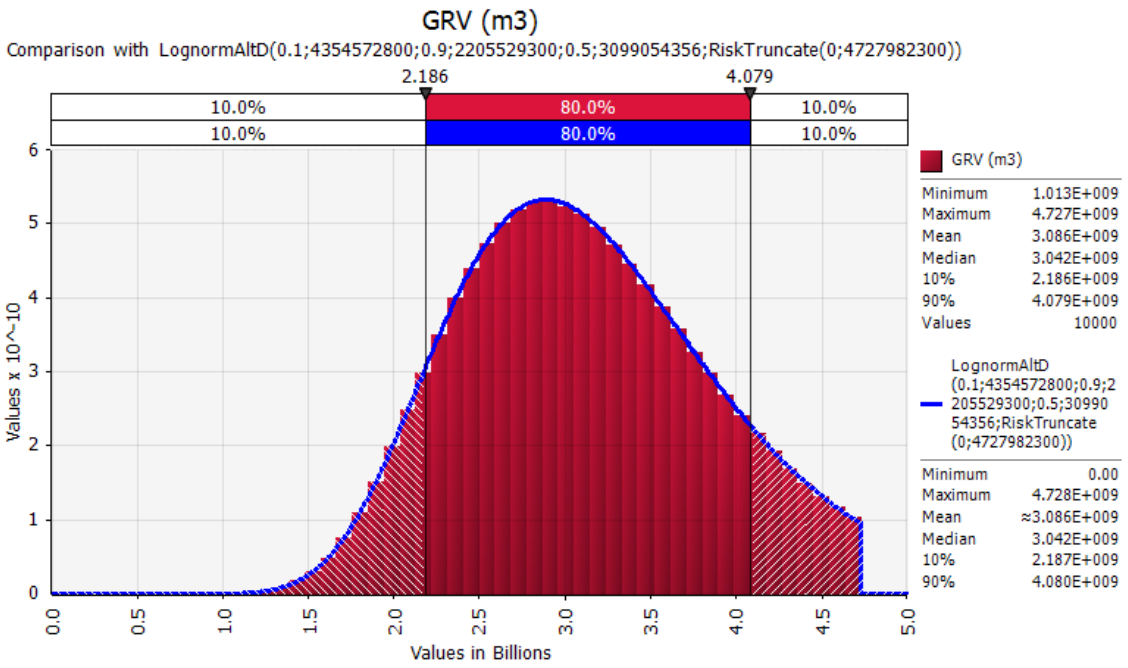

Fig. 74 – *GRV* distribution of Jasper

- Net to Gross:

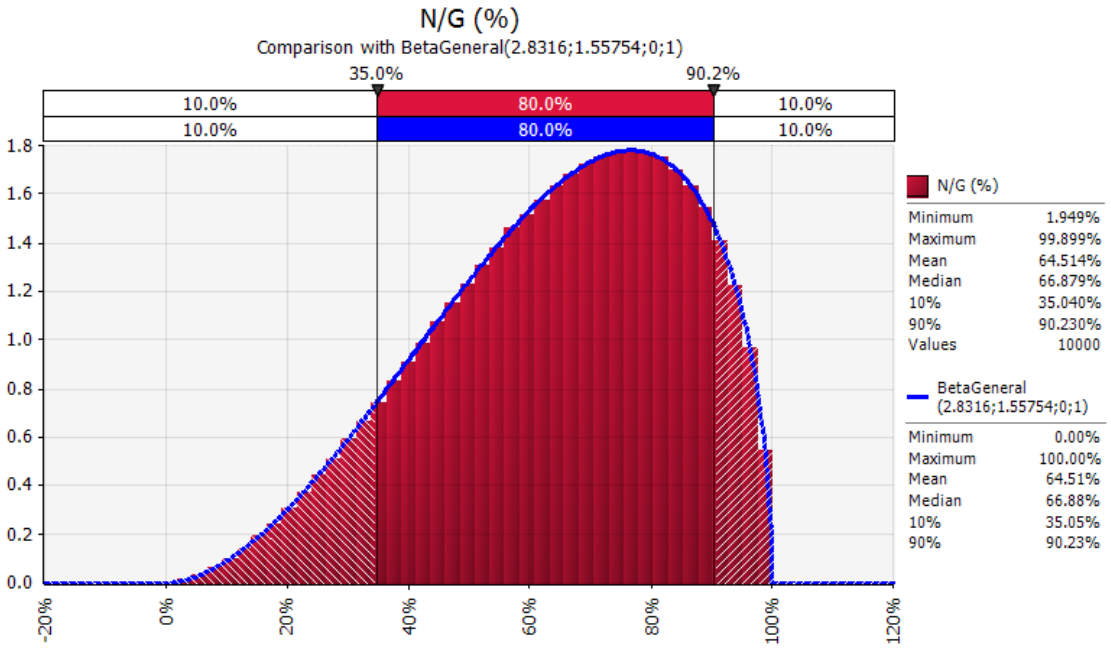

Fig. 75 – *N/G* distribution at Jasper

- Porosity:

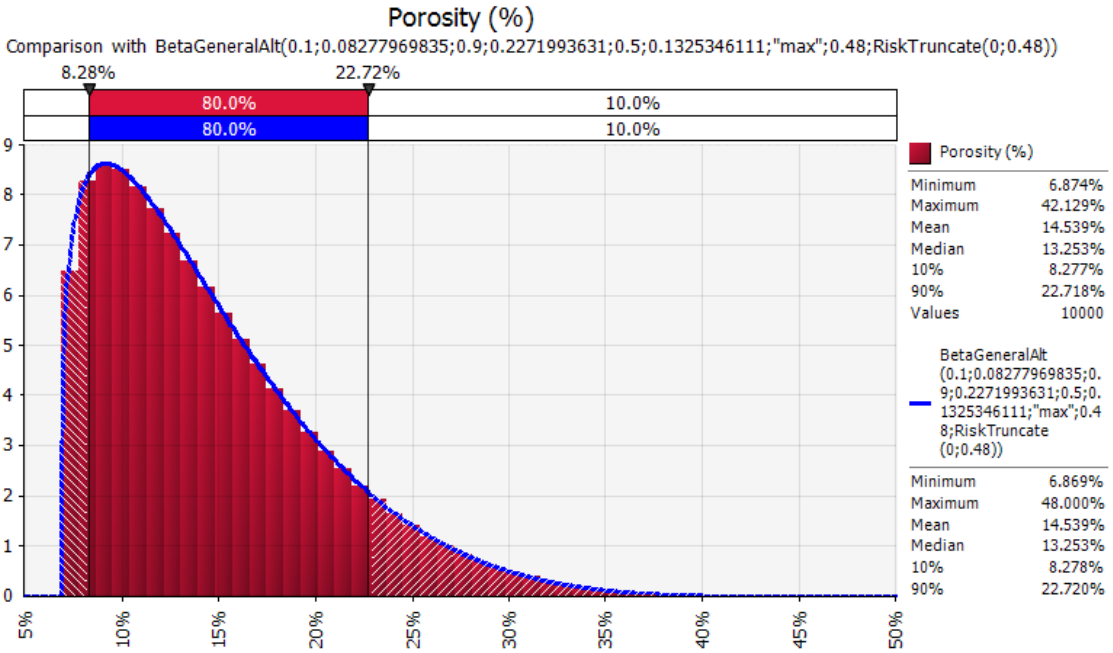

Fig. 76 – Porosity distribution at Jasper

- Water Saturation:

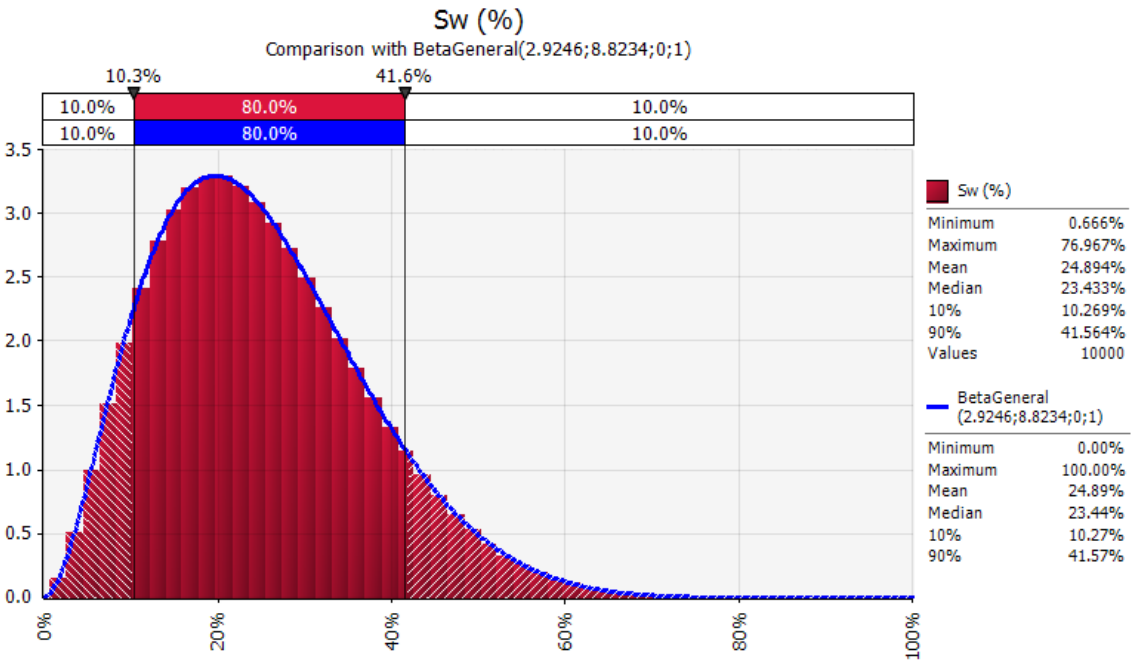

Fig. 77 – *Sw* distribution at Jasper

- Gas/Oil Ratio:

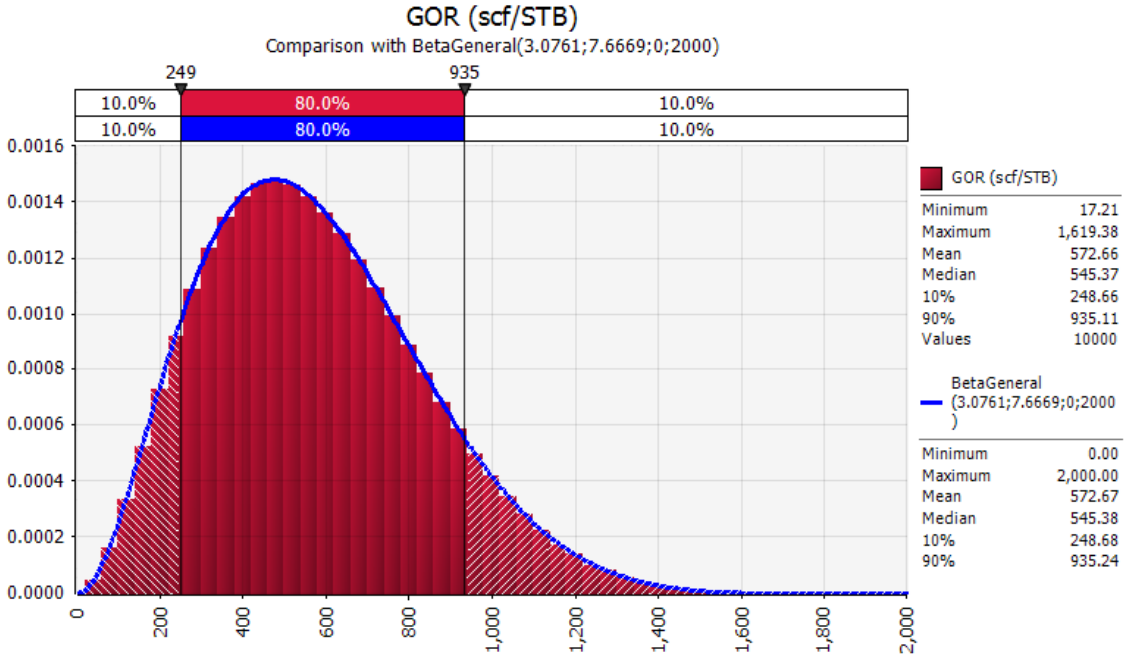

Fig. 78 – *GOR* distribution at Jasper

- Initial formation volume factor:

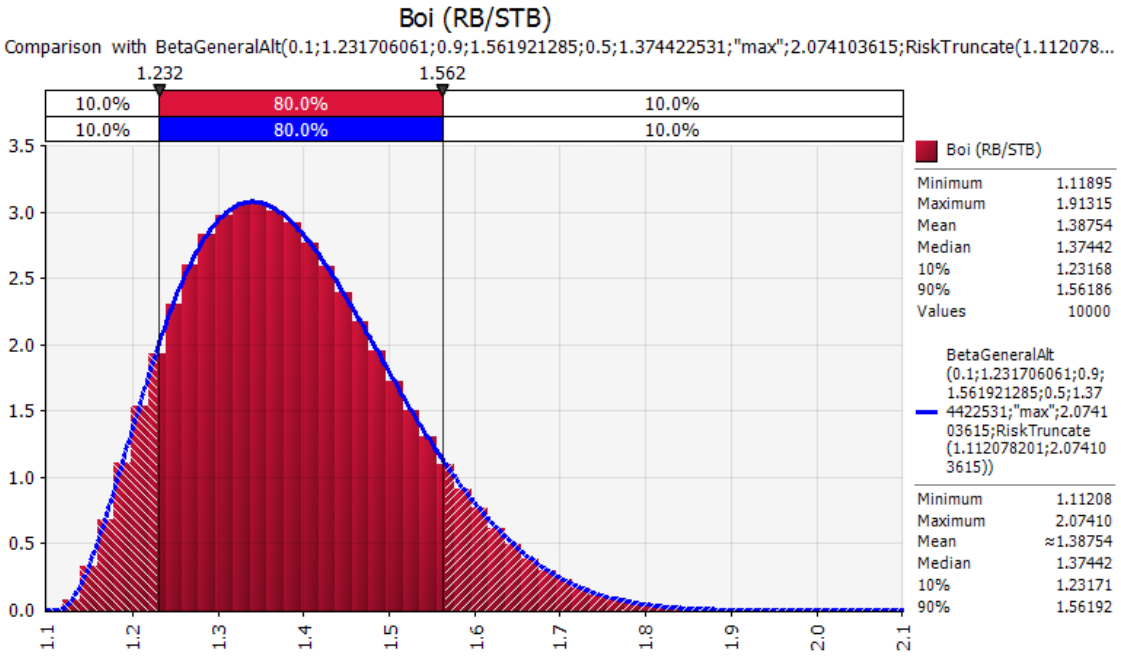

Fig. 79 – *Boi* distribution at Jasper

- Recovery Factor:

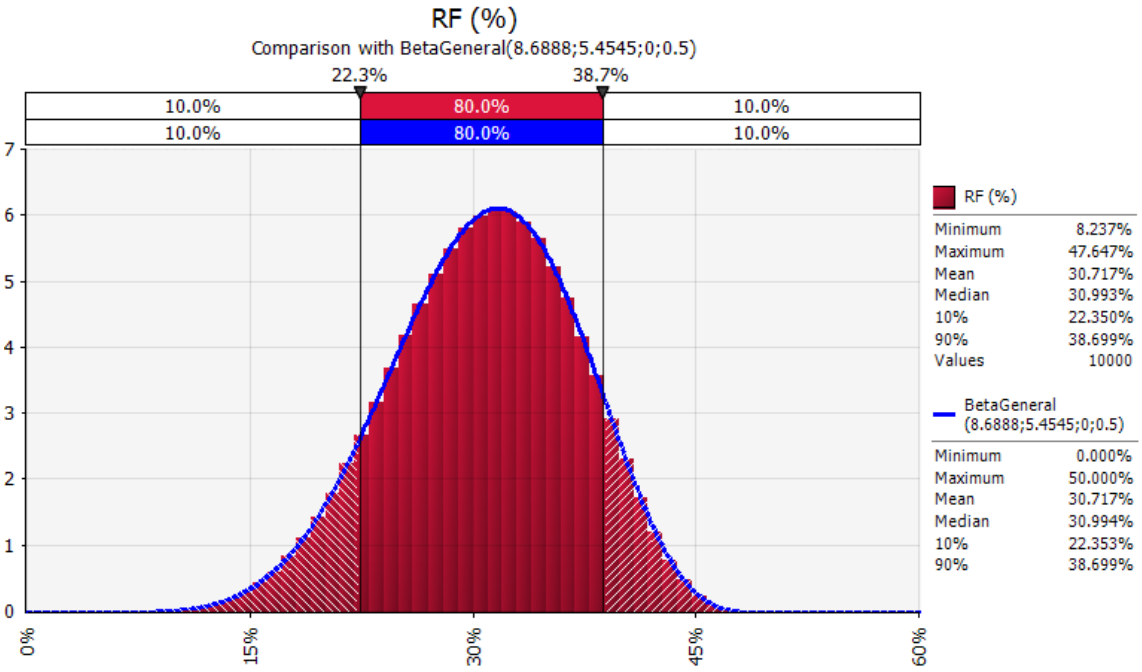

Fig. 80 – *RF* distribution at Jasper

6.3.6 – Results of the probabilistic analysis for Jasper

After all the inputs were set, and the output defined as the oil EUR then an @Risk simulation of 10,000 iterations was run using Latin Hypercube sampling. **Fig. 81** and **Fig. 82** show the resulting EUR distribution graphs for oil and associated gas, respectively:

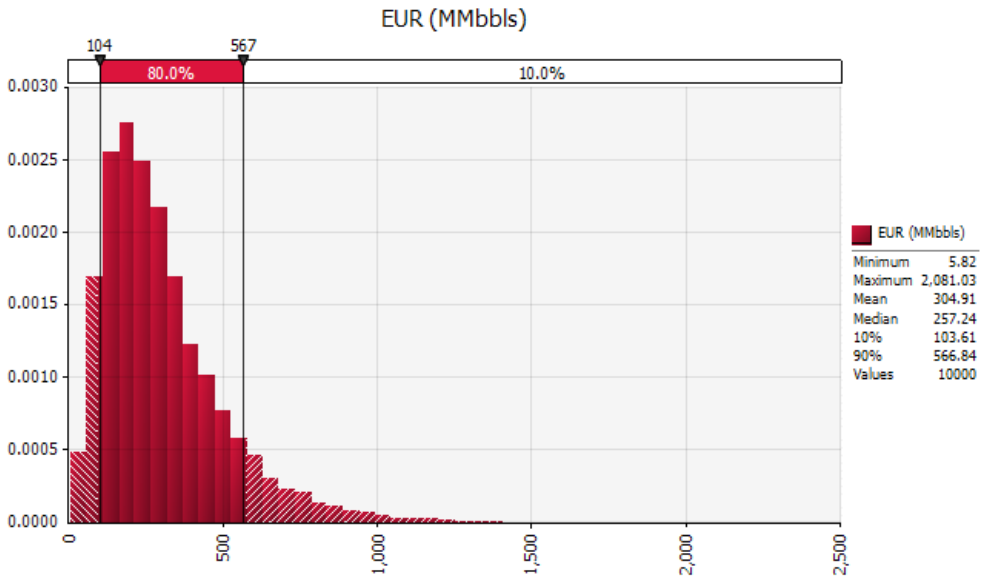

Fig. 81 – Jasper Oil EUR

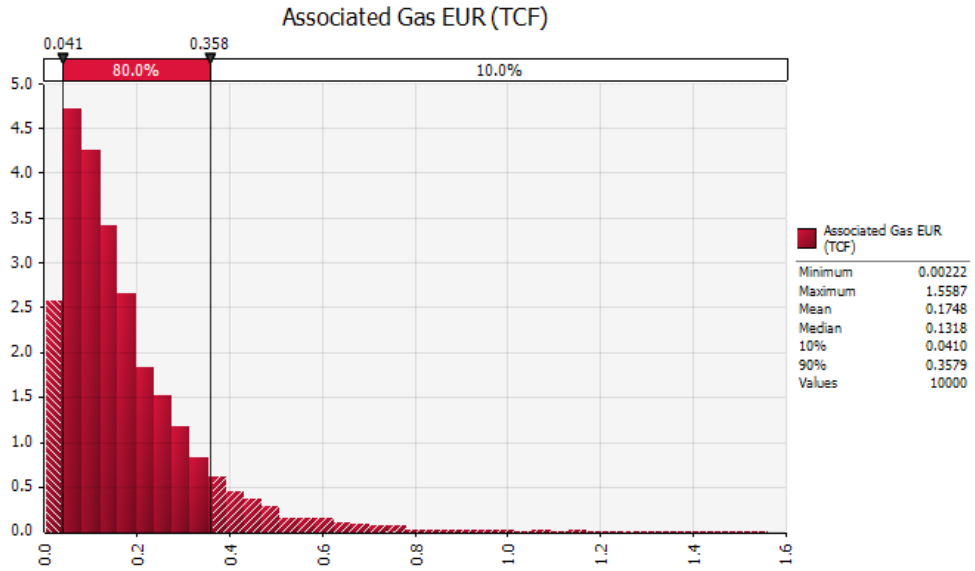

Fig. 82 – Jasper Associated Gas EUR

According to the Petroleum Resources Management System (SPE 2007), for this study case, the calculated resources can be classified as "Prospective Resources" and categorized as follows:

	Oil	Associated Gas
Low estimate Prospective Resources:	103.612 MMbbls	0.041 TCF
Best estimate Prospective Resources:	257.236 MMbbls	0.132 TCF
High estimate Prospective Resources:	566.839 MMbbls	0.358 TCF

Table 8 – Estimation of Jasper Prospective Resources

Sensibility Analysis

A tornado chart with the relative influence of the main variables on the oil EUR for this prospect is shown in **Fig. 83.**

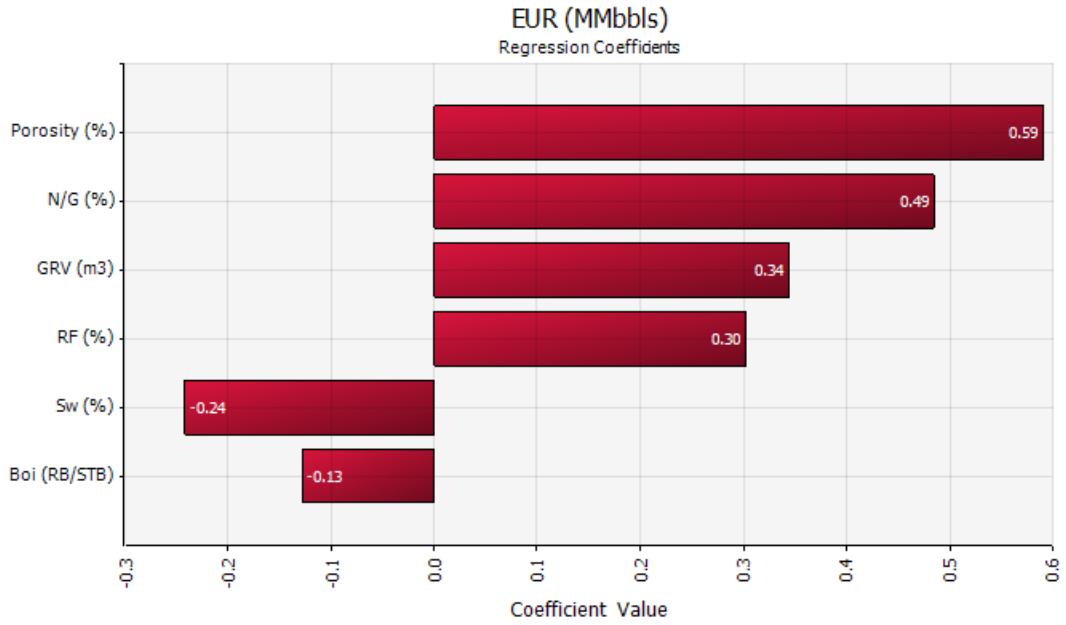

Fig. 83 – Tornado chart for Jasper Oil EUR

Fig. 84 shows a tornado chart with the relative influence of the main variables on the associated gas EUR for this prospect.

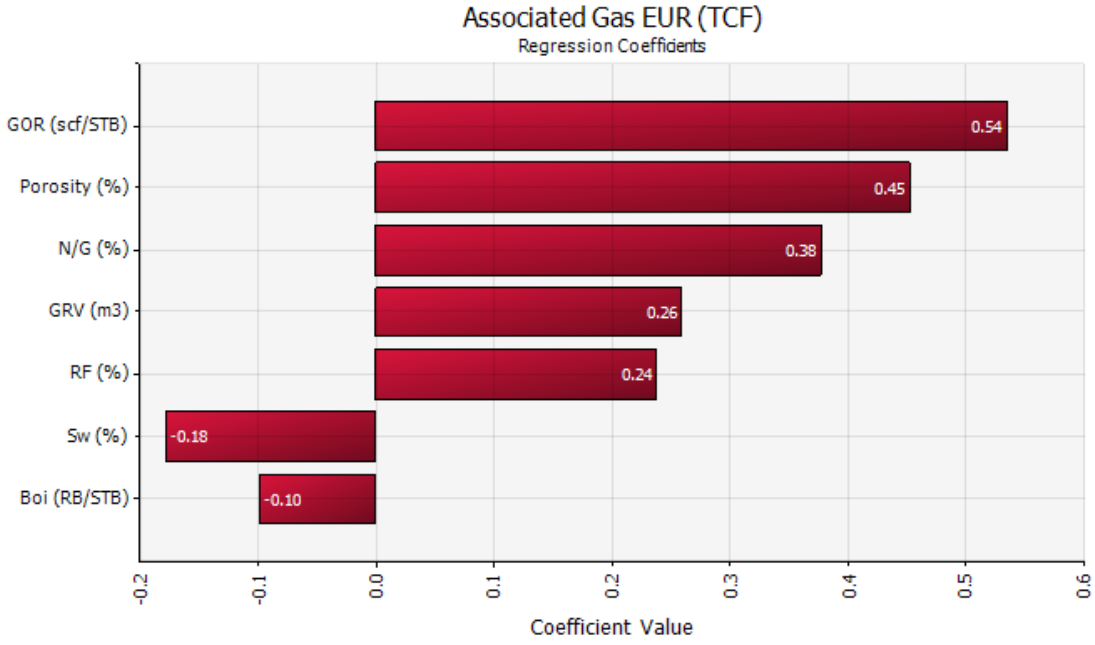

Fig. 84 – Tornado chart for Jasper Associated Gas EUR

From these tornado charts, it can be concluded that porosity and N/G are the parameters which oil EUR is most sensible to. On the other hand, for associated gas EUR, GOR is the most sensible parameter.
For this prospect, the uncertainty in GRV is not very significant and therefore it is not the input that has the greatest influence on the EUR calculation.

6.4 – Analysis of Prospect 4 – Emerald-Deep

Prospect Name: Emerald-Deep

Seismic Survey Used: UR13_3D

Source Rock: Marine Aptian shales

Reservoir: Confined Campanian-Maastrichtian turbidites

Seal: Maastrichtian shales

Trap: Combined stratigraphic-structural trap with an updip sealing fault

Migration: vertically through faults and laterally through carrier beds

6.4.1 – Interpretation of 3D seismic data

For this prospect approximately 600 km^2 of a 2,076 km^2 PSTM converted to depth, 3D seismic survey (UR13_3D survey shown in Fig. 3) were interpreted.

The structural map at top of the prospect, overlaid with a polygon that depicts its interpreted maximum extension, is shown in **Fig. 85.**

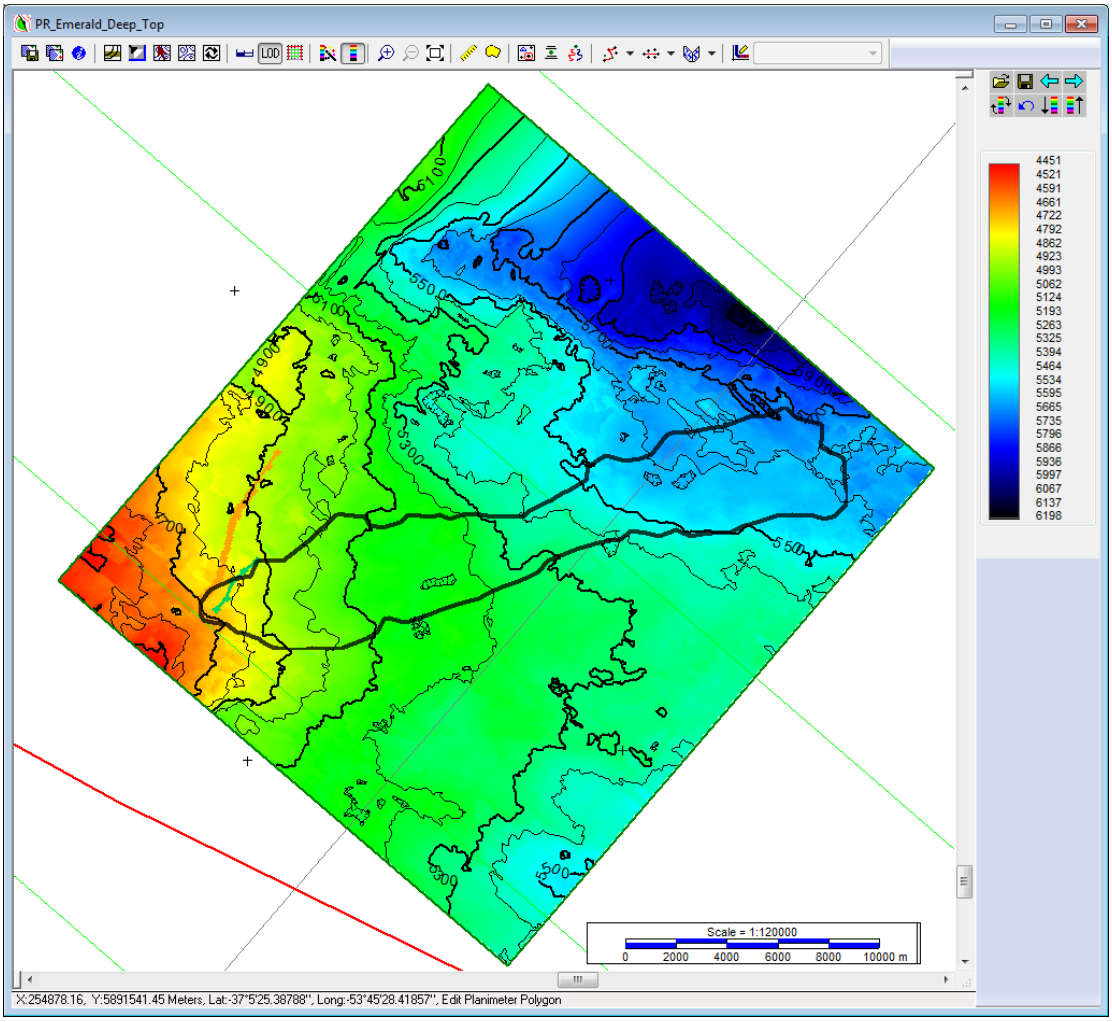

Fig. 85 – Structural map at the top of Emerald-Deep

An arbitrary seismic line through Emerald-Deep is shown in **Fig. 86.** The green horizon depicts the top of the prospect and the pink horizon its base.

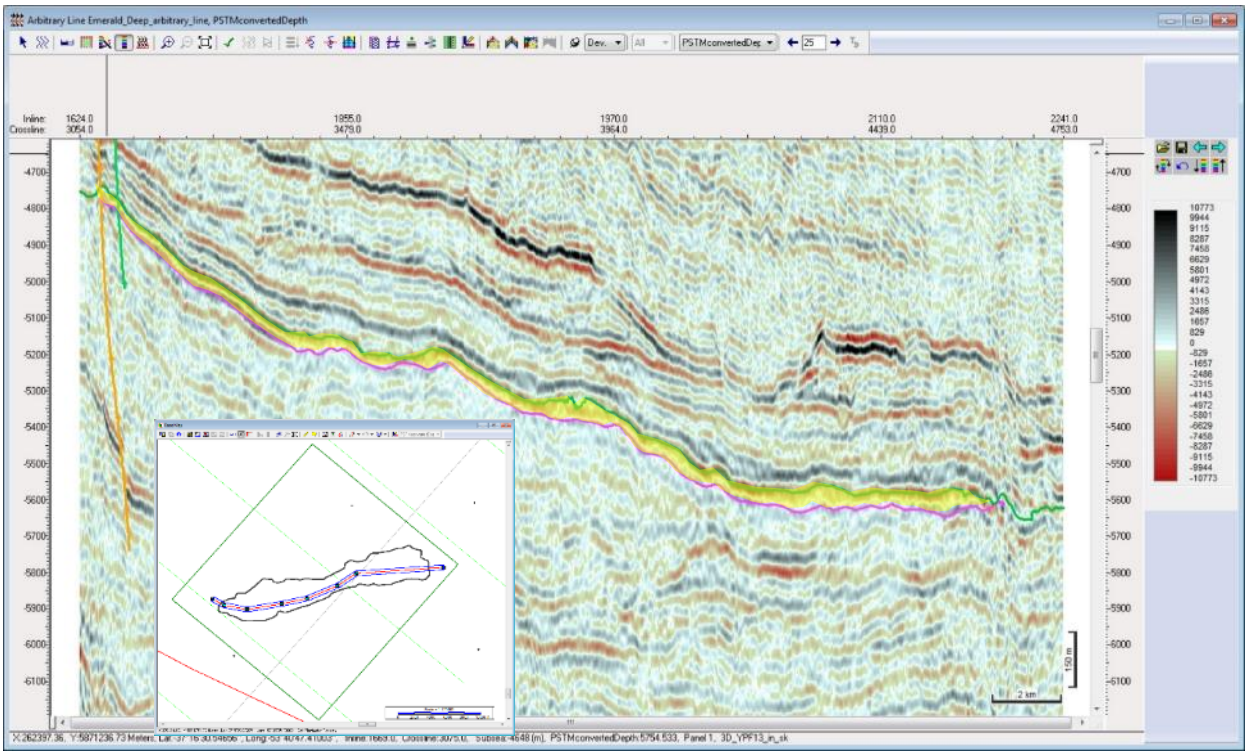

Fig. 86 – Arbitrary line along Emerald-Deep (courtesy of ANCAP)

The lobular shape of Emerald-Deep, in the transversal direction, is shown in **Fig. 87.**

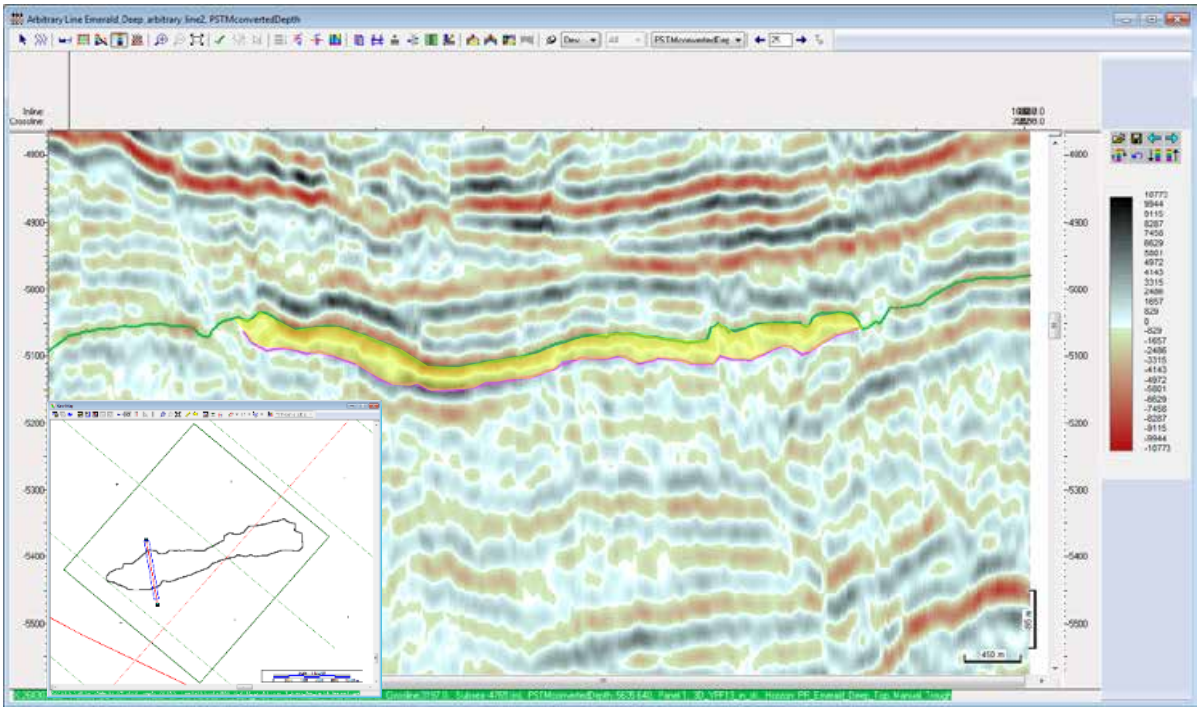

Fig. 87 – Arbitrary line across Emerald-Deep (courtesy of ANCAP)

Fig. 88 shows the different elements of the proposed petroleum system for the case of Emerald-Deep.

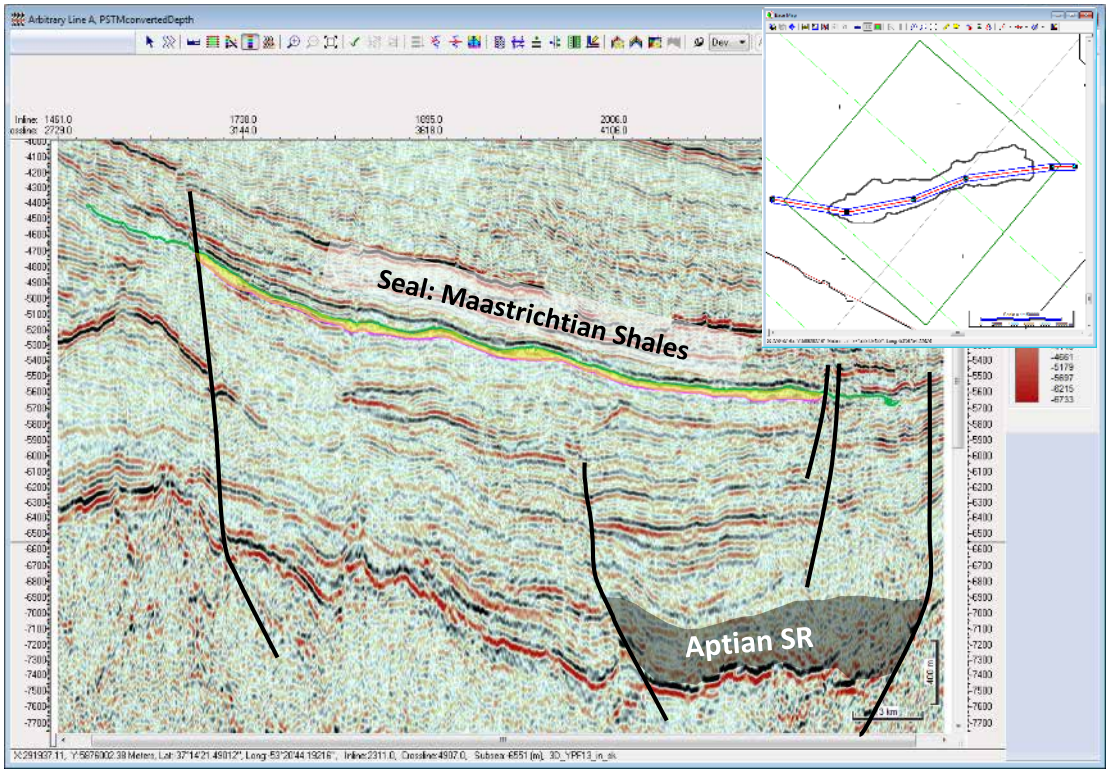

Fig. 88 – Arbitrary line through Emerald-Deep with interpreted petroleum system elements (courtesy of ANCAP)

Fig. 89 shows the seismic amplitude map at the top of the prospect, overlaid with, the contours of the structural map from Fig. 85 and the defined delimitation polygon that accounts for its maximum extension.

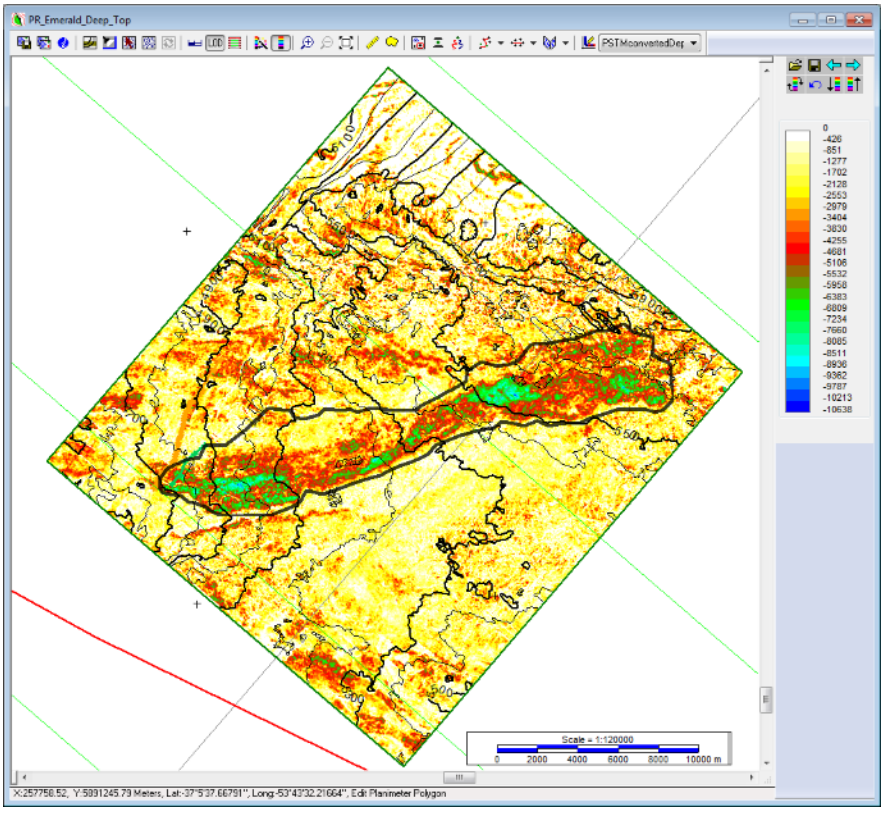

Fig. 89 – Amplitude map of Emerald-Deep

Fig. 90 shows the seismic amplitude map at the top of the prospect with its defined P10 delimitation polygon.

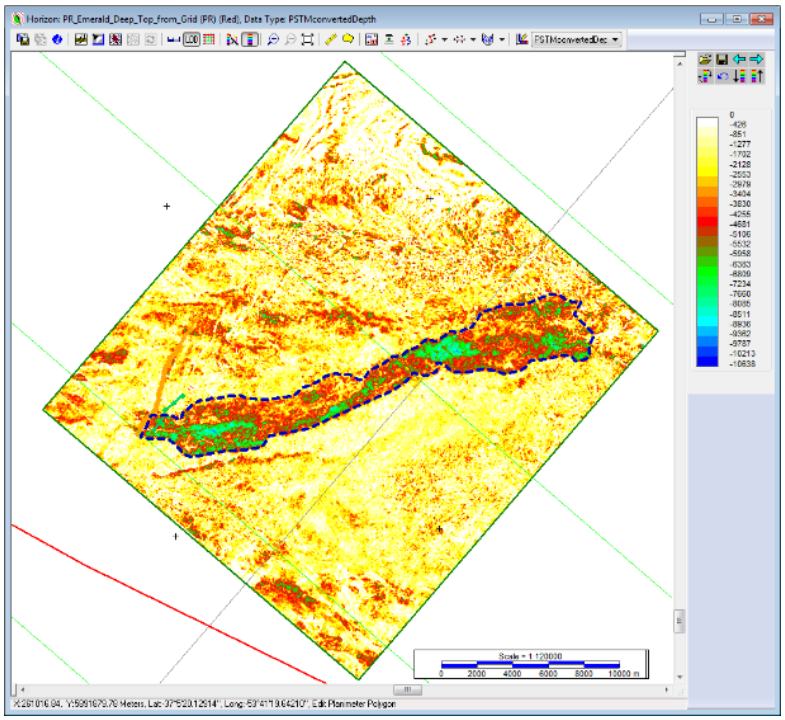

Fig. 90 – Amplitude map of Emerald-Deep with P10 polygon overlaid

Finally, **Fig. 91** shows the seismic amplitude map at the top of the prospect, but with a delimitation polygon showing its P90 extension:

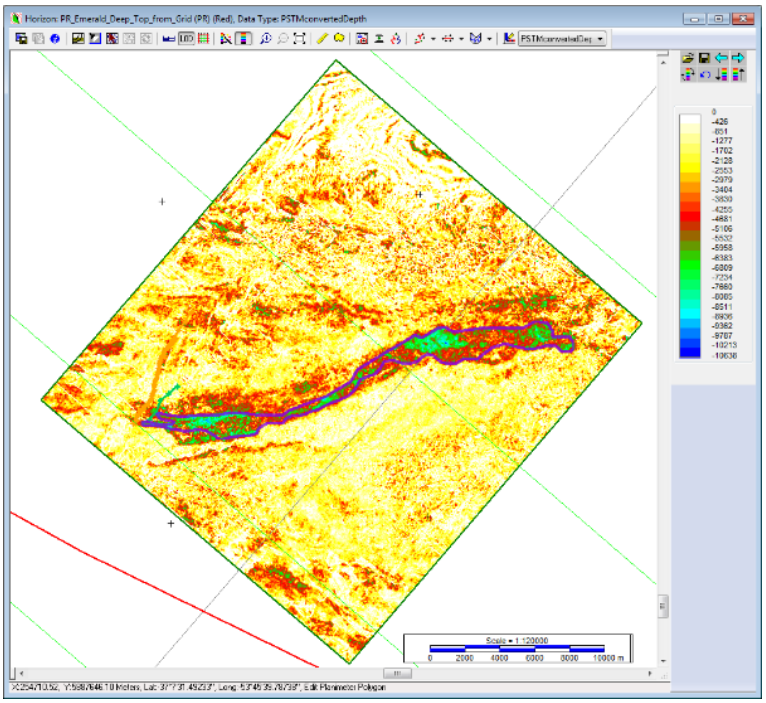

Fig. 91 – Amplitude map of Emerald-Deep with P90 polygon overlaid

The delimitation polygons shown in this study were used to restrict the volumetric calculation in order to get estimated values of a maximum, an optimistic (P10) and a conservative (P90) GRV.

From the interpretation of the seabed in the seismic data, it follows that this potential turbidite lies between a minimum and a maximum water depth of 1,250 m and 1,800 m, respectively **(Fig. 92).**

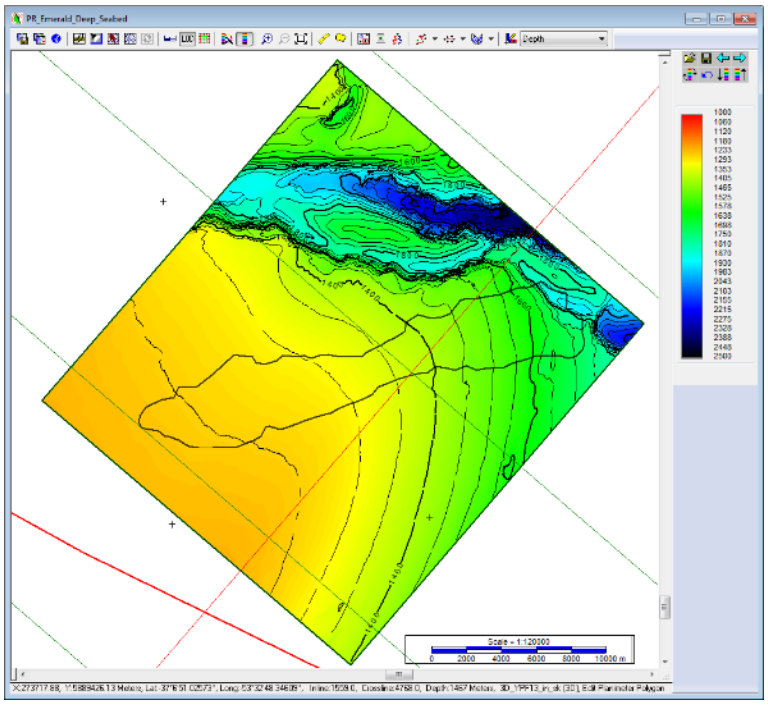

Fig. 92 – Seabed map at Emerald-Deep area of study

The sedimentary overburden is determined by subtracting the seabed grid with the grid that corresponds to the top of the prospect. In this case, this results in an overburden between 3,438 m to 4,197 m **(Fig. 93),** therefore, an average sedimentary overburden of 3,817.5 m was assumed for reservoir and oil properties estimation (porosity and B_{oi}).

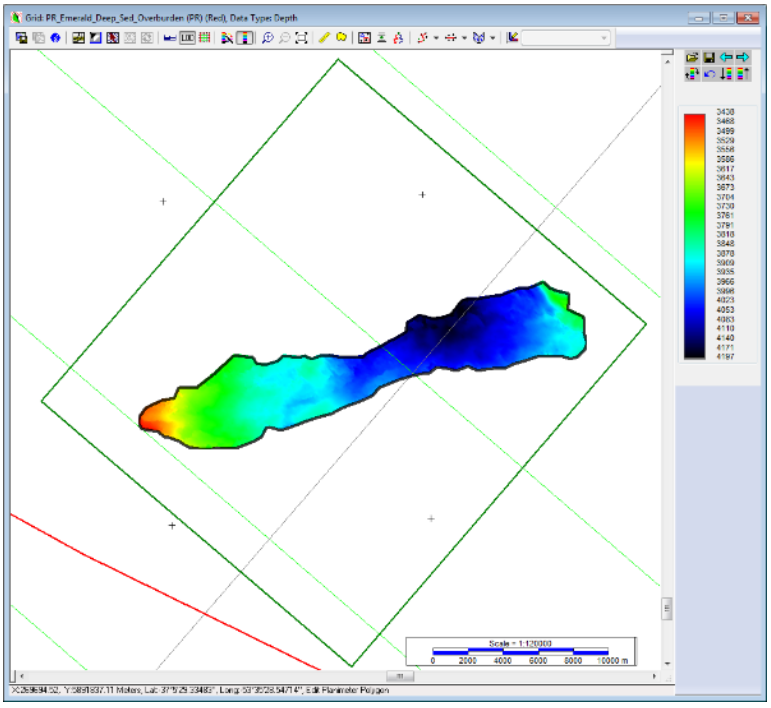

Fig. 93 – Sedimentary overburden map at Emerald-Deep

6.4.2 – Estimation of Oil Formation Volume Factor

In order to define a realistic probability distribution function for the initial formation volume factor (B_{oi}) the following assumptions were made:

- $T_{seabed} = 2.957$ °C, this temperature is obtained from the World Ocean Atlas (2013) at a point with coordinates: 53.63W, 37.38S.

- Geothermal Gradient = 30 °C/km, which is the worldwide average temperature gradient.

Considering these two assumptions the estimated average reservoir temperature is:

$$T_r = T_{seabed} + 30\frac{°C}{km} * 3.8175\ km = 117.48\ °C = 243.47\ °F$$

- Oil gravity was assumed 30°API ⇒ $\gamma_o = \frac{141.5}{121.5+30} \cong 0.93$

- Assuming $p_r > p_b$ and c_o negligible ⇒ $B_{oi} \cong B_{ob}$ ⇒ applying Levitan and Murtha (1999) correlation for B_{ob}:

$$B_{oi} \cong B_{ob} = 1 + 0.0005 * GOR * \left(\frac{\gamma_g}{\gamma_o}\right)^{0.25} + \frac{0.0004 * (T_r - 60)}{\gamma_o * \gamma_g}$$

Where T_r is reservoir temperature in °F.

For the case GOR=0 scf/STB then:

$$B_{oi} \cong 1 + 0.0005 * 0 * \left(\frac{0.8}{0.93}\right)^{0.25} + \frac{0.0004 * (243.47 - 60)}{0.93 * 0.8} = 1.10\ RB/STB$$

Finally, applying the same equation for the rest of the cases (see Table 2 for GOR values):

- GOR=248.7 scf/STB ⇒ $B_{oi} \cong 1.22$ RB/STB
- GOR=545.4 scf/STB ⇒ $B_{oi} \cong 1.36$ RB/STB
- GOR=935.2 scf/STB ⇒ $B_{oi} \cong 1.55$ RB/STB
- GOR=2,000 scf/STB ⇒ $B_{oi} \cong 2.06$ RB/STB

These values are used to define Emerald-Deep PDF for oil formation volume factor.

6.4.3 – Estimation of Porosity

For the case of Emerald-Deep, which is approximately beneath 3.8175 km of sediments, the porosity values obtained through the equations derived from Ehrenberg and Nadeau (2005) analysis give the following results:

$$\varphi_{P90} = -0.0917 * (3.8175)^2 - 0.8773 * (3.8175) + 14.019 = 9.0\%$$

$$\varphi_{P50} = -0.0191 * (3.8175)^2 - 2.2925 * (3.8175) + 23.457 = 14.4\%$$

$$\varphi_{P10} = -0.0636 * (3.8175)^2 - 1.863 * (3.8175) + 31.309 = 24.0\ \%$$

These values are used to define Emerald-Deep PDF for porosity.

6.4.4 – Computation of Gross Rock Volume

The GRV reports created by IHS Kingdom, using the surfaces interpreted for the top and base of Emerald-Deep and the three different restriction polygons, are as follows:

- Maximum Case:

```
Volumetric Model:          Single Structure
Grid:      PR_Emerald-Deep_Top
Polygons Used:   PR_Emerald-Deep_P01
Lower Contact:   PR_Emerald-Deep_Base

Polygon PR_Emerald-Deep_P01
-------------------------------------------------
Polygon Area:     87.3891    10^6 M2
Polygon Area within the Grid(s):     85.9993    10^6 M2
Gross Volume:     3,251.8062    10^6 M3
```

- Optimistic Case:

```
Volumetric Model:          Single Structure
Grid:      PR_Emerald-Deep_Top
Polygons Used:   PR_Emerald-Deep_P10
Lower Contact:   PR_Emerald-Deep_Base

Polygon PR_Emerald-Deep_P10
-------------------------------------------------
Polygon Area:     60.9347    10^6 M2
Polygon Area within the Grid(s):     60.7756    10^6 M2
Gross Volume:     2,422.5214    10^6 M3
```

- Conservative Case

```
Volumetric Model:          Single Structure
Grid:      PR_Emerald-Deep_Top
Polygons Used:   PR_Emerald-Deep_P90
Lower Contact:   PR_Emerald-Deep_Base

Polygon PR_Emerald_Deep_P90
-------------------------------------------------
Polygon Area:     24.0361    10^6 M2
Polygon Area within the Grid(s):     24.0361    10^6 M2
Gross Volume:     979.5454    10^6 M3
```

This variable, GRV, is defined as a LogNormal distribution, therefore three parameters are required in @Risk for its definition: P10, P50 and P90 values. The P50 value is calculated, as a function of the P10 and P90 values using the formula: $\mathrm{P50} = \mathrm{e}^{(\mathrm{LN(P90)+LN(P10)})/2}$ (Wright 2015).

For the case of Emerald-Deep, this results in a P50 value for *GRV* = 1,540,444,642 m^3.

6.4.5 – Inputs used for the probabilistic analysis of Emerald-Deep

A summary of the inputs used for the probabilistic volumetric analysis of Emerald-Deep, based on the previous results, is shown in **Table 9.**

Parameter	MIN	Low Estimate	Best Estimate	High Estimate	MAX	Distr. Type
GRV (m^3)	0	979,545,400	1,540,444,642	2,422,521,400	3,251,806,200	LogNormal
N/G (%)	0	34.8%	66.6%	90%	100%	Beta
Phi (%)	0	9.0%	14.4%	24.0%	48%	Beta
S_w (%)	0	10.3%	23.4%	41.6%	100%	Beta
GOR (scf/STB)	0	248.7	545.4	935.2	2,000	Beta
B_{oi} (RB/STB)	1.10	1.22	1.36	1.55	2.06	Beta
RF (%)	0	22.4%	31%	38.7%	50%	Beta

Table 9 – Reservoir and fluid properties used for the volumetric analysis of Emerald-Deep

The following figures (**Fig. 94** to **Fig. 100**) show the detail of the input distributions defined in @Risk and its simulation results:

- Gross Rock Volume:

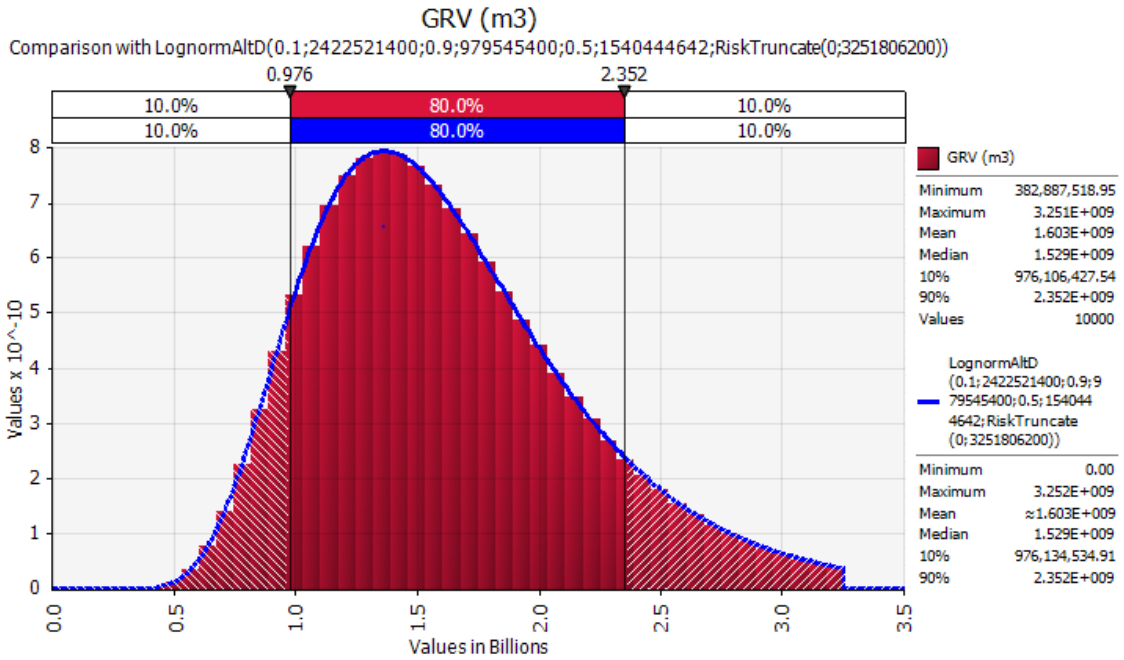

Fig. 94 – *GRV* distribution of Emerald-Deep

- Net to Gross:

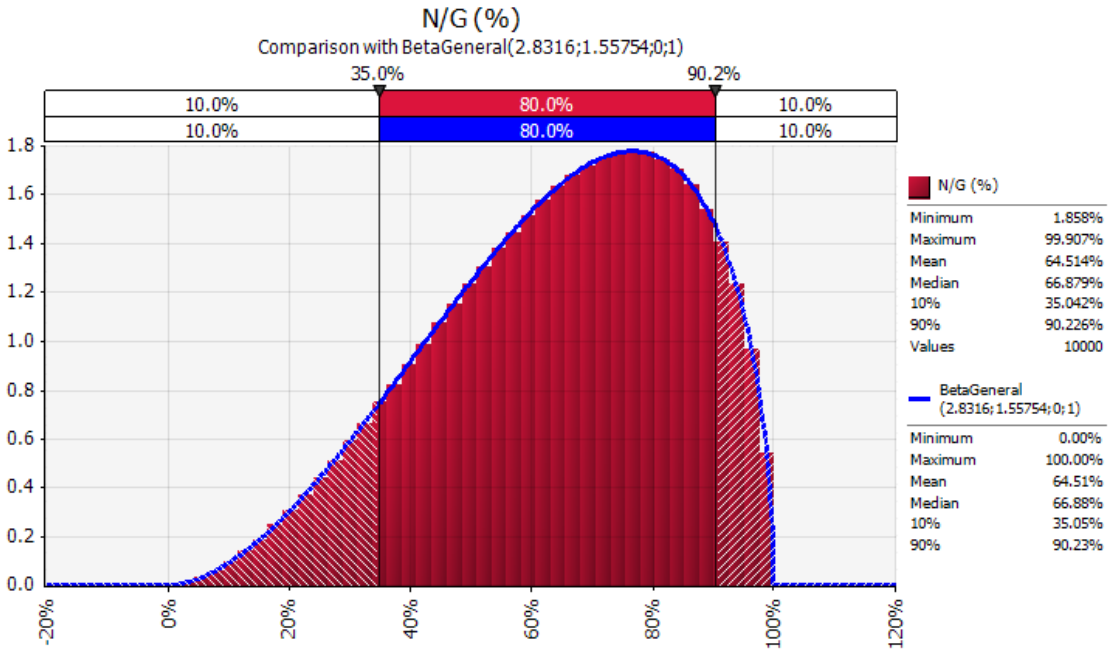

Fig. 95 – *N/G* distribution at Emerald-Deep

- Porosity:

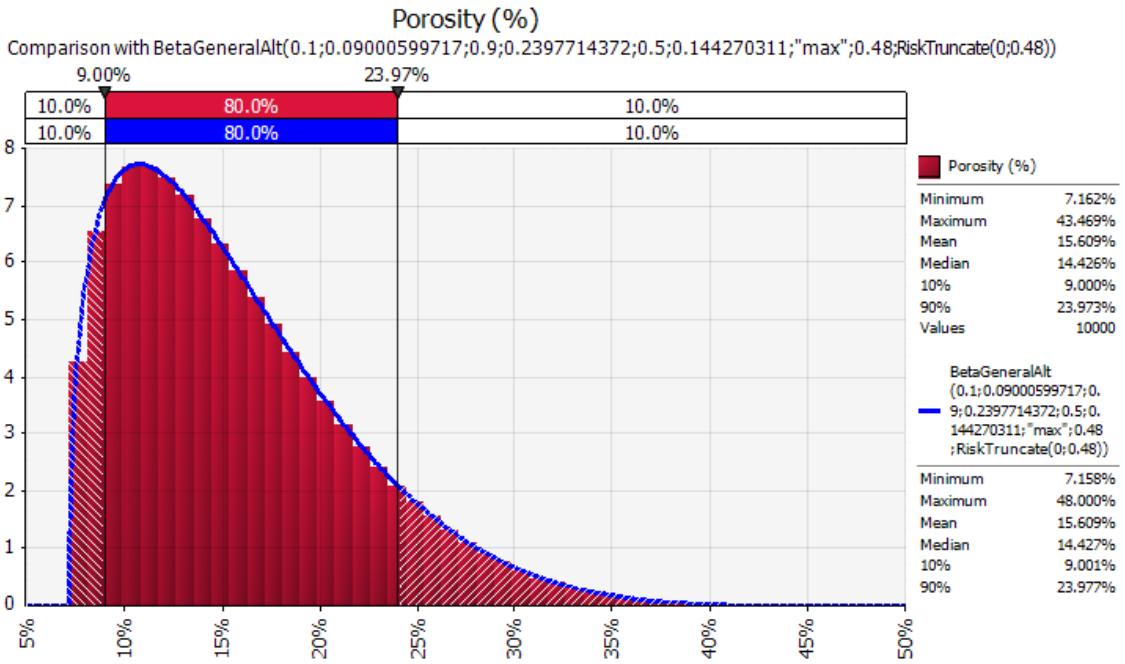

Fig. 96 – Porosity distribution at Emerald-Deep

- Water Saturation:

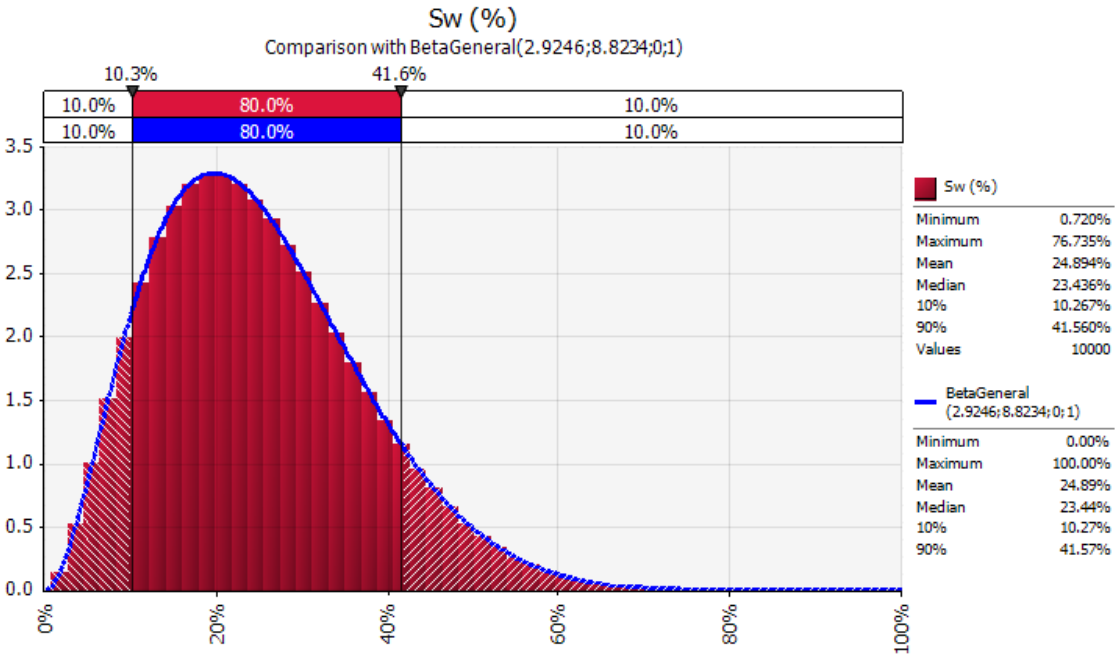

Fig. 97 – *Sw* distribution at Emerald-Deep

- Gas/Oil Ratio:

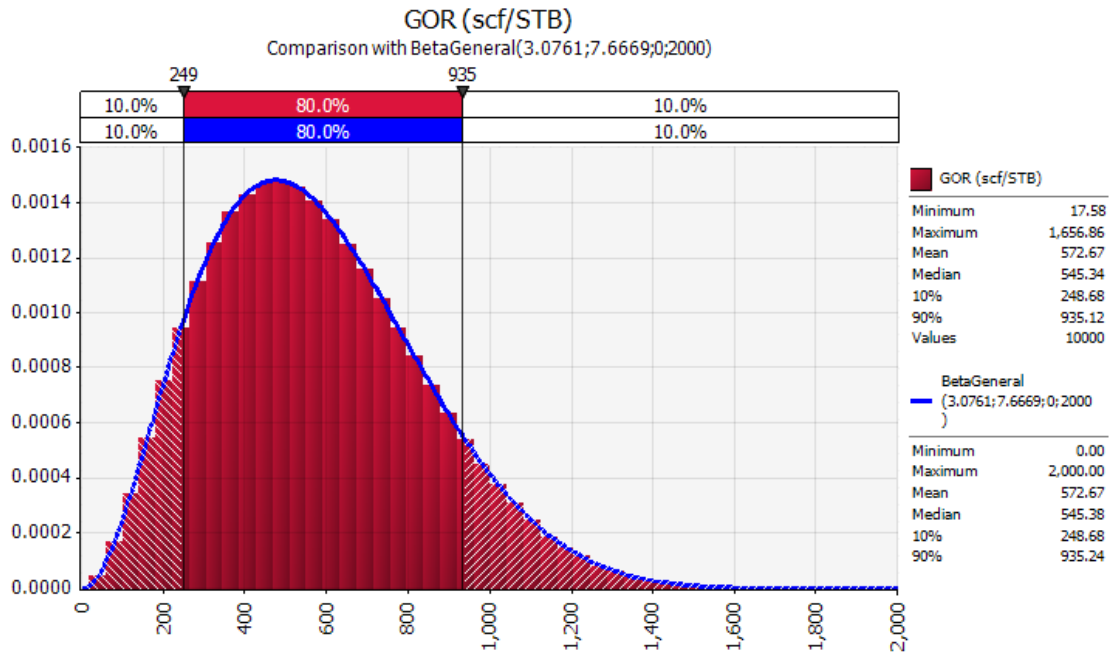

Fig. 98 – *GOR* distribution at Emerald-Deep

- Initial formation volume factor:

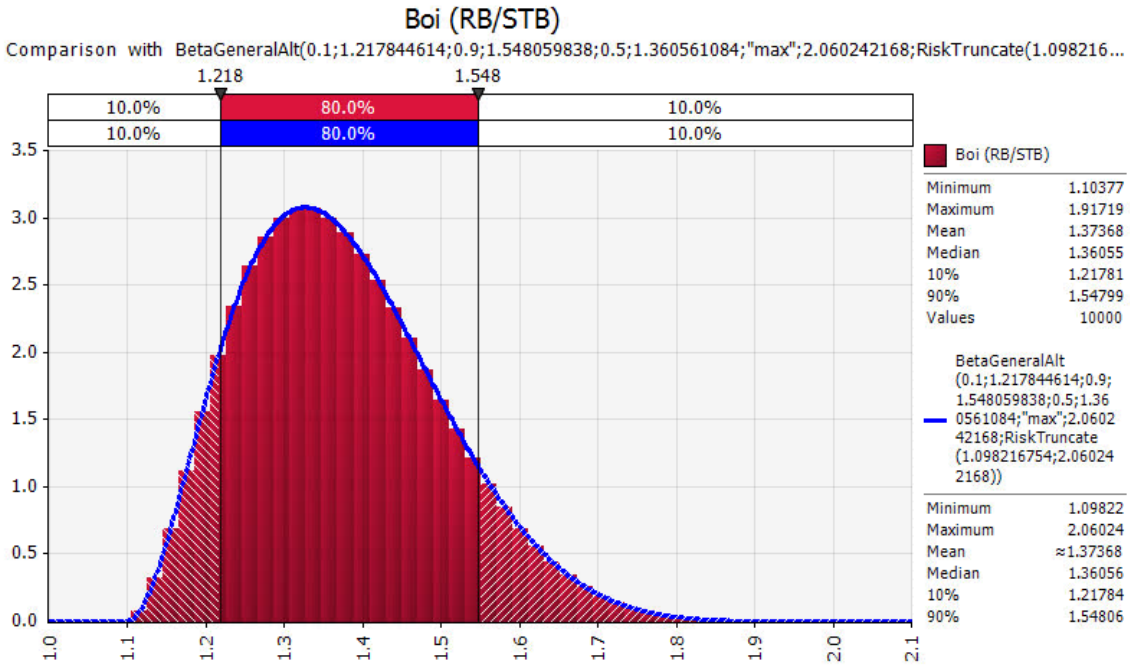

Fig. 99 – *Boi* distribution at Emerald-Deep

- Recovery Factor:

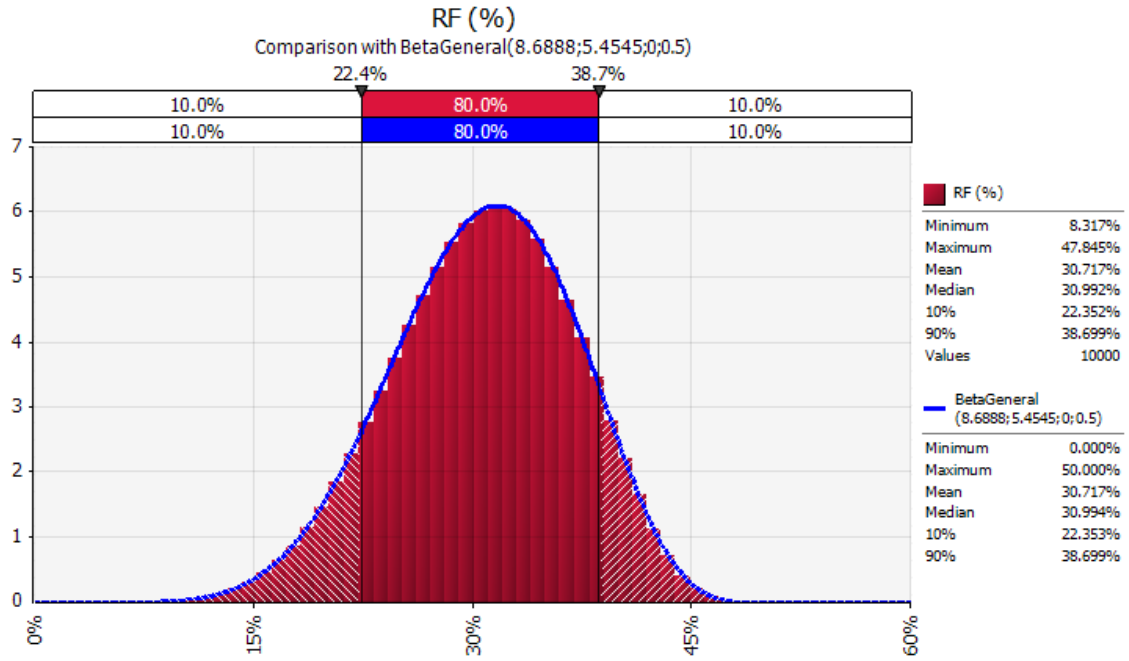

Fig. 100 – *RF* distribution at Emerald-Deep

6.4.6 – Results of the probabilistic analysis for Emerald-Deep

After all the inputs were set, and the output defined as the oil EUR then an @Risk simulation of 10,000 iterations was run using Latin Hypercube sampling. **Fig. 101** and **Fig. 102** show the resulting EUR distribution graphs for oil and associated gas, respectively:

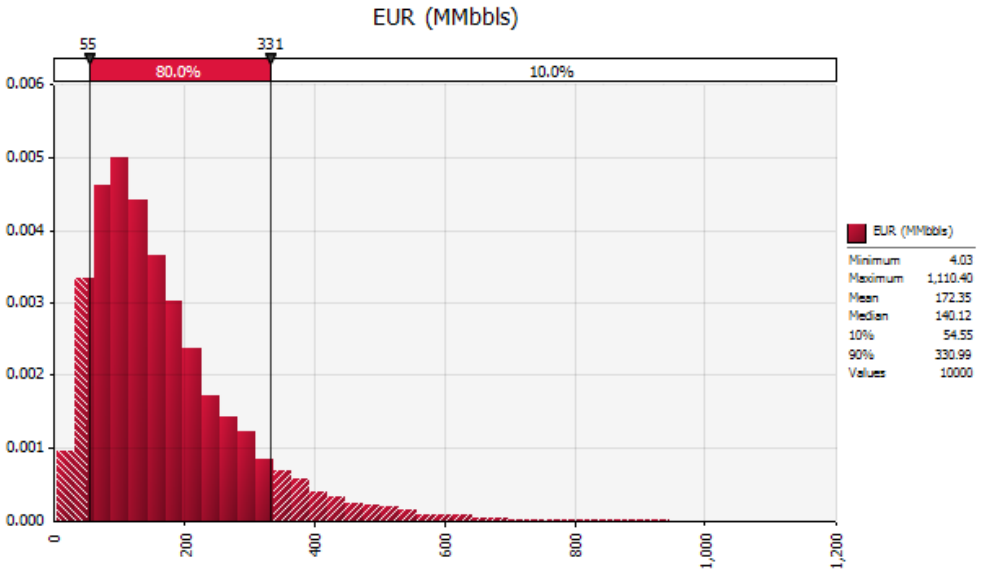

Fig. 101 – Emerald-Deep Oil EUR

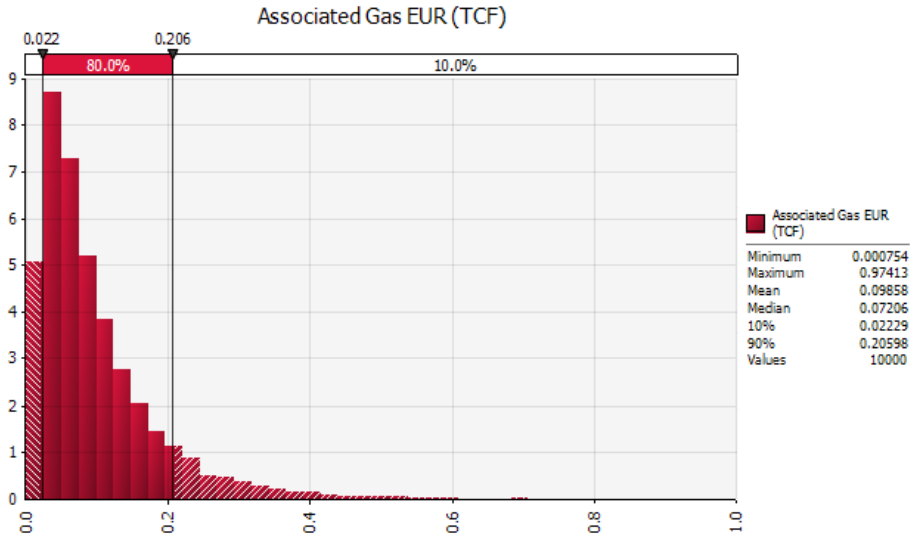

Fig. 102 – Emerald-Deep Associated Gas EUR

According to the Petroleum Resources Management System (SPE 2007), for this study case, the calculated resources can be classified as "Prospective Resources" and categorized as follows:

	Oil	Associated Gas
Low estimate Prospective Resources:	54.548 MMbbls	0.022 TCF
Best estimate Prospective Resources:	140.121 MMbbls	0.072 TCF
High estimate Prospective Resources:	330.994 MMbbls	0.206 TCF

Table 10 – Estimation of Emerald-Deep Prospective Resources

Sensibility Analysis

A tornado chart with the relative influence of the main variables on the oil EUR for this prospect is shown in **Fig. 103.**

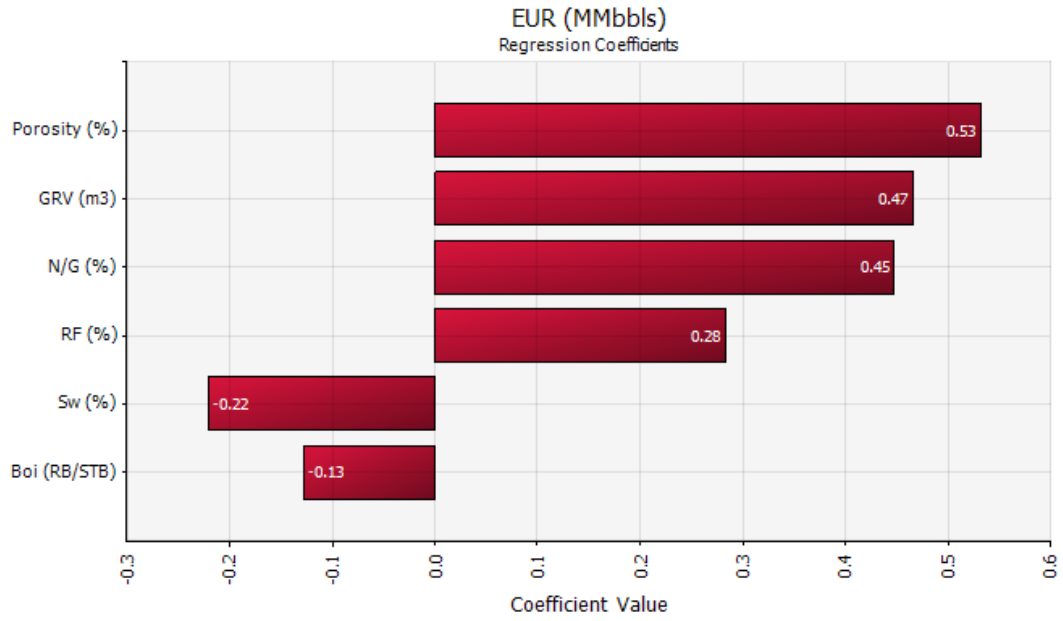

Fig. 103 – Tornado chart for Emerald-Deep Oil EUR

Fig. 104 shows a tornado chart with the relative influence of the main variables on the associated gas EUR for this prospect.

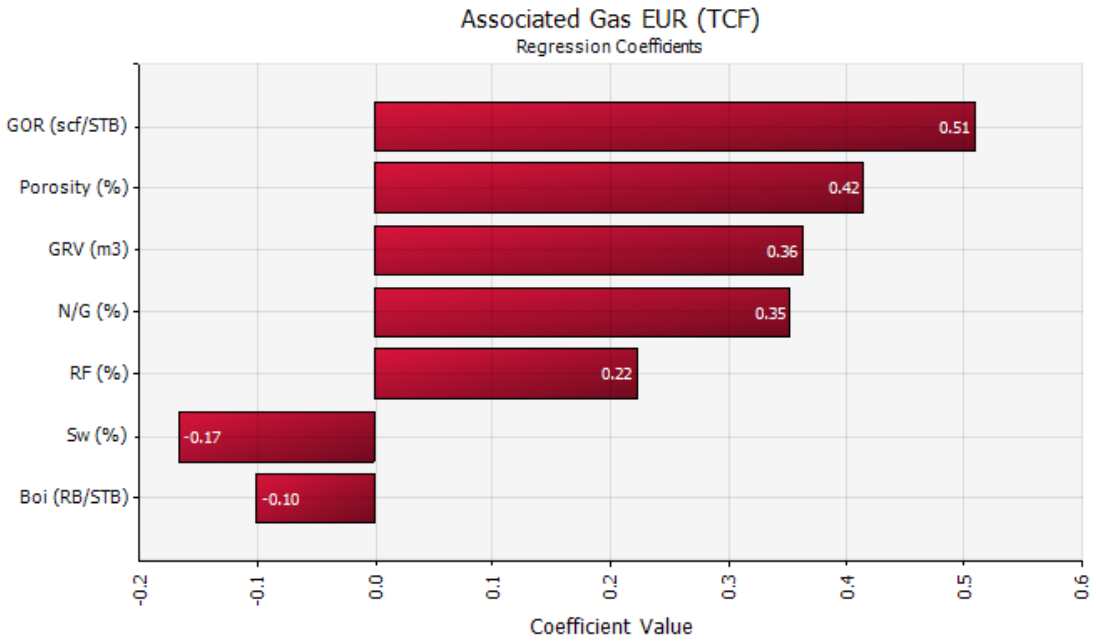

Fig. 104 – Tornado chart for Emerald-Deep Associated Gas EUR

From these tornado charts, it can be concluded that porosity, GRV and N/G are the parameters which oil EUR is most sensible to. On the other hand, for associated gas EUR, GOR is the most sensible parameter.
For this prospect, the uncertainty in GRV variable is significant but it is not the input that has the greatest influence on the EUR calculation.

6.5 – Analysis of Prospect 5 – Emerald

Prospect Name: Emerald

Seismic Survey Used: UR13_3D

Source Rock: Marine Aptian shales

Reservoir: Confined Campanian-Maastrichtian turbidites

Seal: Maastrichtian-Paleocene regional shales

Trap: Combined stratigraphic-structural trap with updip sealing faults

Migration: vertically through faults and laterally through carrier beds

6.5.1 – Interpretation of 3D seismic data

For this prospect approximately 600 km^2 of a 2,076 km^2 PSTM converted to depth, 3D seismic survey (UR13_3D survey shown in Fig. 3) were interpreted.

The structural map at top of the prospect, overlaid with a polygon that depicts its interpreted maximum extension, is shown in **Fig. 105.**

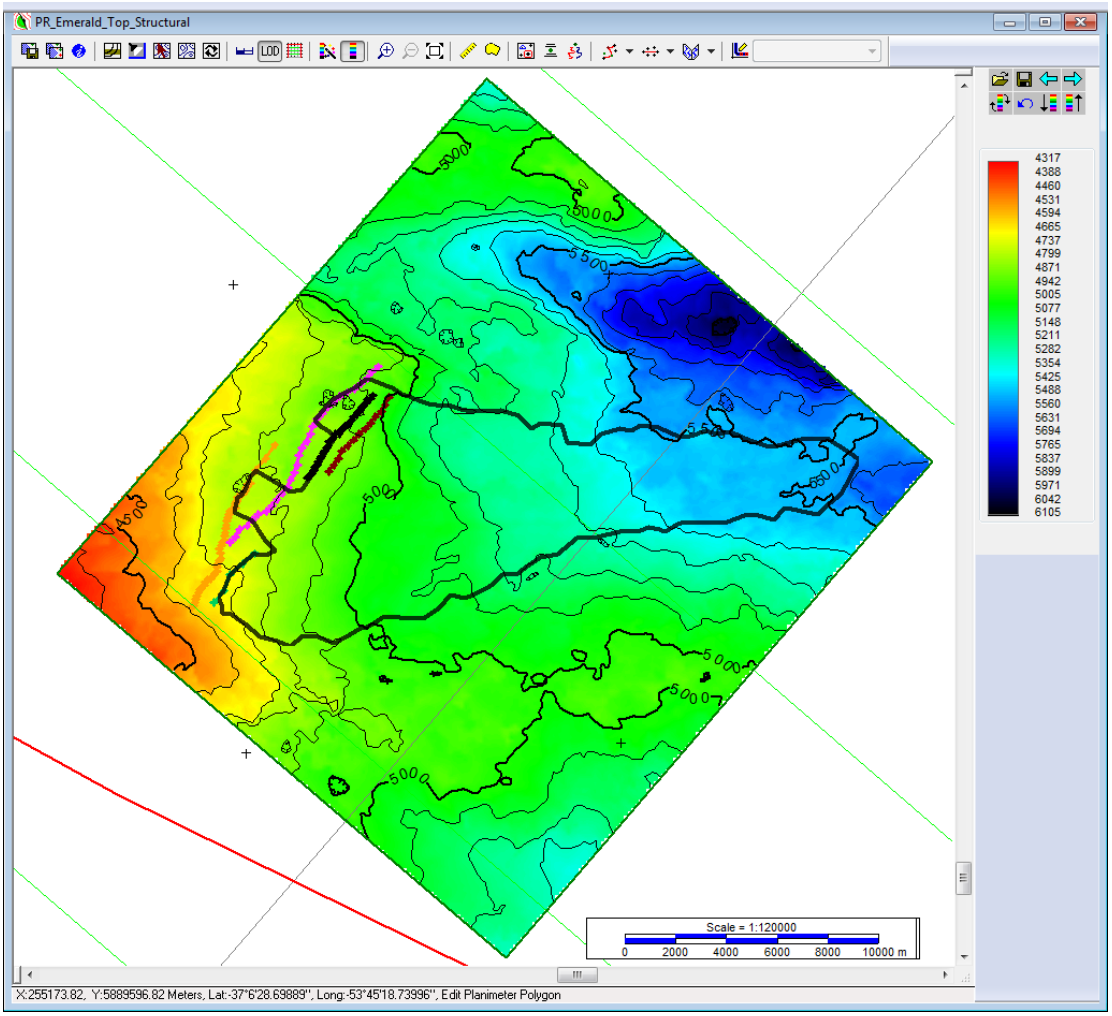

Fig. 105 – Structural map at the top of Emerald

An arbitrary seismic line through Emerald-Deep is shown in **Fig. 106.** The green horizon depicts the top of the prospect and the pink horizon its base.

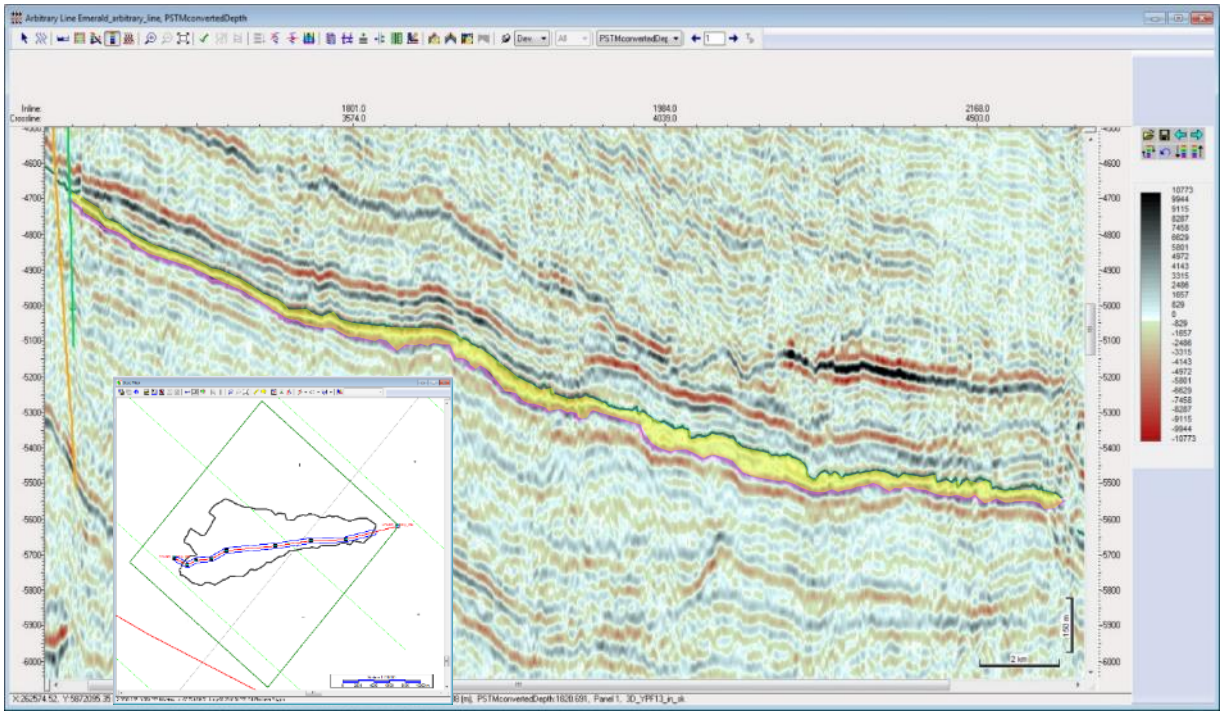

Fig. 106 – Arbitrary line along Emerald (courtesy of ANCAP)

The lobular shape of Emerald, in the transversal direction, is shown in **Fig. 107.**

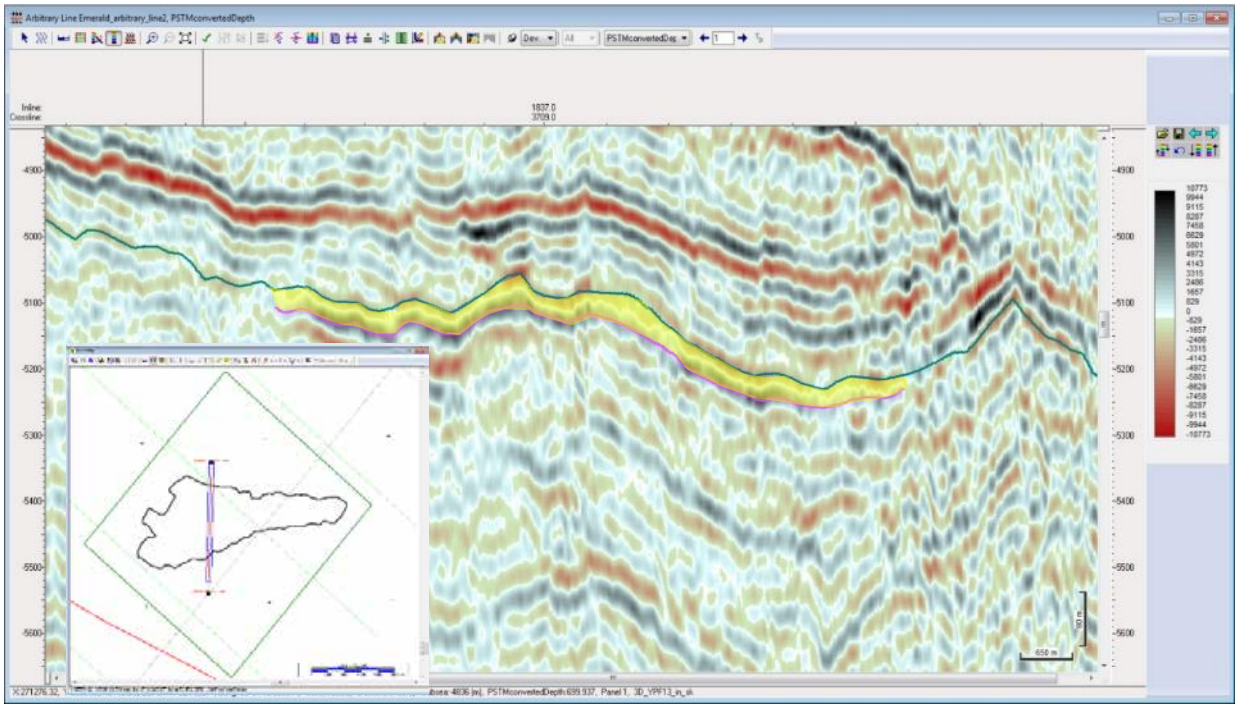

Fig. 107 – Arbitrary line across Emerald (courtesy of ANCAP)

Fig. 108 shows the different elements of the proposed petroleum system for the case of Emerald.

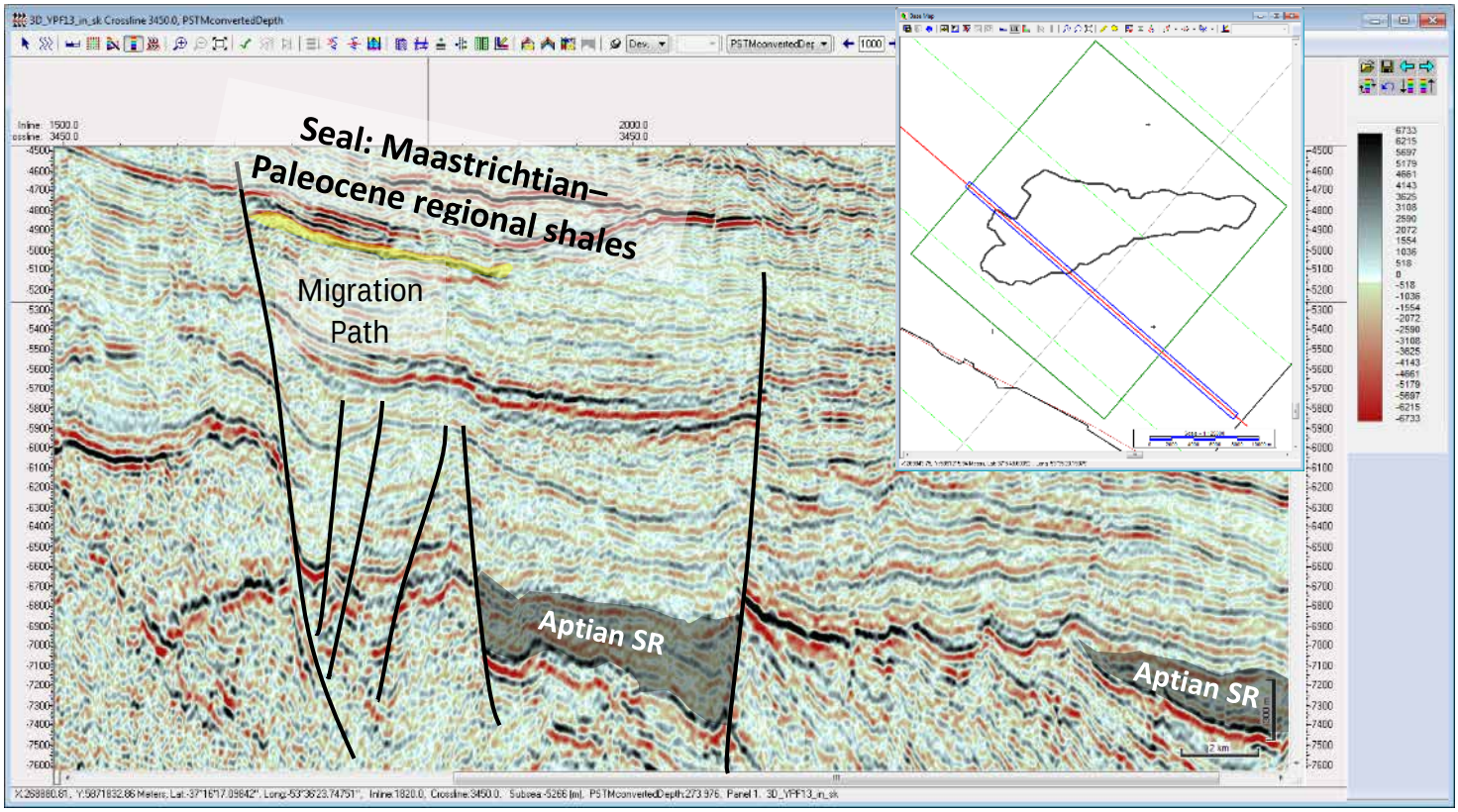

Fig. 108 – Crossline through Emerald with interpreted petroleum system elements (courtesy of ANCAP)

Fig. 109 shows the seismic amplitude map at the top of the prospect, overlaid with, the contours of the structural map from Fig. 105 and the defined delimitation polygon that accounts for its maximum extension.

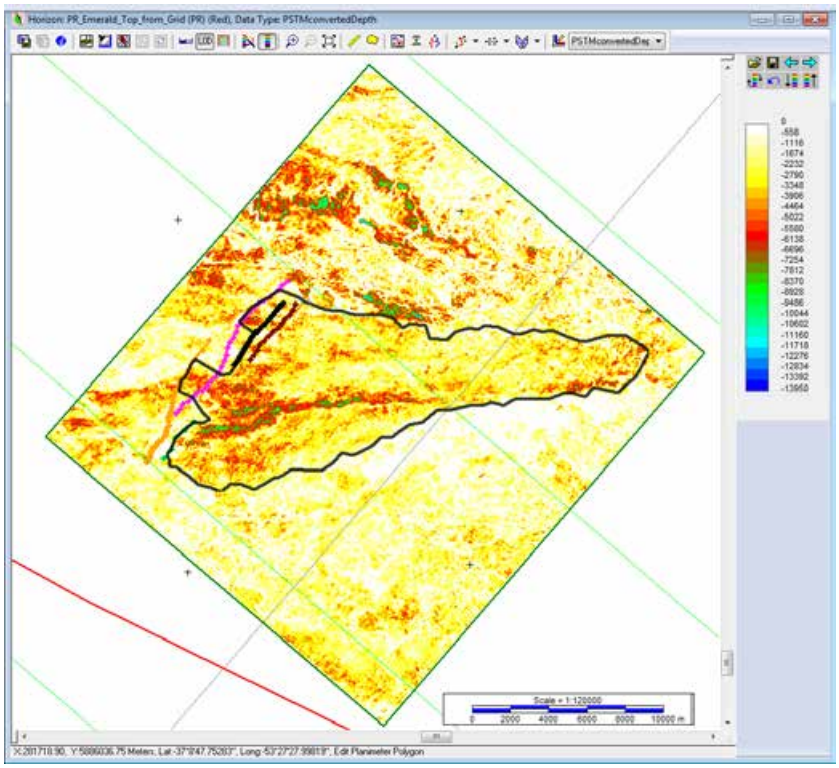

Fig. 109 – Amplitude map of Emerald

Fig. 110 shows the seismic amplitude map at the top of the prospect with its defined P10 delimitation polygon.

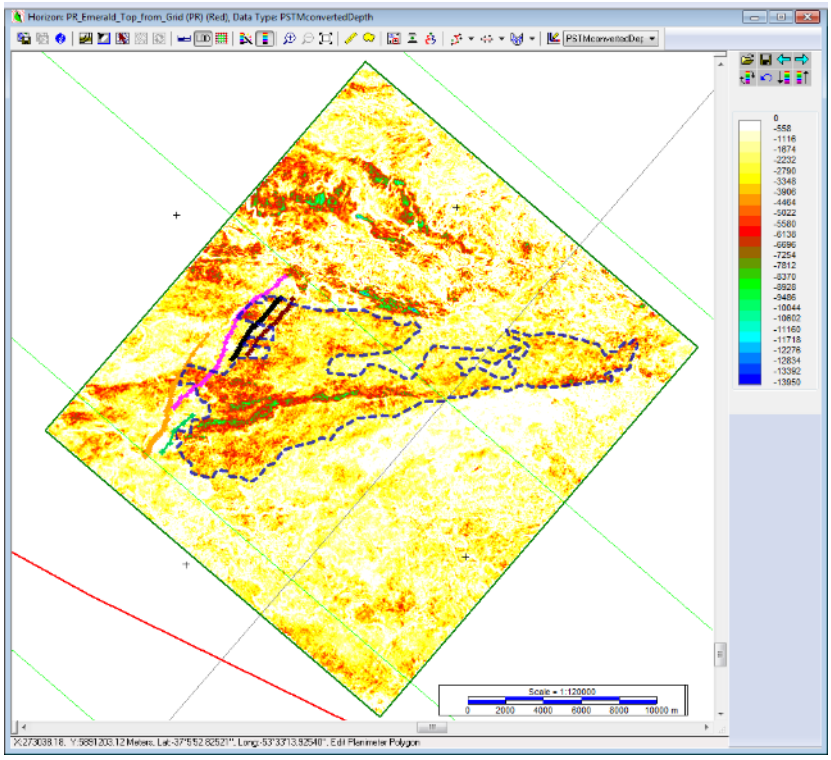

Fig. 110 – Amplitude map of Emerald with P10 polygon overlaid

Finally, **Fig. 111** shows the seismic amplitude map at the top of the prospect, but with a delimitation polygon showing its P90 extension:

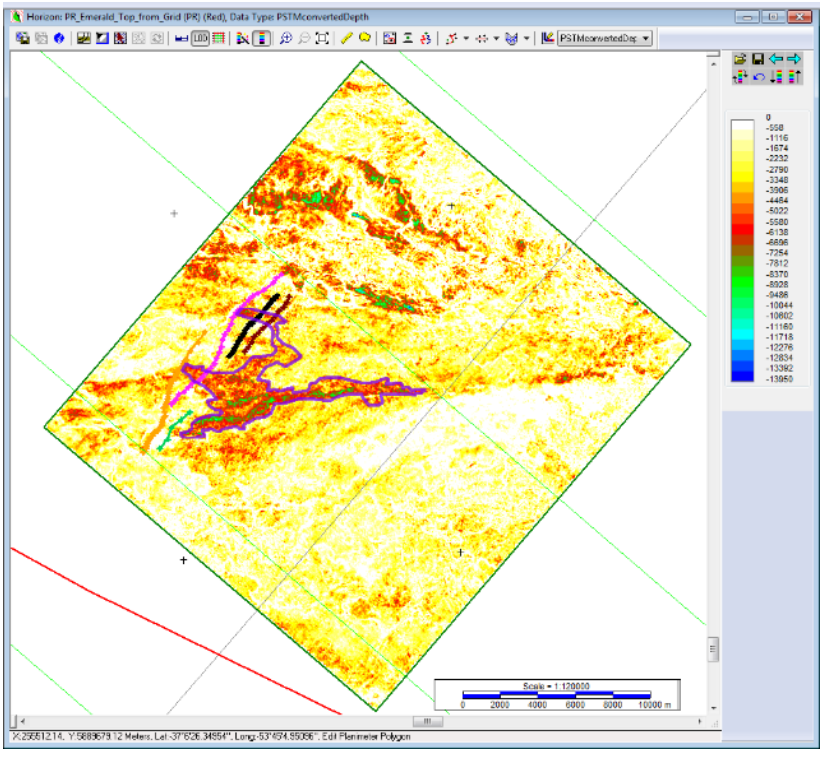

Fig. 111 – Amplitude map of Emerald with P90 polygon overlaid

The delimitation polygons shown in this study were used to restrict the volumetric calculation in order to get estimated values of a maximum, an optimistic (P10) and a conservative (P90) GRV.

From the interpretation of the seabed in the seismic data, it follows that this potential turbidite lies between a minimum and a maximum water depth of 1,250 m and 1,800 m, respectively **(Fig. 112).**

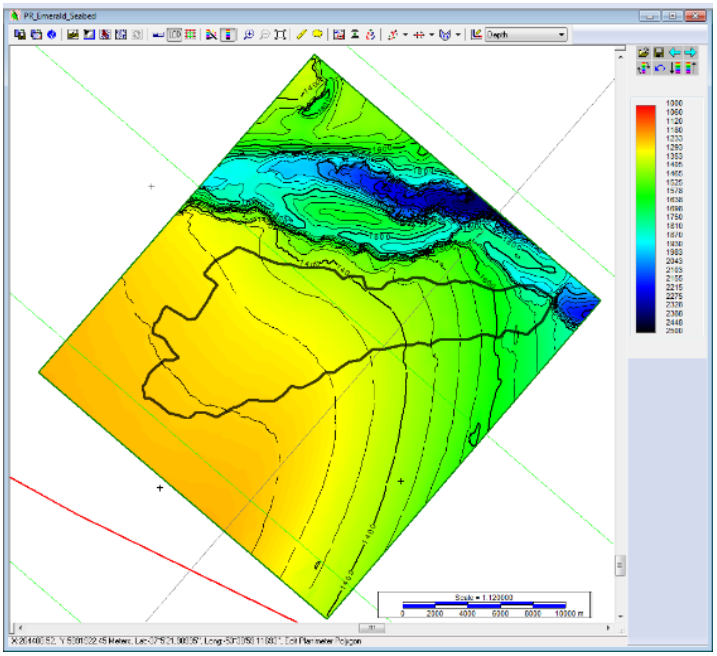

Fig. 112 – Seabed map at Emerald area of study

The sedimentary overburden is determined by subtracting the seabed grid with the grid that corresponds to the top of the prospect. In this case, this results in an overburden between 3,422m to 4,077 m **(Fig. 113),** therefore, an average sedimentary overburden of 3,749.5 m was assumed for reservoir and oil properties estimation (porosity and B_{oi}).

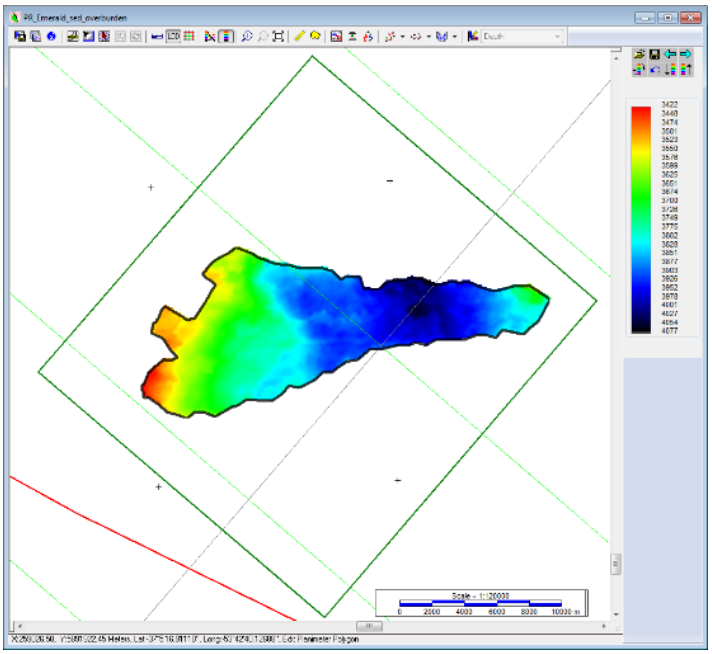

Fig. 113 – Sedimentary overburden at Emerald

6.5.2 – Estimation of Oil Formation Volume Factor

In order to define a realistic probability distribution function for the initial formation volume factor (B_{oi}) the following assumptions were made:

- $T_{seabed} = 2.957\ ^{\circ}\text{C}$, this temperature is obtained from the World Ocean Atlas (2013) at a point with coordinates: 53.63W, 37.38S.

- Geothermal Gradient = $30\ ^{\circ}\text{C/km}$, which is the worldwide average temperature gradient.

Considering these two assumptions, the estimated average reservoir temperature is:

$$T_r = T_{seabed} + 30\frac{^{\circ}\text{C}}{\text{km}} * 3.7495\ \text{km} = 115.44\ ^{\circ}\text{C} = 239.8\ ^{\circ}\text{F}$$

- Oil gravity was assumed 30°API $\Rightarrow \gamma_o = \frac{141.5}{121.5+30} \cong 0.93$

- Assuming $p_r > p_b$ and c_o negligible $\Rightarrow B_{oi} \cong B_{ob} \Rightarrow$ applying Levitan and Murtha (1999) correlation for B_{ob}:

$$B_{oi} \cong B_{ob} = 1 + 0.0005 * GOR * \left(\frac{\gamma_g}{\gamma_o}\right)^{0.25} + \frac{0.0004 * (T_r - 60)}{\gamma_o * \gamma_g}$$

Where T_r is reservoir temperature in °F.

For the case GOR=0 scf/STB then:

$$B_{oi} \cong 1 + 0.0005 * 0 * \left(\frac{0.8}{0.93}\right)^{0.25} + \frac{0.0004 * (239.8 - 60)}{0.93 * 0.8} = 1.10\ \text{RB/STB}$$

Finally, applying the same equation for the rest of the cases (see Table 2 for GOR values):

- GOR=248.7 scf/STB $\Rightarrow B_{oi} \cong 1.22\ \text{RB/STB}$
- GOR=545.4 scf/STB $\Rightarrow B_{oi} \cong 1.36\ \text{RB/STB}$
- GOR=935.2 scf/STB $\Rightarrow B_{oi} \cong 1.55\ \text{RB/STB}$
- GOR=2,000 scf/STB $\Rightarrow B_{oi} \cong 2.06\ \text{RB/STB}$

These values are used to define Emerald PDF for oil formation volume factor.

6.5.3 – Estimation of Porosity

For the case of Emerald, which is approximately beneath 3.7495 km of sediments, the porosity values obtained through the equations derived from Ehrenberg and Nadeau (2005) analysis give the following results:

$$\varphi_{P90} = -0.0917 * (3.7495)^2 - 0.8773 * (3.7495) + 14.019 = 9.2\%$$

$$\varphi_{P50} = -0.0191 * (3.7495)^2 - 2.2925 * (3.7495) + 23.457 = 14.6\%$$

$$\varphi_{P10} = -0.0636 * (3.7495)^2 - 1.863 * (3.7495) + 31.309 = 24.0\ \%$$

These values are used to define Emerald PDF for porosity.

6.5.4 – Computation of Gross Rock Volume

The GRV reports created by IHS Kingdom, using the surfaces interpreted for the top and base of Maspoli and the three different restriction polygons, are as follows:

- Maximum Case:

```
Volumetric Model:          Single Structure
Grid:      PR_Emerald_Top
Polygons Used:   PR_Emerald_P01
Lower Contact:   PR_Emerald_Base

Polygon PR_Emerald_P01
-------------------------------------------------
Polygon Area:     131.1975    10^6 M2
Polygon Area within the Grid(s):     120.3750    10^6 M2
Gross Volume:     5,245.3756    10^6 M3
```

- Optimistic Case:

```
Volumetric Model:          Single Structure
Grid:      PR_Emerald_Top
Polygons Used:   PR_Emerald_P10
Lower Contact:   PR_Emerald_Base

Polygon PR_Emerald_P10
-------------------------------------------------
Polygon Area:     94.2879    10^6 M2
Polygon Area within the Grid(s):     92.8860    10^6 M2
Gross Volume:     4,109.6645    10^6 M3
```

- Conservative Case

```
Volumetric Model:          Single Structure
Grid:      PR_Emerald_Top
Polygons Used:   PR_Emerald_P90
Lower Contact:   PR_Emerald_Base

Polygon PR_Emerald_P90
-------------------------------------------------
Polygon Area:     20.4696    10^6 M2
Polygon Area within the Grid(s):     20.4243    10^6 M2
Gross Volume:     966.6965    10^6 M3
```

This variable, GRV, is defined as a LogNormal distribution, therefore 3 parameters are required in @Risk for its definition: P10, P50 and P90 values. The P50 value is calculated, as a function of the P10 and P90 values using the formula: $P50 = e^{(LN(P90)+LN(P10))/2}$ (Wright 2015).

For the case of Emerald, this results in a P50 value for *GRV* = 1,993,187,971 m^3.

6.5.5 – Inputs used for the probabilistic analysis of Emerald

A summary of the inputs used for the probabilistic volumetric analysis of Emerald, based on the previous results, is shown in **Table 11.**

Parameter	MIN	Low Estimate	Best Estimate	High Estimate	MAX	Distr. Type
GRV (m^3)	0	966,696,500	1,993,187,971	4,109,664,500	5,245,375,600	LogNormal
N/G (%)	0	34.8%	66.6%	90%	100%	Beta
Phi (%)	0	9.2%	14.6%	24.0%	48%	Beta
S_w (%)	0	10.3%	23.4%	41.6%	100%	Beta
GOR (scf/STB)	0	248.7	545.4	935.2	2,000	Beta
B_{oi} (RB/STB)	1.10	1.22	1.36	1.55	2.06	Beta
RF (%)	0	22.4%	31%	38.7%	50%	Beta

Table 11 – Reservoir and fluid properties used for the volumetric analysis of Emerald

The following figures (**Fig. 114** to **Fig. 120**) show the detail of the input distributions defined in @Risk and its simulation results:

- Gross Rock Volume:

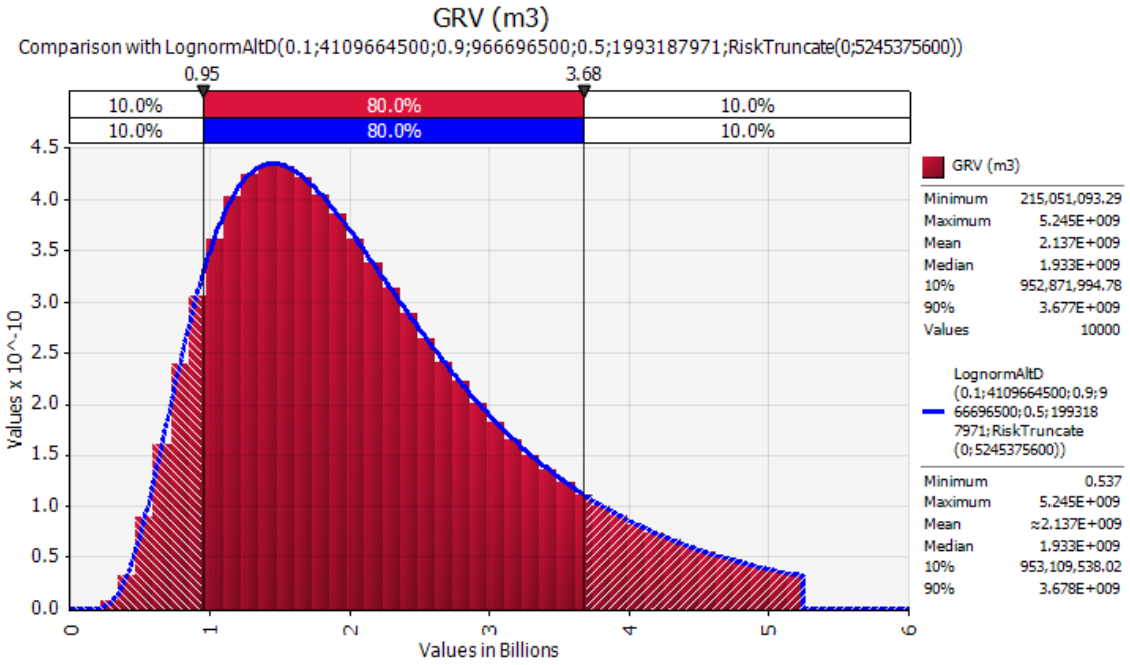

Fig. 114 – *GRV* distribution of Emerald

- Net to Gross:

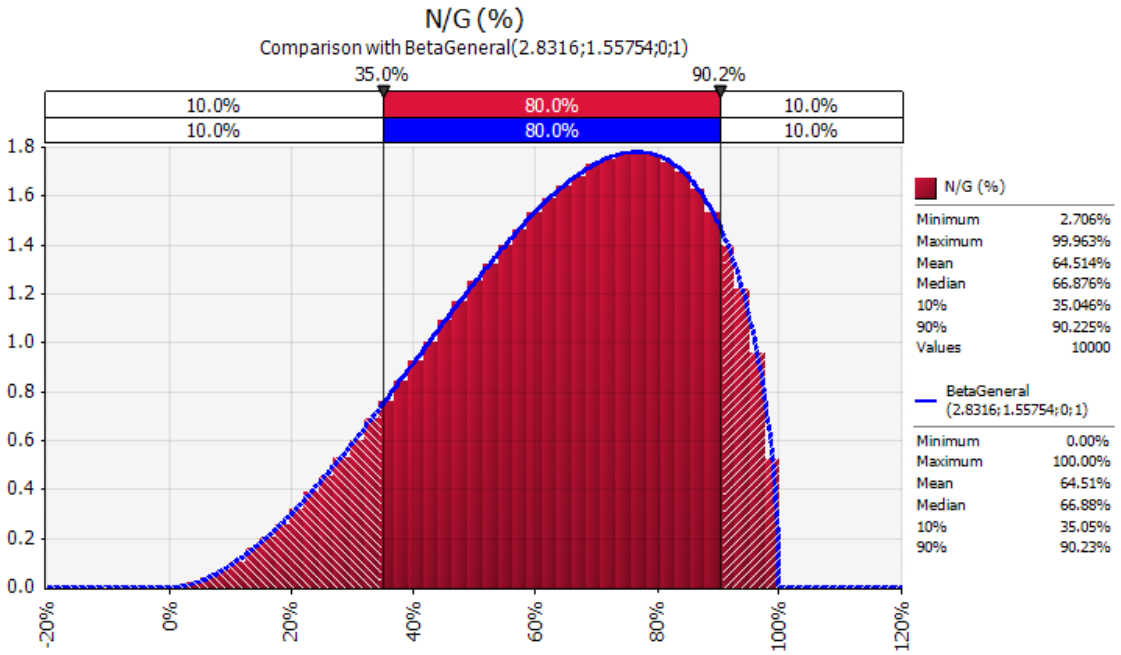

Fig. 115 – *N/G* distribution at Emerald

- Porosity:

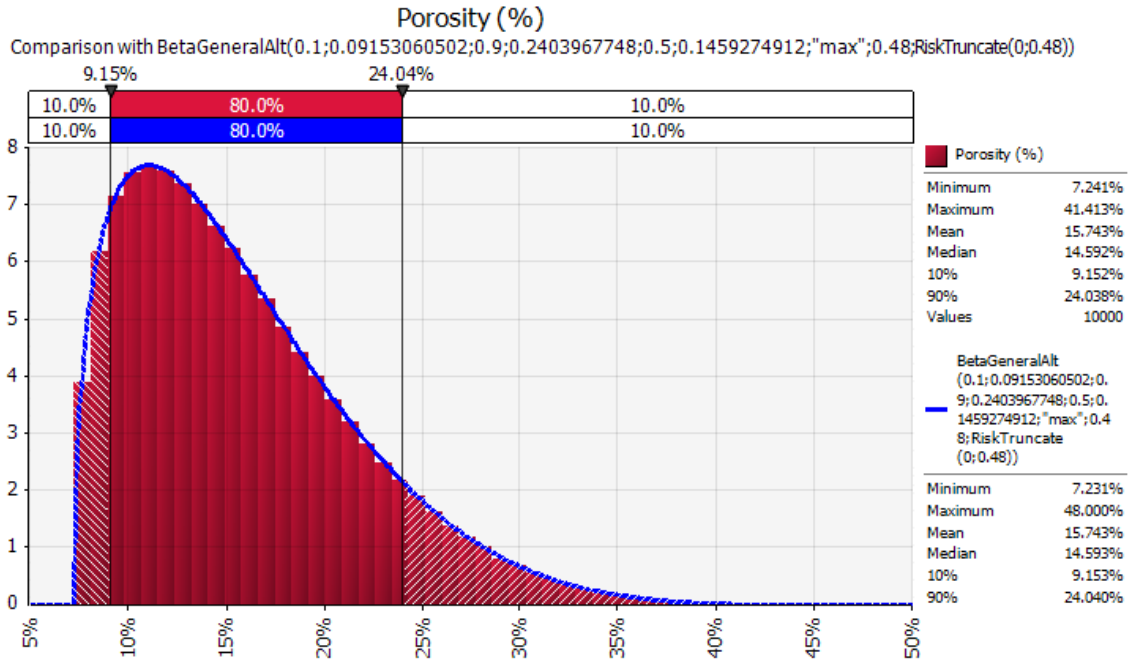

Fig. 116 – Porosity distribution at Emerald

- Water Saturation:

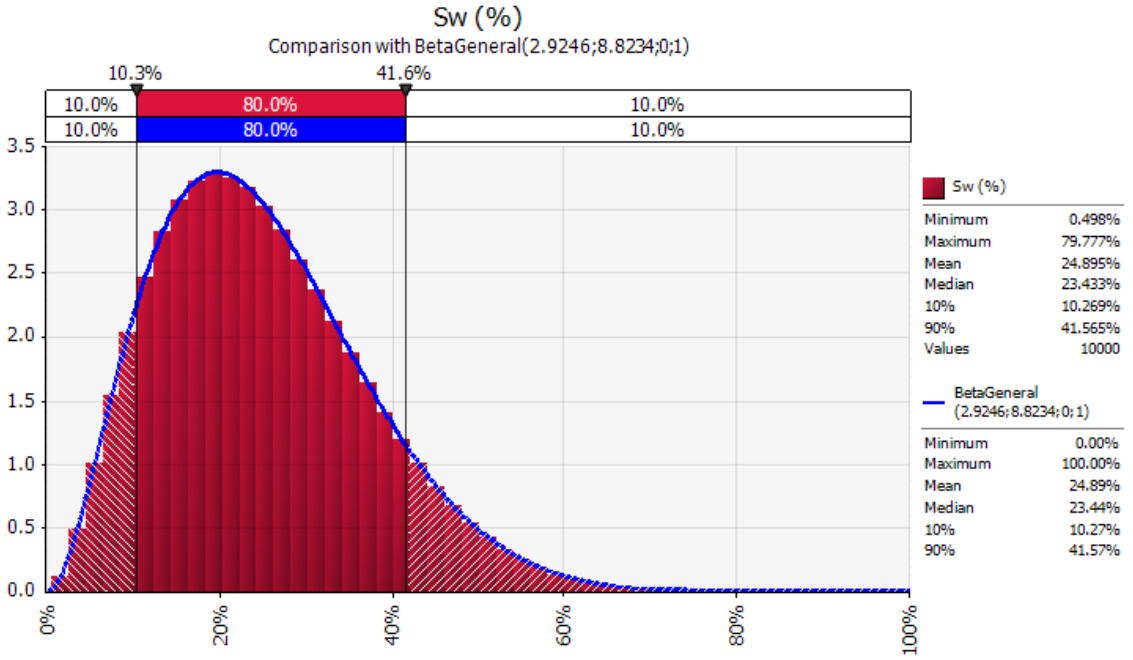

Fig. 117 – *Sw* distribution at Emerald

- Gas/Oil Ratio:

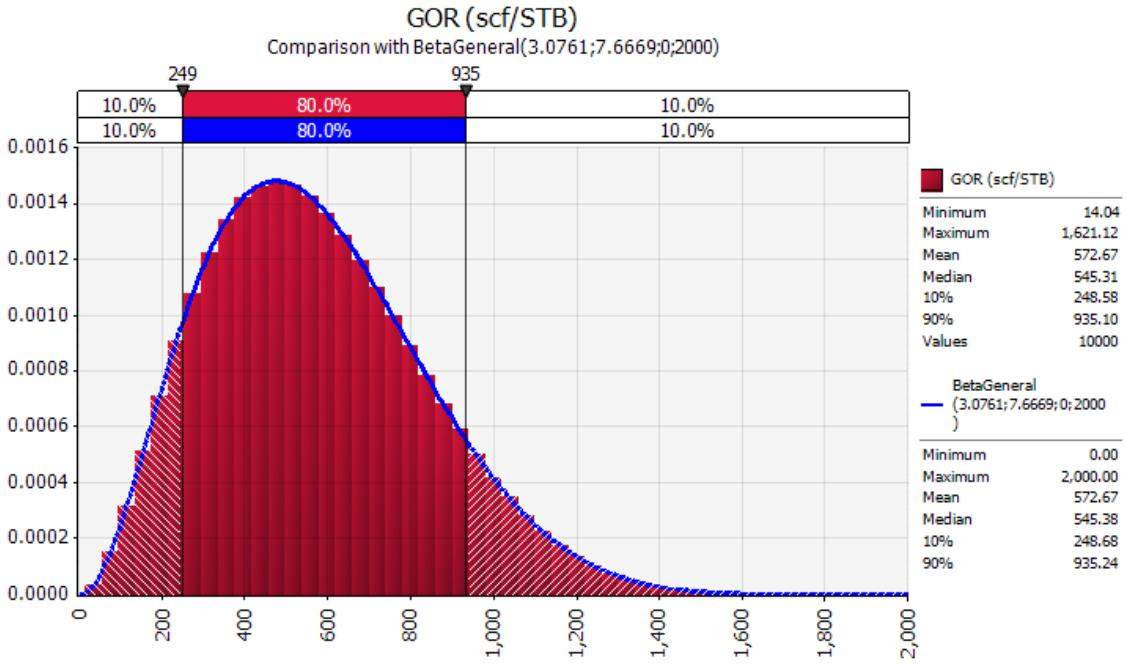

Fig. 118 – *GOR* distribution at Emerald

- Initial formation volume factor:

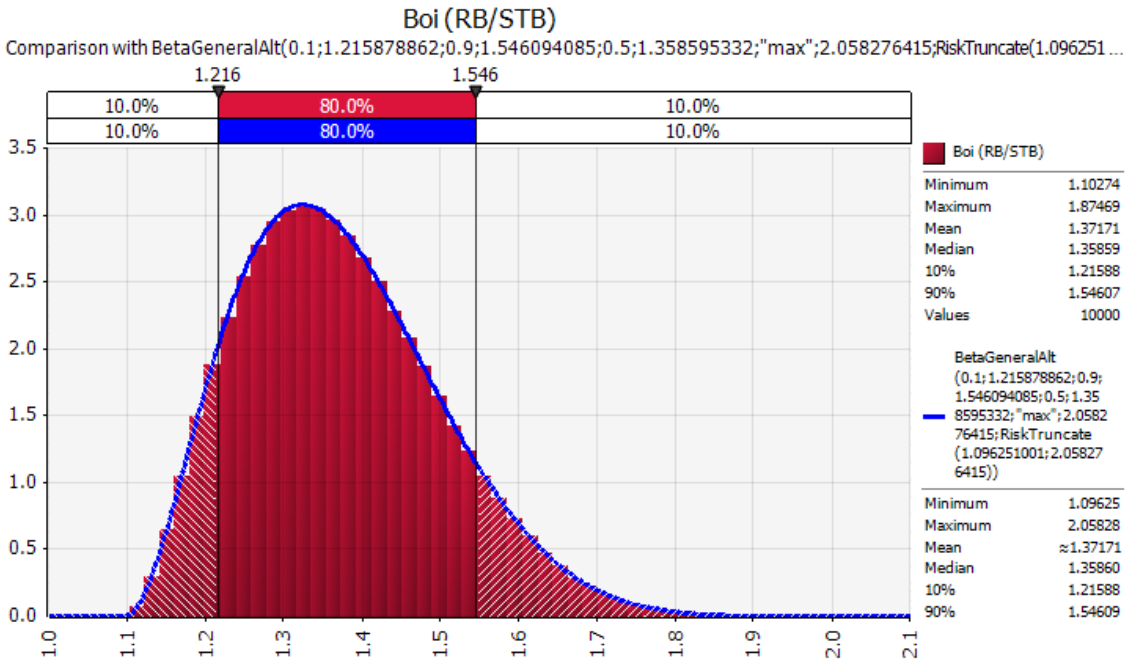

Fig. 119 – *Boi* distribution at Emerald

- Recovery Factor:

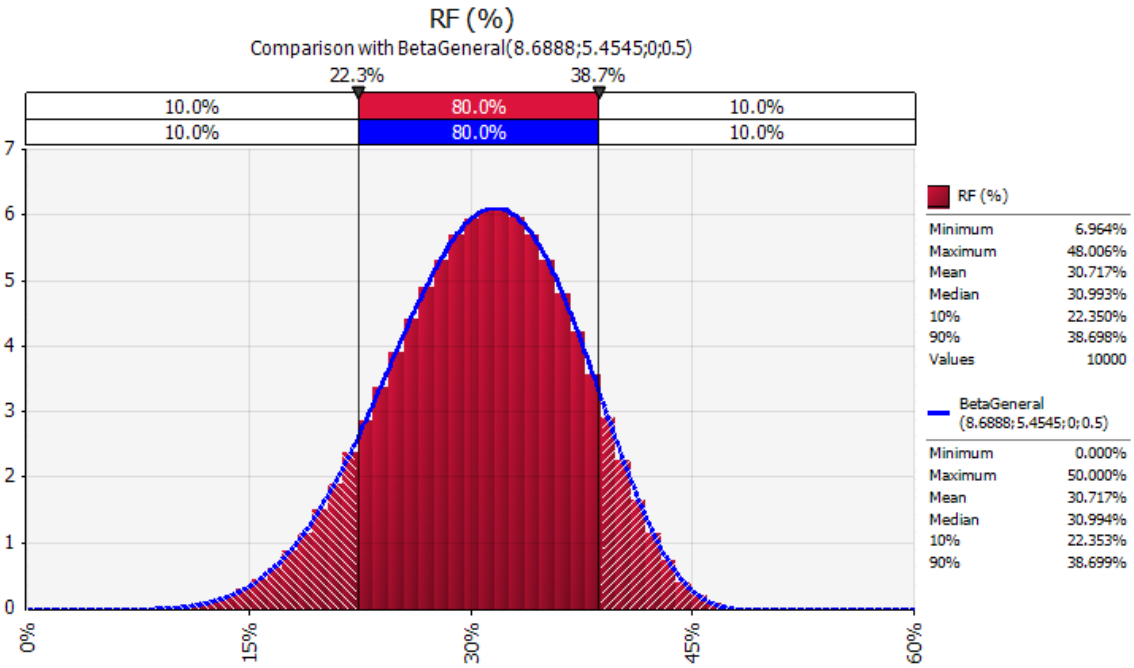

Fig. 120 – *RF* distribution at Emerald

6.4.6 – Results of the probabilistic analysis for Emerald

After all the inputs were set, and the output defined as the oil EUR then an @Risk simulation of 10,000 iterations was run using Latin Hypercube sampling. **Fig. 121** and **Fig. 122** show the resulting EUR distribution graphs for oil and associated gas, respectively:

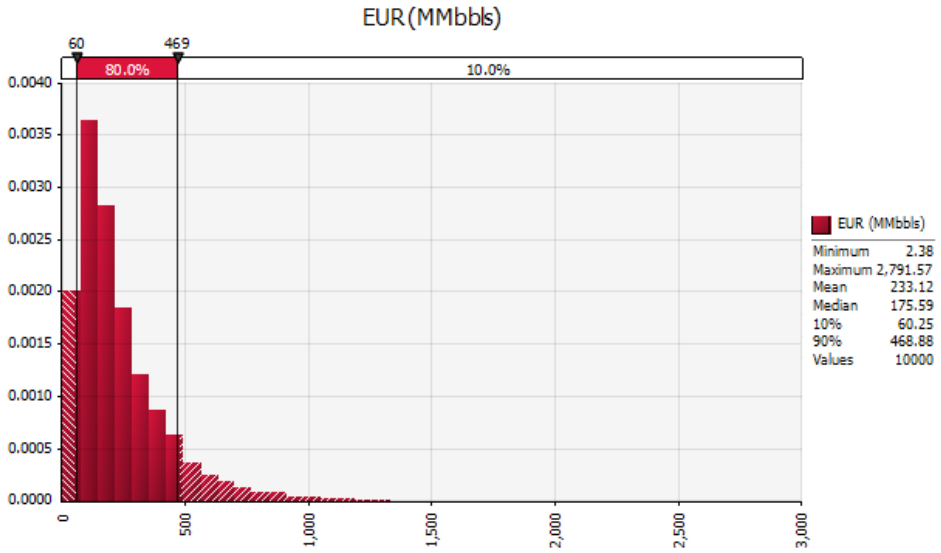

Fig. 121 – Emerald Oil EUR

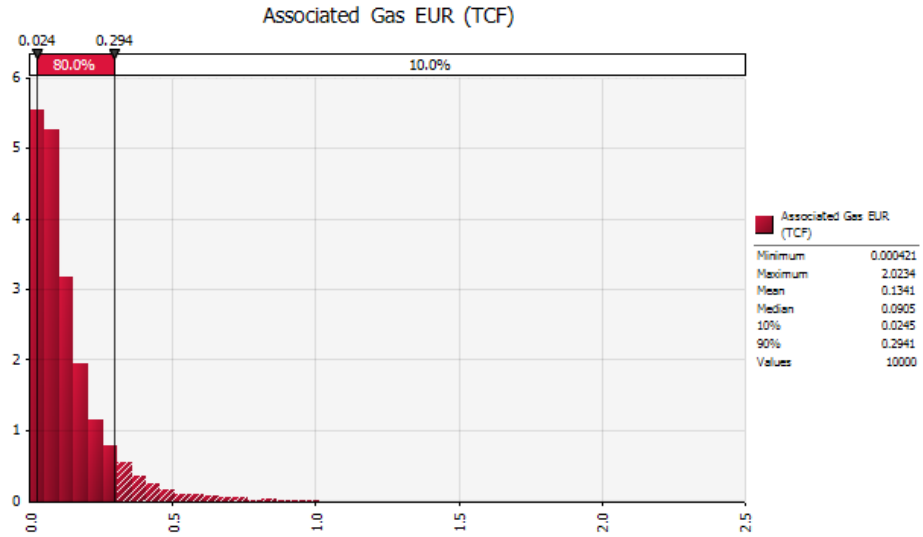

Fig. 122 – Emerald Associated Gas EUR

According to the Petroleum Resources Management System (SPE 2007), for this study case, the calculated resources can be classified as "Prospective Resources" and categorized as follows:

	Oil	Associated Gas
Low estimate Prospective Resources:	60.253 MMbbls	0.024 TCF
Best estimate Prospective Resources:	175.587 MMbbls	0.090 TCF
High estimate Prospective Resources:	468.880 MMbbls	0.294 TCF

Table 12 – Estimation of Emerald Prospective Resources

Sensibility Analysis

A tornado chart with the relative influence of the main variables on the oil EUR for this prospect is shown in **Fig. 123.**

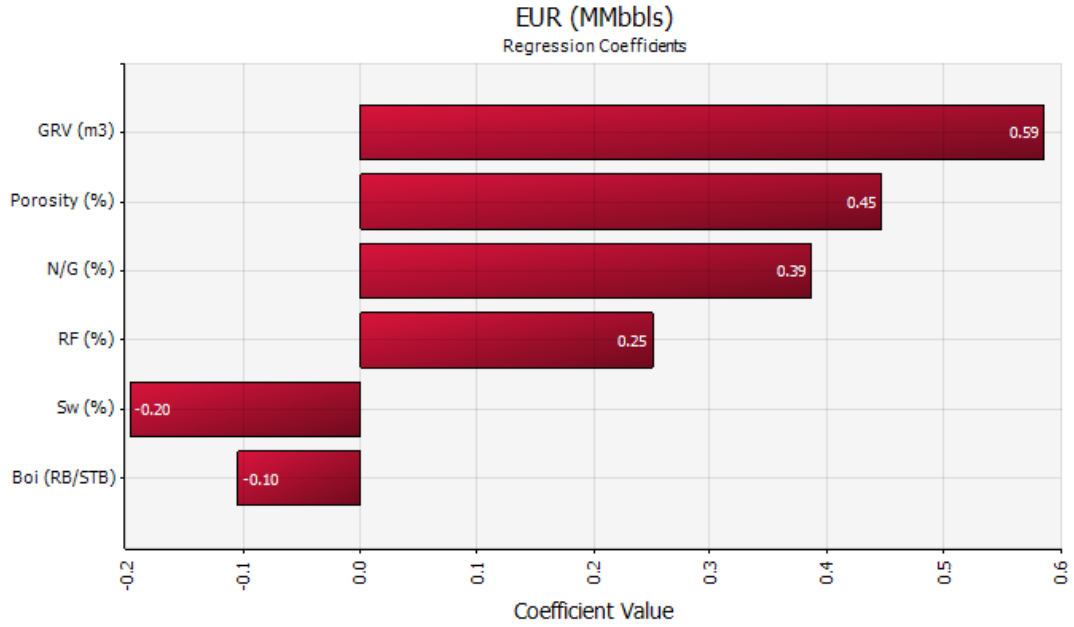

Fig. 123 – Tornado chart for Emerald Oil EUR

Fig. 124 shows a tornado chart with the relative influence of the main variables on the associated gas EUR for this prospect.

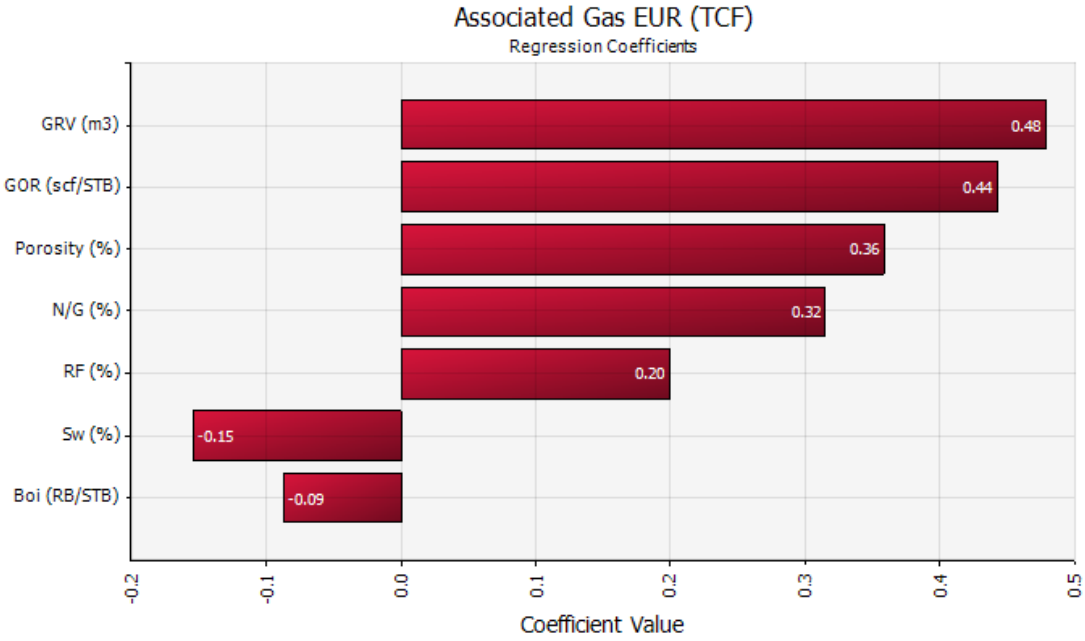

Fig. 124 – Tornado chart for Emerald Associated Gas EUR

From these tornado charts, it can be concluded that GRV is the parameter which oil EUR is most sensible to. On the other hand, for associated gas EUR, GRV and GOR are the most sensible parameters.
For this prospect, the uncertainty in GRV is significant and therefore it is the input that has the greatest influence on the EUR calculation.

7. Discussion

In this project, gross rock volumes are obtained directly from the interpretation of 3D seismic data. Regarding this, some factors that were not considered for EUR calculation, which could affect the quality of the interpretation and add uncertainty to the GRV calculation are:

- The vertical resolution of the seismic data; it is approximately 10 m for the Cenozoic prospect (Maspoli) and 20 m for the Cretaceous prospects (Chafalote, Jasper, Emerald-Deep and Emerald). The smaller prospects, Jasper, Emerald and Emerald-Deep are more affected by this issue because their thickness is in the same order of magnitude of the vertical resolution of the seismic data used for their recognition.
- Potential errors in the seismic velocities used in the processing sequence of the seismic data. Since the UR13_3D survey was processed in the time domain and was later converted to depth (stretched to depth), the prospects analyzed within it (Jasper, Emerald-Deep and Emerald) are more affected by this issue. On the other hand, the advanced processing sequences used to process the BG12_3D and TO12_3D surveys, anisotropic PSDM, minimizes potential errors in the depth imaging of Maspoli and Chafalote.

The definition of Maspoli P10 and P01 areas may be larger; they are constrained because the outer data limits of the BG12_3D survey are reached. For this prospect, only the most conservative area, the P90, lies completely within its seismic survey boundaries. Taking this into account, the best and high estimate volumes calculated for Maspoli should be higher. In **Fig. 125** there is a sketch of a potential maximum extension of this prospect.

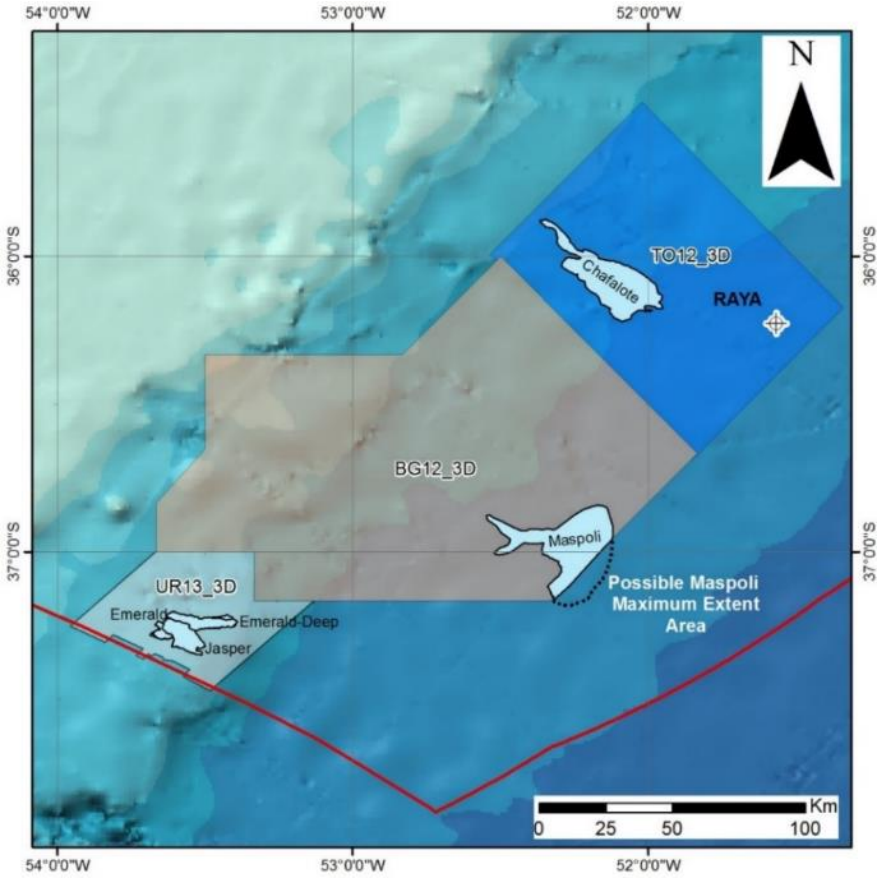

Fig. 125 – Map of analyzed turbidites with potential maximum extent area for Maspoli

For the prospects recognized in the UR13_3D survey (Jasper, Emerald-Deep and Emerald), the seismic response within the turbidite bodies is quite homogeneous. In those cases, there are some internal faults, but they are not likely to compartmentalize the reservoir since they do not present significant displacements. The main faults, which also conform the traps, act as seals, and this is supported by the fact that seismic amplitudes vanish after them (Fig. 69, Fig. 89 and Fig. 109).

Emerald is the prospect most affected by faulting. **Fig. 126** shows an arbitrary line through it with some interpreted faults. From that seismic line, it seems quite probable that the different zones of Emerald are interconnected.

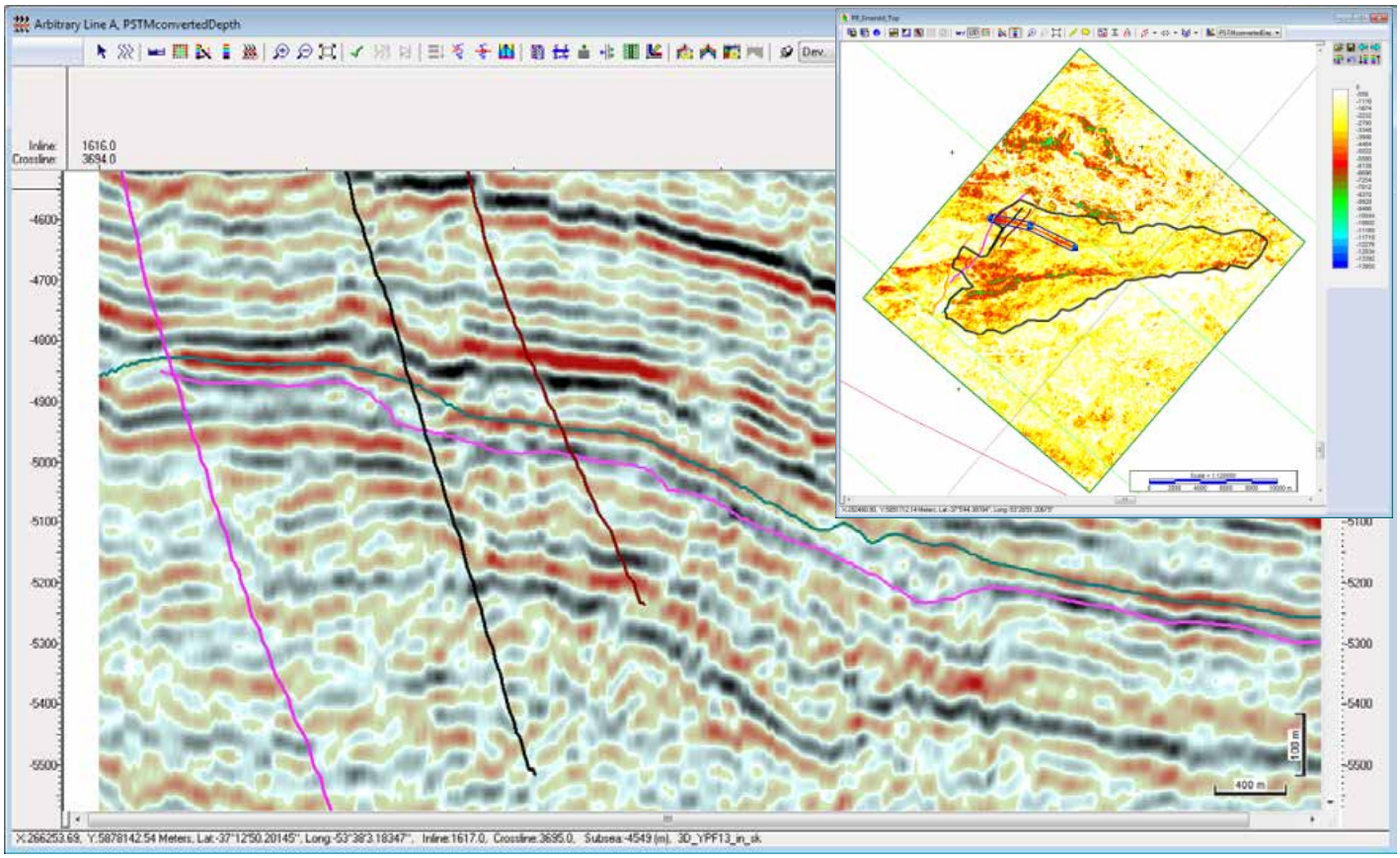

Fig. 126 – Arbitrary seismic line through Emerald (courtesy of ANCAP)

From the seismic response of the largest prospects, Maspoli and Chafalote, internal stratification and faults are recognized. This is a signal of potential isolated production zones within the recognized turbidite bodies. In the case of Maspoli, the variability of facies is not very significant. It is simply composed by two lobes, and according to the seismic data, it is highly probable that both lobes are interconnected (see the areas circled in red in **Fig. 127** and **Fig. 128**). On the other hand, Chafalote presents a more complex case, up to 5 turbidite bodies can be recognized (this prospect is a stack of turbidites), but most of them (if not all) are interconnected, as it happens with Maspoli, because there are zones where the lobes are potentially in contact. It is the same situation that happens with Roncador field in the Campos Basin and with the Sea Lion complex in the North Falkland Basin and it is a quite common situation with this kind of prospects.

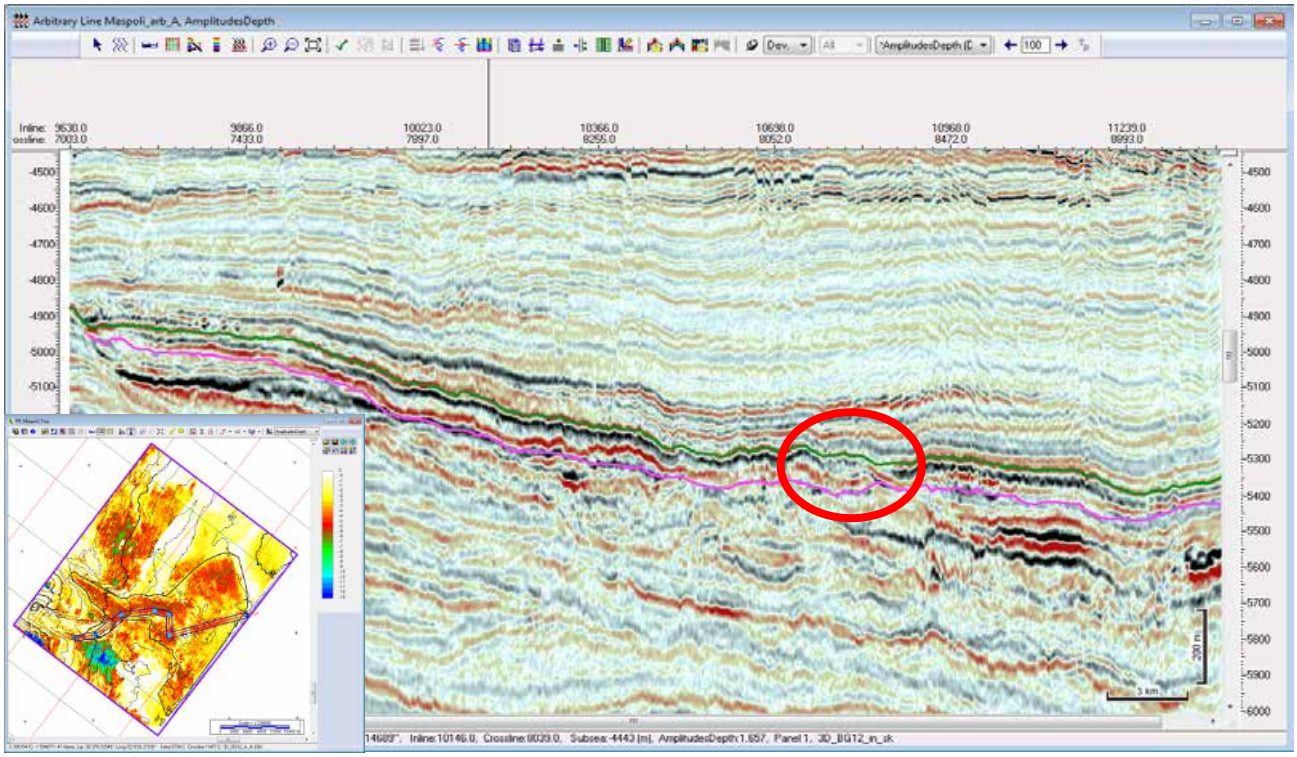

Fig. 127 – Potential interconection between Maspoli lobes (courtesy of ANCAP)

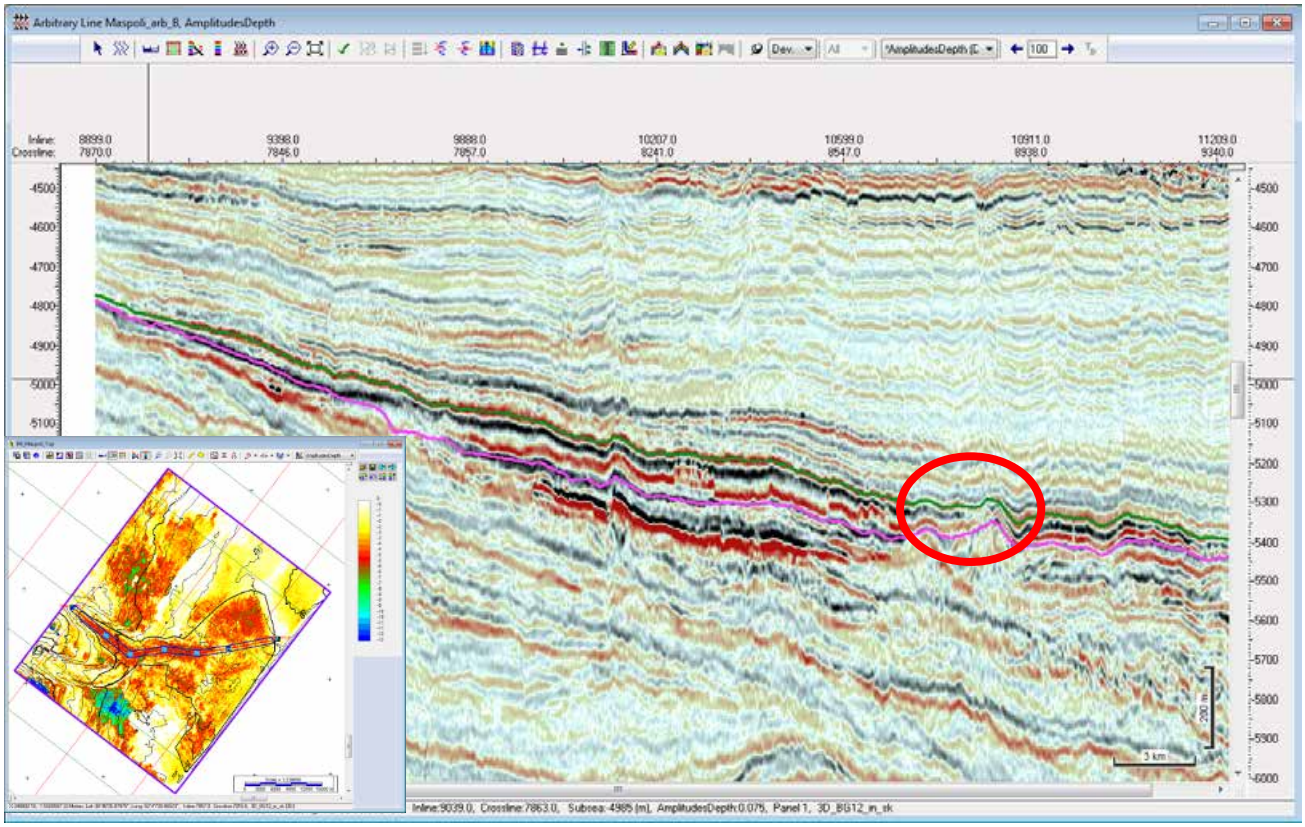

Fig. 128 – Potential interconection between Maspoli lobes (courtesy of ANCAP)

8. Final Results

In this project, a database of turbidite reservoir and fluids parameters was constructed from scientific publications (Table 1). It is composed of turbidites from offshore Brazil, Ghana and Falkland Islands. It was used to construct probability distribution functions for the volumetric evaluation of potential turbidite prospects recognized in the offshore Uruguay.

For this report, three different 3D seismic surveys were analyzed and five turbidite prospects were interpreted in detail: Chafalote, Maspoli, Jasper, Emerald and Emerald-Deep. Their locations are shown in the map presented in Fig. 125.

The probabilistic volumetric evaluation of the turbidite prospects studied in this project is summarized in the following table of prospective resources:

	Oil (MMbbls)			Associated Gas (TCF)		
Prospect	**Low Estimate**	**Best Estimate**	**High Estimate**	**Low Estimate**	**Best Estimate**	**High Estimate**
Chafalote	759.82	1,828.47	4,020.55	0.299	0.932	2.532
Maspoli	905.06	2,224.96	4,680.26	0.355	1.146	3.020
Jasper	103.61	257.24	566.84	0.041	0.132	0.358
Emerald-Deep	54.55	140.12	330.99	0.022	0.072	0.206
Emerald	60.25	175.59	468.88	0.024	0.090	0.294

Table 13 – Prospective Resources per prospect

In "PETE692 – Professional Study" this work will be extended with a probabilistic economic evaluation for each prospect.

9. References

Acosta, M., Farias, R., Vilela, A.J. et al. 2007. SPE 96910 Deepwater Horizontal Openhole Gravel Packing in Marlim Sul Field, Campos Basin, Brazil - Completion Project Learning Curve and Optimization. Presented at the SPE Annual Technical Conference and Exhibition, Dallas, Texas, 9-12 October. SPE-96910-MS. http://dx.doi.org/10.2118/96910-MS

Albertao, G.A., Grell, A.P., Badolato, D. et al. 2005. SPE 95612 3D Geological Modeling in a Turbidite System With Complex Stratigraphic-Structural Framework-An Example From Campos Basin, Brazil. Presented at the SPE Annual Technical Conference and Exhibition, Dallas, Texas, 9-12 October. SPE-95612-MS. http://dx.doi.org/10.2118/95612-MS

Alves, M.M., Maciel, W.B., Reis, L.C. et al. 2005. OTC 17053 Campos Basin Tertiary Reservoirs Of Barracuda And Caratinga Fields: Development Strategy And Main Reservoir Management Issues. Presented at the Offshore Technology Conference, Houston, Texas, 2-5-May. OTC-17053-MS. http://dx.doi.org/10.4043/17053-MS

ANP - Agência Nacional do Petróleo, Gás Natural e Biocombustíveis. 2016a. Plano de Desenvolvimento do Campo Espadarte. http://www.anp.gov.br/images/planos_desenvolvimento/Espadarte.pdf (accessed 17 Jun 2018).

ANP - Agência Nacional do Petróleo, Gás Natural e Biocombustíveis. 2016b. Plano de Desenvolvimento do Campo Frade. http://www.anp.gov.br/images/planos_desenvolvimento/Frade.pdf (accessed 13 June 2018).

Assis, O.C., Becker, M.R., Melo, J.R.C. et al. 1998. OTC 8879 Barracuda and Caratinga giant oil fields, deep water Campos Basin, Brazil. Presented at the Offshore Technology Conference, Houston, Texas, 4-7 May. OTC-8879-MS. http://dx.doi.org/10.4043/8879-MS

Awad, S.P. 1997. OTC 8468 Albacora Field FPS: Another Deepwater Development Offshore Brazil. Presented at the Offshore Technology Conference, Houston, Texas. 5-8 May. OTC-8468-MS. http://dx.doi.org/10.4043/8468-MS

Bacoccoli, G., Morales, R.G. and Campos, O.A.J. 1980. The Namorado Oil Field: A Major Oil Discovery in the Campos Basin, Brazil. In *Giant Oil and Gas Fields of the Decade: 1968-1978. AAPG Memoir 30*, ed. M.T. Halbouty, 329-338.

Bampi, D. and Costa, O.J. 2010. SPE 139376 Marlin Field: An Optimization Study for a Mature Field. Society of Petroleum Engineers. Presented at the SPE Latin American and Caribbean Petroleum Engineering Conference, Lima, Peru, 1-3 December. SPE-139376-MS. http://dx.doi.org/10.2118/139376-MS

Bergeron, J.M. and Parvez, N. 2007. SPE 107706 The Frade Development Asset: How Robust Project Management Drove the Asset From Economically Marginal to Chevron's Cornerstone Development Project in Brazil. Presented at the Latin American & Caribbean Petroleum Engineering Conference, Buenos Aires, Argentina, 15-18 April. SPE-107706-MS. http://dx.doi.org/10.2118/107706-MS

Bonet, L., Romeu, R.K., Barroso, A.S. et al. 1999. SPE 53986 Flow Simulation Study of the Namorado Sandstone (Albacora Field, offshore Brazil) Accounting for Scaling of Petrophysical Properties. Presented at the SPE Latin American and Caribbean Petroleum Engineering Conference, Caracas, Venezuela. 21-26 April. SPE-53986-MS. http://dx.doi.org/10.2118/53986-MS

Brown, A.R. 2011. Interpretation of Three-Dimensional Seismic Data. Dallas, Texas: AAPG & SEG. https://doi.org/10.1190/1.9781560802884

Bunt, R.J.W. 2015. Sea Lion Field, North Falkland Basin: The use of seismic attributes in fan and reservoir definition. *Petroleum Geoscience* **21** (2-3): 137–149. http://dx.doi.org/10.1144/petgeo2014-055

Candido, A. and Cora, C.A.G. 1992. The Marlim and Albacora Giant Fields, Campos Basin, Offshore Brazil. In *Giant Oil and Gas Fields of the Decade 1978-1988. AAPG Memoir 54*, ed. M.T. Halbouty, Chap. 8, 123-135. https://doi.org/10.1306/M54555C8

Capeleiro Pinto, A.C., Guedes, S.S., Bruhn, C.H.L. et al. 2001. SPE 69438 Marlim Complex Development: A Reservoir Engineering Overview. Presented at SPE Latin American and Caribbean Petroleum Engineering Conference, Buenos Aires, Argentina, 25-28 March. SPE-69438-MS. http://dx.doi.org/10.2118/69438-MS

Conti, B., Perinotto, J.A.D.J., Veroslavsky, G. et al. 2017. Speculative petroleum systems of the southern Pelotas Basin, offshore Uruguay. *Marine and Petroleum Geology* **83**: 1-25. http://dx.doi.org/10.1016/j.marpetgeo.2017.02.022

Cronquist, C. 2001. ESTIMATION and CLASSIFICATION of RESERVES of CRUDE OIL, NATURAL GAS, and CONDENSATE. Richardson, Texas: SPE.

Cysne, L., and Mihaguti, M.K. 2008. OTC 19296 Reservoir Aspects and Wells Development Strategy. Presented at the Offshore Technology Conference, Houston, Texas, 5-8 May. OTC-19296-MS. http://dx.doi.org/10.4043/19296-MS

Da Costa Filho, F.H. 2005. OTC 17058 Barracuda And Caratinga FPSO Design. Presented at the Offshore Technology Conference, Houston, Texas, 2-5 May. OTC-17058-MS. http://dx.doi.org/10.4043/17058-MS

Da Silva, M.G.F., Calderon, A. and da Motta, E.P. 2004. SPE 90158 The Keys to Successfully Acidizing Horizontal Injection Wells in the Marlim Sul Field. Presented at the SPE Annual Technical Conference and Exhibition, Houston, Texas, 26-29 September. SPE-90158-MS. http://dx.doi.org/10.2118/90158-MS

Dailly, P., Henderson, T., Kanschat, K. et al. 2017. The Jubilee field, Ghana: Opening the late Cretaceous play in the West African transform margin. In Giant fields of the decade 2000–2010. AAPG Memoir 113, ed. R.K. Merrill and C.A. Sternbach, 257–272. http://dx.doi.org/10.1306/13572010M1132997

De Gasperi, A. and Catuneanu, O. 2014. Sequence stratigraphy of the Eocene turbidite reservoirs in Albacora field, Campos Basin, offshore Brazil. *AAPG Bulletin* **98** (2): 279–313. http://dx.doi.org/10.1306/07031312117

Ecologus. 2006. Estudo de Impacto Ambiental – EIA. Atividade de Produção de Petróleo no Campo de Frade, Bacia de Campos. http://licenciamento.ibama.gov.br/Petroleo/Producao/Producao%20-%20Bacia%20de%20Campos%20-%20Campo%20de%20Frade%20-%20Chevron/EIA/Texto/EIA%20II.5.1%20Meio%20Fisico/EIA%20II.5.1.4%20-%20Geologia%20e%20Geomormofologia.pdf (accessed 13 June 2018)

Ehrenberg, S.N and Nadeau, P.H. 2005. Sandstone vs. carbonate petroleum reservoirs: A global perspective on porosity-depth and porosity-permeability relationships. *AAPG Bulletin* **89** (4): 435-445. http://dx.doi.org/10.1306/11230404071

Farrimond, P., Green, A. and Williams, L.S. 2015. Petroleum geochemistry of Sea Lion Field, North Falkland Basin. *Petroleum Geoscience* **21** (2-3): 125–135. http://dx.doi.org/10.1144/petgeo2014-052

Ferreira, A.A., Ferreira, D.M., Tavares, A.F.C. et al. 1990. SPE 21140 Scale Problems in Namorado Field. Presented at the SPE Latin America Petroleum Engineering Conference, Rio de Janeiro, Brazil, 14-19 October. SPE-21140-MS. http://dx.doi.org/10.2118/21140-MS

Figueiredo, F.P., Branco, C.C.M., Prais, F. et al. 2007. SPE 107387 The Challenges of Developing a Deep Offshore Heavy-Oil Field in Campos Basin. Presented at the Latin American & Caribbean Petroleum Engineering Conference, Buenos Aires, Argentina, 15-18 April. SPE-107387-MS. http://dx.doi.org/10.2118/107387-MS

Graton, L.C. and Fraser, H.J. 1935. Systematic Packing of Spheres-with Particular Relation To Porosity And Permeability. *The Journal of Geology* **43** (8): 785-909. https://doi.org/10.1086/624386

Griffiths, A.G. 2015. The reservoir characterization of the Sea Lion Field. *Petroleum Geoscience* **21** (2-3): 199–209. http://dx.doi.org/10.1144/petgeo2014-041

Guardado, L.R., Gamboa, L.A.P. and Lucchesi C.F. 1989. Petroleum Geology of the Campos Basin, Brazil, a Model for a Producing Atlantic Type Basin. In *Divergent/Passive Margin Basins. AAPG Memoir 48*, ed. J.D. Edwards and P.A. Santogrosi, 3-79.

Hanley, D., Hill, N., Mutimer, K. et al. 2009. Jubilee Field: A Step Change for Ghana. Presented at the 8th PESGB-HGS Conference on African E&P, London, 9-10 September

Hernandes, R., Melo, V.L., Santos, J.A.M. et al. 2008. SPE 114112 Scale Management in Espadarte Field. Presented at the SPE International Oilfield Scale Conference, Aberdeen, UK, 28-29 May. SPE-114112-MS. http://dx.doi.org/10.2118/114112-MS

Lemos, W.P., de Castro, M.R.B., Soares, C.M. et al. 2006. OTC 18056 Albacora Leste Field Development: Reservoir Aspects and Development Strategy. Presented at the Offshore Technology Conference, Houston, Texas, 1-4 May. OTC-18056-MS. http://dx.doi.org/10.4043/18056-MS

Levitan, L.L. and Murtha, M. 1999. New correlations estimate Pb, FVF. *Oil and Gas Journal* **97** (10): 70-76. https://www.ogj.com/articles/print/volume-97/issue-10/in-this-issue/production/new-correlations-estimate-p-b-fvf.html

Liner, D. 2016. The Limitations of Lognormal Distributions: Using Subsurface Data to Make More Accurate Resource Estimations. *AAPG Search and Discovery*. Search and Discovery Article #41848 (2016). http://www.searchanddiscovery.com/documents/2016/41848liner/ndx_liner.pdf

Locarnini, R.A., Mishonov, A.V., Antonov, J.I. et al. 2013. NOAA Atlas NESDIS 73 World Ocean Atlas 2013, Volume 1: Temperature, ed. S. Levitus and. A. Mishonov.

Loureiro, R.O., Patrocínio, B.N., Barbosa, B.C. et al. 2006. OTC 17925 Albacora Leste Field Development Project. Presented at the Offshore Technology Conference, Houston, Texas, 1-4 May. OTC-17925-MS. http://dx.doi.org/10.4043/17925-MS

McLaughlin, D.C. 2012. Jubilee Project Overview. OTC 23430 Presented at the Offshore Technology Conference, Houston, Texas, 30 April-3 May. OTC-23430-MS. http://dx.doi.org/10.4043/23430-MS

Minami, K., Cardoso, C.A.B.R., Bezerra, M.C.M. et al. 2000. OTC 12138. Presented at the Offshore Technology Conference, Houston, Texas, 1-4 May. OTC-12138-MS. http://dx.doi.org/10.4043/12138-MS

Morales, E. 2013. *Evolução tectônica e estratigráfica das bacias da margem continental do Uruguai*. PHD Thesis, Universidade Estadual Paulista, Rio Claro, Sao Paulo (September 2013). http://hdl.handle.net/11449/138385

Morales, E., Chang, H.K., Soto, M. et al. 2017a. Tectonic and stratigraphic evolution of the Punta del Este and Pelotas basins (offshore Uruguay). *Petroleum Geoscience* **23** (4): 415-426. https://doi.org/10.1144/petgeo2016-059

Morales, E., Chang, H.K., Soto, M. et al. 2017b. Speculative petroleum systems of the Punta del Este Basin (Offshore Uruguay). *Brazilian Journal of Geology* **47** (4): 645-656. http://dx.doi.org/10.1590/2317-4889201720170078

Nascimento, T.M., Menezes, P.T.L. and Braga, I.L. 2014. High-resolution acoustic impedance inversion to characterize turbidites at Marlim Field, Campos Basin, Brazil. *Interpretation* **2** (3): T143-T153. https://doi.org/10.1190/INT-2013-0137.1

Olea, R.A. 2011. On the Use of the Beta Distribution in Probabilistic Resource Assessments. *Natural Resources Research* **20** (4): 377-388. http://dx.doi.org/10.1007/s11053-011-9153-1

Oliveira, R.M. 2008. The Marlim Field: Incorporating 4D Seismic in Reservoir-Management Decisions. *J Pet Technol* **60** (4): 52-110. SPE-109336-JPT. http://dx.doi.org/10.2118/109336-JPT

Pádua, K.G.O., Stank, C.V., Soares, C.M. et al. 1998. OTC 8875 Roncador Field, Strategy of Exploitation. Presented at the Offshore Technology Conference, Houston, Texas, 4-7 May. OTC-8875-MS. http://dx.doi.org/10.4043/8875-MS

Pires, P.R.D.M., Lira, E.M., Costa, A. et al. 2010. Integration of Static and Dynamic Data to Investigate Interwell Communication: The Case of Module II of Espadarte Field, Campos Basin, Brazil. Presented at the SPE EUROPEC/EAGE Annual Conference and Exhibition, Barcelona, Spain, 14-17 June. SPE-131569-MS. http://dx.doi.org/10.2118/131569-MS

Rangel, H.D., Santos, P.R. and Quintaes, C.M.S.P. 1998. OTC 8876 Roncador Field, a New Giant in Campos Basin, Brazil. Presented at the Offshore Technology Conference, Houston, Texas, 4-7 May. OTC-8876-MS. http://dx.doi.org/10.4043/8876-MS

Rangel, H.D., Guimaraes, P.T. and Spadini A.R. 2003. Barracuda and Roncador giant oil fields, deep-water Campos Basin, Brazil. In *Giant oil and gas fields of the decade 1990– 1999. AAPG Memoir 78*, ed. M.T. Halbouty, Chap. 4, 123-137.

Reid, M.G., Melo, V.L., Lima, L.M. et al. 2009. Water Injection in Espadarte Module I Field. Presented at the Latin American and Caribbean Petroleum Engineering Conference, Cartagena de Indias, Colombia, 31 May-3 June. SPE-122308-MS. http://dx.doi.org/10.2118/122308-MS

Rodriguez-Suarez, C., de Souza, J.A.B., Sarzenski, D.J. et al. 2003. Reservoir Characterization of Roncador, an Ultra-deepwater Giant Field At Campos Basin, Brazil. SEG Technical Program Expanded Abstracts 2003: 1462-1465. https://doi.org/10.1190/1.1817568

Schmoker, J.W and Gautier, D.L. 1988. Sandstone porosity as a function of thermal maturity. *Geology* **16** (11): 1007-1010. https://doi.org/10.1130/0091-7613(1988)016%3C1007:SPAAFO%3E2.3.CO;2

Sills, S.R. and Agyapong, D. 2012. OTC 23451. Jubilee Field Reservoir Description & Waterflood Performance Overview. Presented at the Offshore Technology Conference, Houston, Texas, 30 April-3 May. OTC-23451-MS. http://dx.doi.org/10.4043/23451-MS

Silva, M.F., Malta, M.S., Zapparolli, L. et al. 2007. SPE 107062 Integrated Management on a Mature Field in the Brazilian Continental Margin. Presented at the Latin American & Caribbean Petroleum Engineering Conference, Buenos Aires, Argentina, 15-18 April. SPE-107062-MS. http://dx.doi.org/10.2118/107062-MS

Soto, M., Conti, B., Gristo, P. et al. 2016. Direct Oil and Gas Evidences from Punta Del Este Basin, Offshore Uruguay: New Data From Fluid Inclusions. *AAPG Search and Discovery*. Search and Discovery Article #10833 (2016). http://www.searchanddiscovery.com/documents/2016/10833conti/ndx_conti.pdf

Souza, J. M., Scarton, J. C., Candido, A. et al. 1989. The Marlim and Albacora Fields: Geophysical, Geological, and Reservoir Aspects. Presented at the Offshore Technology Conference, Houston, Texas, 1-4 May. OTC-5894-MS. http://dx.doi.org/10.4043/5894-MS

Society of Petroleum Engineers (SPE). 2007. Petroleum Resources Management System, http://www.spe.org/industry/docs/Petroleum_Resources_Management_System_2007.pdf

Tavella, G.F. and Wright, C.G. 1996. Cuenca del Salado. In Geología y Recursos Naturales de la Plataforma Continental Argentina, ed. V.A. Ramos and M.A. Turic, Chap. 6, 95-116. Buenos Aires, Argentina: Asociación Geológica Argentina and Instituto Argentino del Petróleo.

Weimer, P. and Slatt, R.M. 2004. Petroleum Systems of Deepwater Settings. Tulsa, Oklahoma: Society of Exploration Geophysicists and European Association of Geoscientists and Engineers.

Wood Group Mustang. 2018. 2018 Deepwater Solutions & Records for Concept Selection. Houston, Texas: Offshore Magazine.

Wright, J.D. 2015. Oil & Gas Property Evaluation. Golden, Colorado: Thompson-Wright, LLC.